**Investigating Chromium Cycling in Global Oxygen Deficient Zones with Chromium Isotopes**

By

Tianyi Huang

B. Sc. Chemistry, Peking University, 2015

Submitted to the Department of Earth, Atmospheric and Planetary Sciences in Partial Fulfillment of the Requirements for the Degree of

Doctor of Philosophy

at the

MASSACHUSETTS INSTITUTE OF TECHNOLOGY

and the

WOODS HOLE OCEANOGRAPHIC INSTITUTION

September 2021



Signature of Author _____

Joint Program in Oceanography/Applied Ocean Science and Engineering
Massachusetts Institute of Technology and Woods Hole Oceanographic Institution
August 17, 2021

Certified by _____

Prof. Edward A. Boyle
Thesis Supervisor
Massachusetts Institute of Technology

Accepted by _____

Dr. Colleen Hansel
Chair, Joint Committee for Chemical Oceanography
Woods Hole Oceanographic Institution

**Investigating chromium cycling in global oxygen deficient zones with chromium isotopes**

by

Tianyi Huang

Submitted to the Department of Earth, Atmospheric and Planetary Sciences on August 17, 2021
in Partial Fulfillment of the Requirements for the Degree of Doctor of Philosophy

## ABSTRACT

Chromium (Cr) isotopes have shown great potential as a paleo-redox proxy to trace the redox conditions of ancient oceans and atmosphere. However, its cycling in modern environments is poorly constrained. In my thesis, I attempt to fill in the gap of our understanding of chromium cycling in the modern ocean, with a focus on the redox processes in global oxygen deficient zones (ODZs).

Firstly, we developed a method to analyze Cr isotopes of different Cr redox species. Tests on processing conditions demonstrated its robustness in obtaining accurate Cr isotope data. It is applicable to both frozen and fresh samples. This method allows us to investigate the redox cycling of Cr that is hard to unravel by existing total Cr methods. Secondly, in the Eastern Tropical North Pacific (ETNP), Eastern Tropical South Pacific (ETSP) and Arabian Sea ODZs, their total dissolved Cr profiles show preferential reduction of isotopically light Cr(VI) to Cr(III), which is scavenged and exported to deeper oceans. Applying our new method to ETNP and ETSP ODZ seawater samples, we observed Cr(VI) reduction in both ODZs with a similar fractionation factor. This indicates similar mechanisms may be controlling Cr(VI) reduction in the two ODZs. Cr(III) maximum coincides with Fe(II) and secondary nitrite maximums in the upper core of both ODZs. Shipboard incubations with spiked Fe(II) showed fast Cr(VI) reduction occurring in the ETNP ODZ. But neither Fe(II) nor microbes were reducing Cr(VI) directly. Thirdly, we calculated the isotope effects of Cr scavenging in the ETNP and ETSP ODZs. The two ODZs show a similar isotope partitioning during Cr scavenging. And spatial variability is observed in the ETNP ODZ. Our calculated scavenged Cr isotope ratio is lighter than that of the total dissolved Cr from the same depth. It is also comparable to that of reducing or anoxic sediments, which implies that Cr isotopes can be used as an archive for local redox conditions.

Thesis supervisor: Edward A. Boyle
Title: Professor of Ocean Geochemistry

**Acknolwdgments**

First and foremost, I would like to thank my advisor, Prof. Edward Boyle. Ed has been providing tremendous support to me in my research and giving guidance on my career path. He also provided me with a lot of opportunities for cruises and international conferences, so that I could get the best scientific training and make the most from my PhD years. Ed not only supported me in my research, but also showed me how to be a good scientist. In all ways, he has been a role model for me in academia. I am grateful for his encouragement and belief in me in my hardest times of PhD. As I was facing difficulties as an international student, Ed showed his full understanding. He kindly invited me to join his family for Thanksgiving, making my new life in the US start with love and warmth.

I would also like to thank my committee: Colleen Hansel, Sune Nielsen and Mak Saito. They always gave me helpful feedback throughout my PhD, and brought new insights into my project from their expertise. I spent two summers in Woods Hole working with Sune. He provided me with an open and inclusive environment for my first research experience in the US. I am especially thankful for his generous support and guidance.

I am very grateful to numerous collaborators throughout the US. Gabrielle Rocap, Rick Keil and Al Devol generously offered me opportunities to join their two cruises to the Eastern Tropical North Pacific. A majority of my data in this thesis were produced with samples collected from the two cruises. Jim Moffett and his trace metal team on the two cruises provided their sampling devices and shared their water budget with me. A lot of students and PIs on these cruises make these adventures fruitful and fun: Kenny Bolster, Shun-Chung Yang, Natalya Evans, Rin Moriyasu, and many more. Katherine Barbeau generously shared their frozen samples from the GEOTRACES EPZT cruise, which makes an important part of my thesis. Sebastien Bigorre collected samples for us in the Argentine Basin. Ryan Woosley shared their seawater standard with us.

I would also like to thank my labmates in Boyle lab. Rick Kayser helped me a lot in the lab on tedious but crucial work. I am also really grateful for his help for cruise preparation and shipment when I need to go on to cruises on my own. He is professional and of great experience, making everything much easier and less terrifying to me. Cheryl Zurbrick and Simone Moos were lovely labmates during my early PhD years. They helped me settle down in Boston when I first arrived. I really enjoyed working with them all.

I also want to give thanks to a lot of friends and peers in the Joint Program and elsewhere. Liping Zhou from Peking University first led me into the world of oceanography. He offered me a precious cruise opportunity in my senior year, after which I made up my mind to shift to Chemical Oceanography. His support throughout my PhD years meant a lot to me. Na Qian was my labmate in Zhou's lab and we extended our friendship and caring for each other in the past years. Muntsa Martí and Ben Uveges, I felt lucky to have you as my mentors. Ronni Schwartz, Kris Kipp, Melody Abedinejad and Erin Chin made EAPS and E25 such a pleasant, lovely and supportive community. I am also lucky to have a lot of friends and their support in the Join Program: Marianne Acker, Jingxuan Li, Christopher Kinsley, Kelsey Moore, Jeemin Rhim, Jen Karolewsky, Jianhua Gong, Lizzie Wallace, and many more. Yang Xiang and Sun Xin are great peers. I always felt excited when we met in conferences and catched up with each other.

I would also like to give special thanks to all my friends in MITCEF and CBCGB. They were my family in Boston. Ruoxi Wang and Siyi Ye are my best sisters. I enjoy every moment with you and cherish our friendship. Especially during the pandemic, your love and company made this hard time full of sparkling sweetness. Nan Li, Eric Ma, Ning Qiao, Jirong Wang, Juta Pan, Chaoluan Kao, Chaw-Bing Chang and Kia-Ling Chang offered their endless love and care to me. I am thankful for many friends who have accompanied me through my ups and downs at different stages of my PhD: Liang Xiang, Siyu Chen, Shuo Jiang, Manyuan Lu, Wenzhu Song, Zhekai Hu, Yuyangguang Mu.

Finally, I owe so many thanks to my parents. You are always my support emotionally and professionally. Although we were far apart from each other in the last six years and only got to reunite a few times, your deepest love held me on this difficult path.

This research was supported by an anonymous MIT Fellowship, Praceis Presidential Fellowship, Frederick A. Middleton Fellowship, the US National Science Foundation (NSF Award No. OCE-1459287, OCE-1736996, OCE-1924050 and DEB-1542240) and the Center for Microbial Oceanography: Research and Education (C-MORE, NSF-OIA Award No. EF-0424599).

# List of Tables

# List of Figures

# Chapter 1 Introduction

## 1.1 Marine biogeochemistry of chromium

Chromium (Cr) is a redox sensitive trace metal in the ocean. Its concentration varies between 1.2 and 6.5 nmol/kg (i.e. Scheiderich et al., 2015; Huang et al., 2021). Cr has nutrient-like profiles in the Atlantic, Pacific and Arctic Oceans (Jeandel and Minister, 1987; Scheiderich et al., 2015). It increases with depth with a partial depletion in the surface and correlates with silicate (more so) and phosphate (less so) in some ocean basins (Jeandel and Minister, 1987; Rickli et al., 2019). Similar to nutrients, the deep Pacific is enriched in Cr by ~50% compared to the Atlantic. These features indicate that Cr may have similar cycling to nutrients - it is biologically taken up in the surface, transported by sinking particles, and regenerated in deeper oceans. Therefore, Cr is accumulated along the global thermohaline circulation, resulting in an enrichment in the deep Pacific Ocean.

Trivalent Cr (Cr(III)) and hexavalent Cr (Cr(VI)) in the form of oxyanion (chromate) are the two thermodynamically stable redox species of Cr in aquatic environments. Cr(VI) is stable in oxic seawater and is the dominant form of Cr in the ocean, whereas Cr(III) could be present in anoxic waters (Cranston and Murray, 1978; Rue et al., 1997). Chromate is toxic to organisms at high levels. Its structural resemblance to sulfate can cause its accidental uptake by organisms (Cervantes et al., 2001). In the oxic ocean, biological activity and photochemistry can reduce a small fraction (<5%) of Cr(VI) to Cr(III) in the near-surface waters (Achterberg and van den Berg, 1997; Connelly et al., 2006; Kieber & Helz, 1992; Janssen et al., 2020). Cr(III) is particle-reactive and can be scavenged by sinking particles (Semeniuk et al., 2016). The scavenged Cr(III) in the deep ocean may be regenerated and re-oxidized on a timescale of months (Murray et al., 1983; Janssen et al., 2021). However, Cr(III) can potentially be complexed with organic ligands (Saad et al., 2017), which might stabilize it in the water column.

Riverine input is the most important source of Cr to the ocean (McClain and Maher, 2016; Qin and Wang, 2017). Oxidative weathering catalyzed by manganese oxides (Fendorf and Zasoski, 1992) releases Cr(VI), which is transported to the ocean by rivers. Other sources such as groundwater, dust deposition and hydrothermal inputs make considerably smaller contributions to overall Cr sources (Izbicki et al., 2012; McClain and Maher, 2016; Qin and Wang, 2017; Sander and Koschinsky, 2000; Bauer et al., 2019). A recent study indicates benthic input as an

important regional source, but its importance for the global ocean still needs to be investigated (Janssen et al., 2021). Sedimentary burial of scavenged and biological Cr is the major sink of Cr in the ocean. The Cr residence time in the ocean are in the range of 3000 to 8000 years (Qin and Wang, 2017; Poppelmeier et al., 2021)

.

**1.2 Cr isotopes**

Cr has four stable isotopes: $^{50}$Cr, $^{52}$Cr, $^{53}$Cr and $^{54}$Cr with a natural abundance of 4.35%, 83.79%, 9.50%, and 2.36%, respectively (Holden, 2011; Shields et al., 1966).

Cr isotopes are usually reported in a delta notation by convention in geological and oceanographic studies:

$$\delta^{53}Cr\ (‰) = [\frac{(^{53}Cr\ /\ ^{52}Cr)_{sample}}{(^{53}Cr\ /\ ^{52}Cr)_{standard}} - 1] \times 1000\ (‰).$$

The Cr standard reference material (SRM) used in this thesis is NIST SRM 979. Therefore, the reported Cr isotopes are expressed as a relative deviation from SRM 979 in permil (‰).

When a process or a reaction generates different Cr isotopic compositions in the product and reactant, this isotopic effect is usually expressed as an isotopic fractionation factor α:

$$\alpha = \frac{R_{product}}{R_{reactant}},$$

where $R_{product}$ and $R_{reactant}$ denote the $^{53}$Cr/$^{52}$Cr ratio in the product and reactant, respectively. Alternatively, an isotope effect could also be expressed as ε in units of ‰, which is defined by the $\delta^{53}$Cr difference between the product and reactant:

$$\epsilon\ (‰) = \delta^{53}Cr_{product} - \delta^{53}Cr_{reactant}.$$

When the isotope effect is small enough, the fractionation factor α would be close to 1, and the following approximation could be used:

$$\epsilon\ (‰) \approx 1000 \times ln(\alpha) \approx 1000 \times (\alpha - 1).$$

So far, the reported Cr isotope effects (ε) are less than 10‰. Therefore, this approximation is applicable to Cr systematics discussed in this thesis.

**1.3 Cr isotope effects of different processes**

Cr isotope fractionations are mass dependent, and can be categorized into equilibrium and kinetic isotope effects.

### 1.3.1 Equilibrium isotope fractionations

Theoretical calculations have found equilibrium Cr isotope fractionations between coexisting species with different oxidation states (Cr(III) and Cr(VI)) and bonding ligands (Schauble et al., 2004). At calculated equilibrium, Cr(VI) in $[CrO_4]^{2-}$ should be isotopically heavier than Cr(III) in $[Cr(H_2O)_6]^{3+}$ by 6~7‰ at 298K. Cr bonded to stronger ligands tend to be heavier than those bound with weaker ligands (i.e. $Cl^-$, $NH_3$). Experimental studies show that the equilibrium isotope fractionation between $[Cr(VI)O_4]^{2-}$ and $[Cr(III)(H_2O)_6]^{3+}$ is 5~6‰ on a timescale of years at high Cr concentration (molar level) and pH 1.2 (Wang et al., 2015). At low Cr concentration (micromolar level) and neutral pH, the isotopic exchange between dissolved Cr(VI) and solid Cr(III) oxyhydroxide is faster on a timescale of months.

### 1.3.2 Kinetic isotope fractionations

Various processes can induce kinetic fractionations for Cr. This kinetic fractionation is usually caused by differences in the strength of the bond that links different Cr isotopes with other bonding elements.

The reduction of Cr(VI) to Cr(III) is a relatively well-studied process in terms of its associated isotope effect. Its kinetic fractionation originates from the weaker bonding between lighter Cr isotope and oxygen in $[Cr(VI)O_4]^{2-}$, which makes lighter Cr(VI) more readily to be reduced and therefore generates negative isotopic fractionation factors (ε). Experimental studies have shown that Cr(VI) could be reduced by various reducing agents through abiotic and biotic pathways. These reductants include organic matter (Kitchen et al., 2012), ferrous Fe (Bauer et al., 2018; Basu and Johnson, 2012; Dossing et al., 2011; Kitchen et al., 2012), magnetite (Ellis et al., 2002) and hydrogen peroxide (Zink et al., 2010). *Shewanella oneidensis* bacteria could also reduce Cr(VI) (Sikora et al., 2008). Their fractionation factors vary from -1.50‰ to -5.0‰ (Table 1.1).

The oxidation of Cr(III) to Cr(VI) is also accompanied with Cr isotope fractionation. The isotopic fractionation of Cr oxidation by $MnO_2$ or $H_2O_2$ varies between -2.5‰ to +0.7‰ in experiments (Ellis et al., 2004; Zink et a., 2010; Bain and Bullen, 2005). In natural settings, this occurs as oxidative weathering processes where Cr(III) is oxidized to the mobile Cr(VI), which enters the ocean via riverine transport. The isotope effect of this process catalyzed by $MnO_2$ has

been used to infer ancient atmospheric oxygen levels during oxidation events (Figure 1.1; i.e. Frei et al., 2009; Crowe et al., 2013). $\delta^{53}Cr$ values of up to 5‰ have been observed in geological records, indicating the rise of oxygen level and the consequent oxidative weathering of Cr.

Non-redox processes might also induce isotopic fractionation for Cr. The dissolution of Cr(III)-(oxy)hydroxide by complexing with organic acids and siderophores can produce slightly positive isotopic fractionation (dissolved $\delta^{53}Cr$(III): −0.27 to 1.23‰; Saad et al., 2017). The enhancement of Cr mobility by siderophores in rock leaching is accompanied with an isotopic effect up to 2.14‰ (Kraemer et al., 2019). The sorption of Cr(VI) onto $\gamma$-$Al_2O_3$ and goethite does not show an isotope effect (Ellis et al., 2004).

### 1.4 Cr isotopes of different terrestrial reservoirs

Distinct Cr isotope signatures of different terrestrial reservoirs reflect various processes occurring in these environments. Qin and Wang (2017) compiled the Cr isotopic compositions of different terrestrial reservoirs (Figure 1.2). Bulk silicate earth (BSE) has a Cr isotope signature of -0.12‰ (Schoenberg et al., 2008). Sedimentary rocks that have undergone oxidative weathering and re-deposition of heavier Cr(VI) tend to have positive $\delta^{53}Cr$ values (i.e. Frei et al., 2009; Crowe et al., 2013). Negative $\delta^{53}Cr$ has been found in some ancient soil profiles (i.e. paleosols) and modern laterites due to Cr loss (i.e. Crowe et al., 2013; Frei and Polat, 2013). Riverine Cr is predominantly Cr(VI) and tends to have positive $\delta^{53}Cr$ values, which reflects oxidative weathering of continental rocks (Cranston and Murray, 1980; Farkaš et al. 2013; Paulukat et al. 2015; D'Arcy et al. 2016; Sun et al., 2019). Seawater $\delta^{53}Cr$ values vary between 0.5‰ to 2‰, which reflects riverine input as the dominant source for oceanic Cr, and also local processes such as Cr reduction and scavenging (i.e. Scheiderich et al., 2015; Goring-Harford et al., 2018; Moos et al., 2020). Groundwater has a wide range of positive Cr isotope signatures (0.7‰ to 5.2‰), which results from Cr reduction (i.e. Ellis et al., 2002; Izbicki et al. 2012; Berna et al. 2010).

### 1.5 Cr isotopes of the global ocean

Recently, there have been more reported seawater Cr isotope data with the advance of seawater Cr analysis techniques. These Cr isotope datasets provide another dimensionality to validate our previous understandings of the global Cr cycling. In the surface, the correlation between [Cr(III)] and net community productivity (NCP) indicates a biological control on Cr

reduction and Cr(III) with an isotopic fractionation of -1.08 ± 0.25 ‰ (Janssen et al., 2020). In the intermediate and deep ocean, the release of Cr from sinking particles produces an isotopic fractionation of -0.66‰, and seems to be related to Cr oxidation by Mn oxides independent from organic carbon respiration (Janssen et al., 2021). Porewater Cr profiles seem to give contrasting implications that sediments could be either a Cr sink or source to the ocean (Shaw et al., 1990; Janssen et al., 2021). In the latter case, the estimated $\delta^{53}$Cr of the benthic source is 0.34 ± 0.25 ‰ (Janssen et al., 2021). An inter-basin difference in $\delta^{53}$Cr is also seen between the deep Atlantic and Pacific, where the deep Pacific is higher in [Cr] with lighter $\delta^{53}$Cr (~4.6 nmol/kg and ~0.7‰) compared to the deep Atlantic (2.8 nmol/kg and 1.1‰) (Goring-Harford et al., 2018; Moos and Boyle, 2019). This is consistent with Cr being a nutrient-like element, and regeneration incubations that show Cr adsorbed onto biogenic particles are lighter (Janssen et al., 2021). The distribution of $\delta^{53}$Cr in the Arctic Ocean and Southern Ocean also implies that mixing is an important process for Cr cycling (Scheiderich et al., 2015; Rickli et al., 2019).

Besides global patterns, oxygen deficient zones (ODZs) provide a unique environment to study the redox processes of Cr. In the hypoxic Atlantic oxygen minimum zone (OMZ) where oxygen level is never below 40 μmol/kg, Cr deficit with heavier isotope signatures up to 1.71 ‰ was observed at minimal oxygen depths (Goring-Harford et al., 2018). Similarly, in the Eastern Tropical North Pacific (ETNP) ODZ where dissolved oxygen is below detection limit, a minor depletion in Cr and slightly heavier $\delta^{53}$Cr was observed (Moos et al., 2020; Huang et al., 2021). In both the ETNP and Eastern Tropical South Pacific (ETSP) ODZs, bottom anoxic water (on the shelf) holds a large Cr deficit with heavier Cr isotopes (Moos et al., 2020; Nasemann et al., 2020). These similar features of Cr in the ODZs indicate Cr reduction that utilizes lighter Cr(VI) preferentially, and subsequent removal of the light Cr(III).

A linear relationship was found between $\delta^{53}$Cr and ln[Cr] globally (Scheiderich et al., 2015). This relationship was consistent with a progressive Rayleigh fractionation model with an apparent Cr isotopic fractionation of -0.8‰. It was proposed to arise from fractionation during the reduction of Cr(VI) in surface waters and oxygen minimum zones, scavenging of isotopically light Cr(III), and subsequent release of this lighter Cr(III) to deeper waters. This hypothesis was supported by recent studies on surface biological controls on Cr(III), deep regeneration of Cr, and Cr isotopes in ODZs. It is worth noting that there are outliers from this relationship observed from the Atlantic OMZ. The outliers are generally above the linear correlation on a low-Cr, high

$\delta^{53}$Cr end. This indicates that some processes related to the continental shelf might exert unique controls on Cr cycling locally.

### 1.6 Cr cycling in oxygen deficient zones

As a redox sensitive trace metal, Cr could potentially be reduced from Cr(VI) to Cr(III) in reducing environments (Figure 1.3). Thermodynamically, the redox potential of Cr(III)-Cr(VI) pair overlaps with some redox pairs that could undergo redox transformations in natural settings (Figure 1.4; Cutter et al., 1997).

As described in 1.5, total dissolved Cr isotopes have been reported in Atlantic OMZ, ETNP ODZ and ETSP ODZ (Goring-Harford et al., 2018; Moos et al., 2020; Nasemann et al., 2020). All these OMZs (ODZs) show total dissolved Cr isotope signatures indicating Cr reduction and subsequent scavenging. This signal is even more pronounced on anoxic continental shelf and in anoxic bottom waters. Two datasets of Cr(III) concentrations have been reported in the ETNP ODZ (Murray et al., 1983; Rue et al., 1997). They show the presence of dissolved Cr(III) in the ODZ, indicating that Cr reduction is occurring in the suboxic/anoxic waters. However, no reliable Cr(III) or Cr(VI) isotope was available prior to this study.

Although Cr reduction is believed to happen in the ODZs, the mechanisms are still unclear. Fe(II) seems to be a potential reducing agent. Kinetic studies show that Cr(VI) reduction by Fe(II) can happen on a timescale of months or less (Sedlak and Chan, 1997; Pettine et al., 1998). The fractionation factor of this reaction was also determined from different Fe(II) materials, varying from -1.8‰ to -3.91‰ (Dossing et al., 2011; Basu and Johnson, 2012; Bauer et al., 2018). Some microbes are also capable of reducing Cr(VI) and could produce an isotopic fractionation of -1.75‰ to -4.11‰ (i.e. Sikora et al., 2008; Zhang et al., 2019). Saito et al. (2020) observed highly abundant nitrite oxidoreductase in the ETNP ODZ, which could be involved in the accidental catalysis of Cr(VI) reduction. Magnetite, organic reductants and hydrogen peroxide could also reduce Cr(VI) with a negative fractionation factor (Ellis et al., 2002; Kitchen et al., 2012; Zink et al., 2010).

### 1.7 Thesis outline

At the outset of my PhD, only a few Cr isotope datasets were published, and all of them were of total dissolved Cr. To better understand the redox cycling of Cr using Cr isotopes, we

developed a seawater Cr(III) and Cr(VI) isotope method which was modified from a total dissolved Cr isotope method (Moos and Boyle, 2019). In chapter 2, we present the procedures of this species-specific Cr isotope method, and investigate the processing conditions and robustness of this method. We also compare the Cr(III) extraction technique used here ($Mg(OH)_2$ co-precipitation) with a Chelex extraction method.

In chapter 3, we apply the Cr(III) and Cr(VI) isotope method to seawater samples in the ETNP ODZ. By doing this, we are able to observe Cr(VI) reduction in the anoxic water column, and determine the associated isotopic fractionation factor. The mechanism of Cr reduction is discussed. We also calculate the amount and isotopic composition of scavenged Cr in this region, and estimate the isotope effect of the scavenging process. Spatial variability of Cr scavenging was also observed.

In chapter 4, the species-specific Cr isotope method is applied to two ETSP ODZ stations. We compare the reduction and scavenging of Cr in this region with that in the ETNP ODZ, and found great similarities. We also analyzed some Arabian Sea ODZ samples for total dissolved Cr, and found similar patterns to the other two ODZs.

In chapter 5, a summary of the thesis and recommendations of future research are presented.

Two side projects are presented in the appendix. The first one is a Cr isotope profile in the Argentine Basin. This measurement is intended to evaluate whether Cr in this region is an anomaly as presented in a published literature (Bonnand et al., 2013). The other one is a shipboard incubation to study Cr(VI) reduction by Fe(II). Seawater spiked with Fe(II) was incubated and analyzed for Cr(III) and total dissolved Cr isotopes. The isotope effect and reaction rate of this reaction are determined.

## Figures and Tables

**Table 1.1 Compilation of the fractionation factors of Cr(VI) reduction adapted from Bauer et al. (2019)**

| Reductant | Fractionation factor (‰) | Reference |
|---|---|---|
| Dissolved and solid phase Fe(II) | -1.8‰ | Bauer et al. (2018) |
| Geothite; siderite; green rust; FeS | -3.91; -2.67; -2.65; -2.11 | Basu and Johnson (2012) |
| Ferrous Fe; 'Green rust' | -3.60; -1.50 | Dossing et al. (2011) |
| Magnetite | -3.51 | Ellis et al. (2002) |
| Low-pH Fe(II); organic reductants | -4.20; -3.11 | Kitchen et al. (2012) |
| *Shewanella oneidensis* bacteria | -4.11; -1.75 | Sikora et al. (2008) |
| Acidic $H_2O_2$; pH-neutral $H_2O_2$ (kinetic) | -3.54; -5.0 | Zink et al. (2010) |

**Figure 1.1 Schematic of the surface chemistry of chromium (adopted from Frei et al., 2009)**

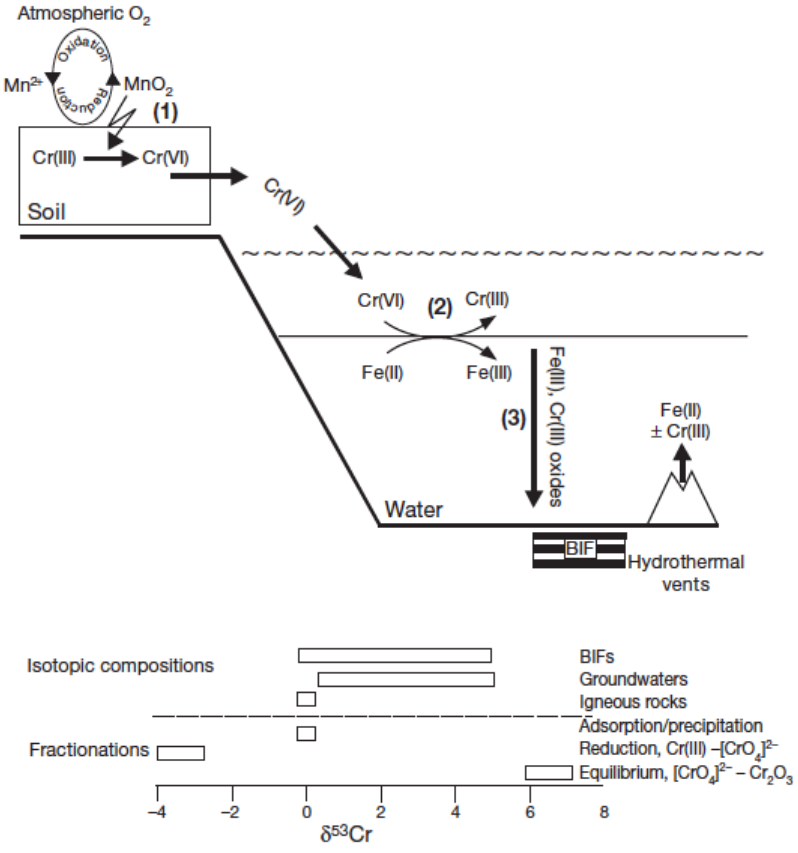

**Figure 1.2 Cr isotopic compositions of different terrestrial reservoirs (adopted from Qin and Wang, 2017)**

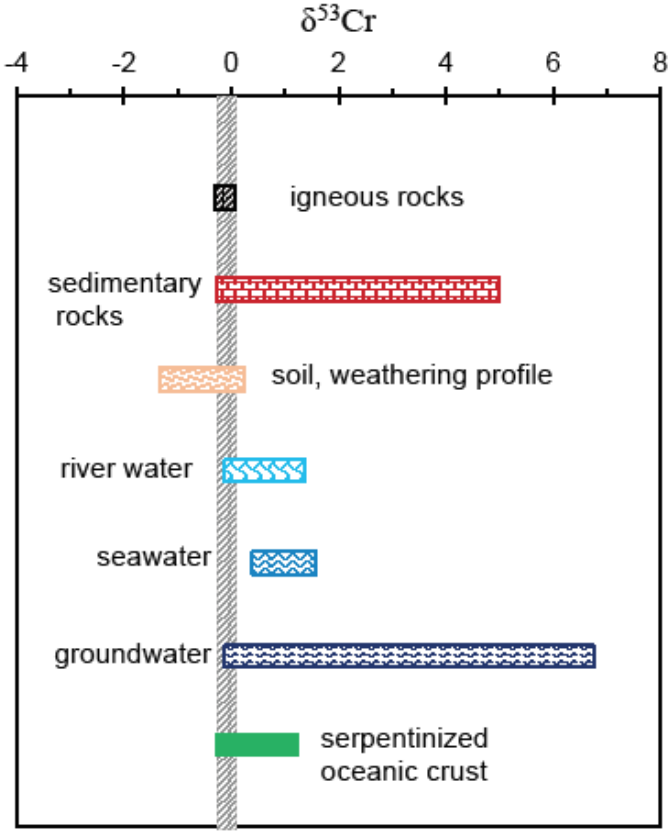

**Figure 1.3 Eh-pH diagram of Cr (adopted from Qin and Wang, 2017)**

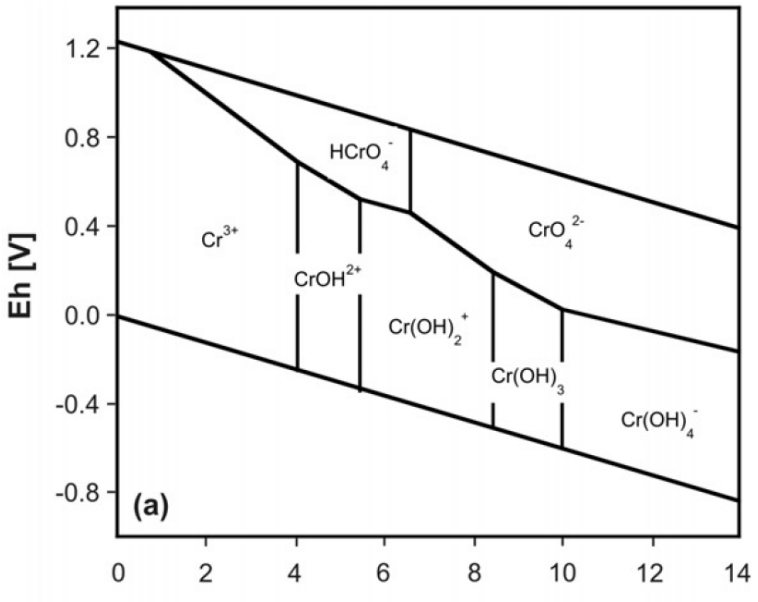


**Figure 1.4 Redox couples and predicted pE ranges for seawater at a pH 7.5 and salinity 35 (Cutter et al., 1997)**

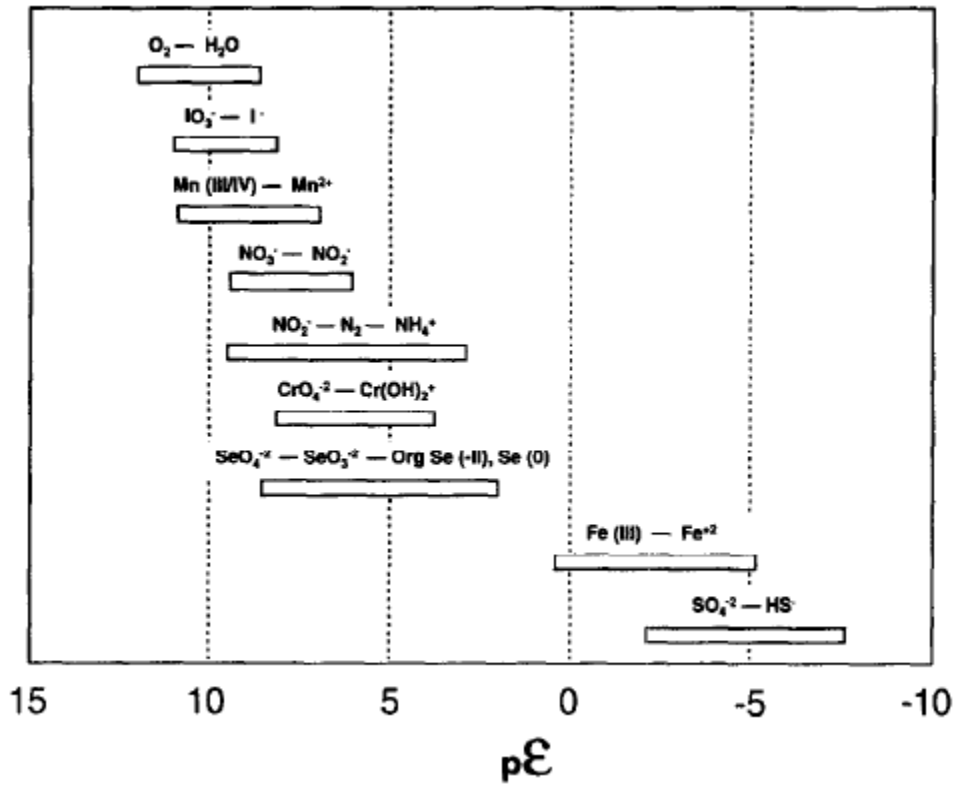

**References**


Achterberg, E. P., & Van Den Berg, C. M. (1997). Chemical speciation of chromium and nickel in the western Mediterranean. *Deep Sea Research Part II: Topical Studies in Oceanography*, *44*(3-4), 693-720.

Bain, D. J., & Bullen, T. D. (2005). Chromium isotope fractionation during oxidation of Cr (III) by manganese oxides. *Geochimica et Cosmochimica Acta Supplement*, *69*(10), A212.

Basu, A., & Johnson, T. M. (2012). Determination of hexavalent chromium reduction using Cr stable isotopes: isotopic fractionation factors for permeable reactive barrier materials. *Environmental science & technology*, *46*(10), 5353-5360.

Bauer, K. W., Gueguen, B., Cole, D. B., Francois, R., Kallmeyer, J., Planavsky, N., & Crowe, S. A. (2018). Chromium isotope fractionation in ferruginous sediments. *Geochimica et Cosmochimica Acta*, *223*, 198-215.

Bauer, K. W., Cole, D. B., Asael, D., Francois, R., Calvert, S. E., Poulton, S. W., ... & Crowe, S. A. (2019). Chromium isotopes in marine hydrothermal sediments. *Chemical Geology*, *529*, 119286.

Berna, E. C., Johnson, T. M., Makdisi, R. S., & Basu, A. (2010). Cr stable isotopes as indicators of Cr (VI) reduction in groundwater: a detailed time-series study of a point-source plume. *Environmental science & technology*, *44*(3), 1043-1048.

Cervantes, C., Campos-García, J., Devars, S., Gutiérrez-Corona, F., Loza-Tavera, H., Torres-Guzmán, J. C., & Moreno-Sánchez, R. (2001). Interactions of chromium with microorganisms and plants. *FEMS microbiology reviews*, *25*(3), 335-347.

Connelly, D. P., Statham, P. J., & Knap, A. H. (2006). Seasonal changes in speciation of dissolved chromium in the surface Sargasso Sea. *Deep Sea Research Part I: Oceanographic Research Papers*, *53*(12), 1975-1988.

Cranston, R. E., & Murray, J. W. (1978). The determination of chromium species in natural waters. *Analytica Chimica Acta*, *99*(2), 275-282.

Cranston, R. E., & Murray, J. W. (1980). Chromium species in the Columbia River and estuary 1. *Limnology and Oceanography*, *25*(6), 1104-1112.

Crowe, S. A., Døssing, L. N., Beukes, N. J., Bau, M., Kruger, S. J., Frei, R., & Canfield, D. E. (2013). Atmospheric oxygenation three billion years ago. *Nature*, *501*(7468), 535-538.

D'Arcy, J., Babechuk, M. G., Døssing, L. N., Gaucher, C., & Frei, R. (2016). Processes controlling the chromium isotopic composition of river water: Constraints from basaltic river catchments. *Geochimica et Cosmochimica Acta*, *186*, 296-315.

Døssing, L. N., Dideriksen, K., Stipp, S. L. S., & Frei, R. (2011). Reduction of hexavalent chromium by ferrous iron: A process of chromium isotope fractionation and its relevance to natural environments. *Chemical Geology*, *285*(1-4), 157-166.

Ellis, A. S., Johnson, T. M., & Bullen, T. D. (2002). Chromium isotopes and the fate of hexavalent chromium in the environment. *Science*, *295*(5562), 2060-2062.

Ellis, A. S., Johnson, T. M., & Bullen, T. D. (2004). Using chromium stable isotope ratios to quantify Cr (VI) reduction: lack of sorption effects. *Environmental science & technology*, *38*(13), 3604-3607.

Farkaš, J., Chrastný, V., Novák, M., Čadkova, E., Pašava, J., Chakrabarti, R., ... & Bullen, T. D. (2013). Chromium isotope variations (δ53/52Cr) in mantle-derived sources and their weathering products: Implications for environmental studies and the evolution of δ53/52Cr in the Earth's mantle over geologic time. *Geochimica et Cosmochimica Acta*, *123*, 74-92.

Fendorf, S. E., & Zasoski, R. J. (1992). Chromium (III) oxidation by. delta.-manganese oxide (MnO2). 1. Characterization. *Environmental Science & Technology*, *26*(1), 79-85.

Frei, R., Gaucher, C., Poulton, S. W., & Canfield, D. E. (2009). Fluctuations in Precambrian atmospheric oxygenation recorded by chromium isotopes. *Nature*, *461*(7261), 250-253.

Frei, R., & Polat, A. (2013). Chromium isotope fractionation during oxidative weathering—implications from the study of a Paleoproterozoic (ca. 1.9 Ga) paleosol, Schreiber Beach, Ontario, Canada. *Precambrian Research*, *224*, 434-453.

Goring-Harford, H. J., Klar, J. K., Pearce, C. R., Connelly, D. P., Achterberg, E. P., & James, R. H. (2018). Behaviour of chromium isotopes in the eastern sub-tropical Atlantic Oxygen Minimum Zone. *Geochimica et Cosmochimica Acta*, *236*, 41-59.

Holden, N. E., Coplen, T. B., Böhlke, J. K., Wieser, M. E., Singleton, G., Walczyk, T., ... & Tarbox, L. V. (2011). IUPAC Periodic Table of the Isotopes. *Chemistry International*, *33*(4).

Huang, T., Moos, S. B., & Boyle, E. A. (2021). Trivalent chromium isotopes in the eastern tropical North Pacific oxygen-deficient zone. *Proceedings of the National Academy of Sciences, 118*(8).

Izbicki, J. A., Bullen, T. D., Martin, P., & Schroth, B. (2012). Delta Chromium-53/52 isotopic composition of native and contaminated groundwater, Mojave Desert, USA. *Applied geochemistry*, *27*(4), 841-853.

Janssen, D. J., Rickli, J., Quay, P. D., White, A. E., Nasemann, P., & Jaccard, S. L. (2020). Biological control of chromium redox and stable isotope composition in the surface ocean. *Global biogeochemical cycles*, *34*(1), e2019GB006397.

Janssen, D. J., Rickli, J., Abbott, A. N., Ellwood, M. J., Twining, B. S., Ohnemus, D. C., ... & Jaccard, S. L. (2021). Release from biogenic particles, benthic fluxes, and deep water circulation control Cr and δ 53 Cr distributions in the ocean interior.

Jeandel, C., & Minster, J. F. (1987). Chromium behavior in the ocean: Global versus regional processes. *Global Biogeochemical Cycles, 1*(2), 131-154.

Kieber, R. J., & Helz, G. R. (1992). Indirect photoreduction of aqueous chromium (VI). *Environmental science & technology*, *26*(2), 307-312.

Kitchen, J. W., Johnson, T. M., Bullen, T. D., Zhu, J., & Raddatz, A. (2012). Chromium isotope fractionation factors for reduction of Cr (VI) by aqueous Fe (II) and organic molecules. *Geochimica et Cosmochimica Acta*, *89*, 190-201.

Kraemer, D., Frei, R., Viehmann, S., & Bau, M. (2019). Mobilization and isotope fractionation of chromium during water-rock interaction in presence of siderophores. *Applied Geochemistry*, *102*, 44-54.

McClain, C. N., & Maher, K. (2016). Chromium fluxes and speciation in ultramafic catchments and global rivers. *Chemical Geology*, *426*, 135-157.

Moos, S. B., & Boyle, E. A. (2019). Determination of accurate and precise chromium isotope ratios in seawater samples by MC-ICP-MS illustrated by analysis of SAFe Station in the North Pacific Ocean. *Chemical Geology*, *511*, 481-493.

Moos, S. B., Boyle, E. A., Altabet, M. A., & Bourbonnais, A. (2020). Investigating the cycling of chromium in the oxygen deficient waters of the Eastern Tropical North Pacific Ocean and the Santa Barbara Basin using stable isotopes. *Marine Chemistry*, *221*, 103756.

Murray, J. W., Spell, B., & Paul, B. (1983). The contrasting geochemistry of manganese and chromium in the eastern tropical Pacific Ocean. In *Trace metals in sea water* (pp. 643-669). Springer, Boston, MA.

Nasemann, P., Janssen, D. J., Rickli, J., Grasse, P., Frank, M., & Jaccard, S. L. (2020). Chromium reduction and associated stable isotope fractionation restricted to anoxic shelf waters in the Peruvian Oxygen Minimum Zone. *Geochimica et cosmochimica acta*, *285*, 207-224.

Paulukat, C., Døssing, L. N., Mondal, S. K., Voegelin, A. R., & Frei, R. (2015). Oxidative release of chromium from Archean ultramafic rocks, its transport and environmental impact–A Cr isotope perspective on the Sukinda valley ore district (Orissa, India). *Applied Geochemistry*, *59*, 125-138.

Pettine, M., D'ottone, L., Campanella, L., Millero, F. J., & Passino, R. (1998). The reduction of chromium (VI) by iron (II) in aqueous solutions. *Geochimica et cosmochimica acta*, *62*(9), 1509-1519.

Pöppelmeier, F., Janssen, D. J., Jaccard, S. L., & Stocker, T. F. (2021). Modeling the marine chromium cycle: New constraints on global-scale processes. *Biogeosciences Discussions*, 1-26.

Qin, L., & Wang, X. (2017). Chromium isotope geochemistry. *Reviews in Mineralogy and Geochemistry*, *82*(1), 379-414.

Rickli, J., Janssen, D. J., Hassler, C., Ellwood, M. J., & Jaccard, S. L. (2019). Chromium biogeochemistry and stable isotope distribution in the Southern Ocean. *Geochimica et cosmochimica acta, 262*, 188-206.

Rue, E. L., Smith, G. J., Cutter, G. A., & Bruland, K. W. (1997). The response of trace element redox couples to suboxic conditions in the water column. *Deep Sea Research Part I: Oceanographic Research Papers*, *44*(1), 113-134.

Saad, E. M., Wang, X., Planavsky, N. J., Reinhard, C. T., & Tang, Y. (2017). Redox-independent chromium isotope fractionation induced by ligand-promoted dissolution. *Nature communications*, *8*(1), 1-10.

Saito, M. A., McIlvin, M. R., Moran, D. M., Santoro, A. E., Dupont, C. L., Rafter, P. A., ... & Waterbury, J. B. (2020). Abundant nitrite-oxidizing metalloenzymes in the mesopelagic zone of the tropical Pacific Ocean. *Nature Geoscience*, *13*(5), 355-362.

Sander, S., & Koschinsky, A. (2000). Onboard-ship redox speciation of chromium in diffuse hydrothermal fluids from the North Fiji Basin. *Marine Chemistry*, *71*(1-2), 83-102.

Schauble, E., Rossman, G. R., & Taylor Jr, H. P. (2004). Theoretical estimates of equilibrium chromium-isotope fractionations. *Chemical Geology*, *205*(1-2), 99-114.

Scheiderich, K., Amini, M., Holmden, C., & Francois, R. (2015). Global variability of chromium isotopes in seawater demonstrated by Pacific, Atlantic, and Arctic Ocean samples. *Earth and Planetary Science Letters, 423*, 87-97.

Schoenberg, R., Zink, S., Staubwasser, M., & von Blanckenburg, F. (2008). The stable Cr isotope inventory of solid Earth reservoirs determined by double spike MC-ICP-MS. *Chemical Geology*, *249*(3-4), 294-306.

Sedlak, D. L., & Chan, P. G. (1997). Reduction of hexavalent chromium by ferrous iron. *Geochimica et Cosmochimica Acta*, *61*(11), 2185-2192.

Semeniuk, D. M., Maldonado, M. T., & Jaccard, S. L. (2016). Chromium uptake and adsorption in marine phytoplankton–Implications for the marine chromium cycle. *Geochimica et Cosmochimica Acta*, *184*, 41-54.

Shaw, T. J., Gieskes, J. M., & Jahnke, R. A. (1990). Early diagenesis in differing depositional environments: the response of transition metals in pore water. *Geochimica et Cosmochimica Acta*, *54*(5), 1233-1246.

Shields, W. R., Murphy, T. J., Catanzaro, E. J., & Garner, E. L. (1966). Absolute isotopic abundance ratios and the atomic weight of a reference sample of chromium. *Journal of research of the National Bureau of Standards. Section A, Physics and chemistry*, *70*(2), 193.

Sikora, E. R., Johnson, T. M., & Bullen, T. D. (2008). Microbial mass-dependent fractionation of chromium isotopes. *Geochimica et Cosmochimica Acta*, *72*(15), 3631-3641.

Stumm, W., & Morgan, J. J. (2012). *Aquatic chemistry: chemical equilibria and rates in natural waters* (Vol. 126). John Wiley & Sons.

Sun, Z., Wang, X., & Planavsky, N. (2019). Cr isotope systematics in the Connecticut River estuary. *Chemical Geology*, *506*, 29-39.

Wang, X., Johnson, T. M., & Ellis, A. S. (2015). Equilibrium isotopic fractionation and isotopic exchange kinetics between Cr (III) and Cr (VI). *Geochimica et Cosmochimica Acta*, *153*, 72-90.

Zhang, Q., Amor, K., Galer, S. J., Thompson, I., & Porcelli, D. (2019). Using stable isotope fractionation factors to identify Cr (VI) reduction pathways: Metal-mineral-microbe interactions. *Water research*, *151*, 98-109.

Zink, S., Schoenberg, R., & Staubwasser, M. (2010). Isotopic fractionation and reaction kinetics between Cr (III) and Cr (VI) in aqueous media. *Geochimica et Cosmochimica Acta*, *74*(20), 5729-5745.

# Chapter 2 Methods: Isotope analysis of different chromium redox species

## 2.1 Introduction

As a redox sensitive element, chromium (Cr) and its isotopes have been measured in different environments (eg. groundwater, sediments, seawater) to investigate related redox processes and the associated isotope effect. Cr isotopes are usually reported in a delta notation by convention, which is defined by:

$$\delta^{53}Cr = [\frac{(^{53}Cr\ /\ ^{52}Cr)_{sample}}{(^{53}Cr\ /\ ^{52}Cr)_{standard}} - 1] \times 1000\ ‰,$$

where the $(^{53}Cr/^{52}Cr)_{sample}$ and $(^{53}Cr/^{52}Cr)_{standard}$ denote the $^{53}Cr/^{52}Cr$ ratio in a sample and a standard, respectively. The Cr standard used in this thesis is NIST SRM 979.

The earliest studies on Cr isotopes are in cosmochemistry to investigate early solar system processes (i.e. Rotaru et al., 1992). More recently, this system has been used to study groundwater processes and the redox evolution of Earth's early ocean-atmosphere system (Ellis et al., 2002 and 2004; Schoenberg et al., 2008; Frei et al., 2009). They demonstrated a promising use of Cr isotopes to track redox processes both in modern and ancient times. This inspired more research to measure Cr isotopes in diverse environments, such as marine sediments (Bruggmann et al., 2019), rocks (Crowe et al., 2013; Frei et al., 2014; Wang et al., 2016), rivers (D'Arcy et al., 2016; Farkaš et al., 2013; Frei et al., 2014; Paulukat et al., 2015; Wu et al., 2017; Sun et al., 2019) and the ocean (Bonnand et al., 2013; Scheiderich et al., 2015; Goring-Harford et al., 2018; Moos and Boyle, 2018; Rickli et al., 2019; Janssen et al., 2020; Nasemann et al., 2020; Moos et al., 2020).

These studies developed analytical methods to purify samples with multi-step chromatography, and determine stable Cr isotope ratios by thermal ionization mass spectrometry (TIMS) or multi-collector inductively-coupled-plasma mass spectrometry (MC-ICP-MS). A double-spike of $^{50}Cr$-$^{54}Cr$ is used to correct for any isotopic fractionation occurring during sample processing and mass spectrometry analysis. Compared with the sample bracketing technique, the double spike technique does not require a quantitative recovery for the element of the interest. Unlike rock or sediment samples where the Cr content is usually high enough for isotope

analyses, seawater samples with nanomolar level of Cr (1-5 nmol/kg) face an extra challenge with pre-concentration. Iron co-precipitation and $Mg(OH)_2$ co-precipitation have shown their robustness as pre-concentration methods (Moos and Boyle, 2018; Bonnand et al., 2013).

However, because of the redox properties of Cr and significant amounts of reduced Cr (Cr(III)) found in reducing waters (Murray et al., 1983; Rue et al., 1997; Cranston and Murray, 1978), it is crucial to develop a method to determine the isotopic composition of different Cr redox species (i.e. Cr(III) and Cr(VI)), which can foster our understanding of the isotopic fractionation associated with Cr redox processes. The key to this method would be to extract Cr(III) while excluding Cr(VI). It is theoretically viable because Cr(III) is a cation while Cr(VI) is an oxyanion. So far there have been only three papers reporting Cr(III) isotopes with two Cr extraction methods. Between the two methods, $Mg(OH)_2$ co-precipitation (Semeniuk et al., 2016; Janssen et al., 2020; Davidson et al., 2020) seems to be more robust than Chelex extraction (Rue et al., 1997; Wang et al., 2019).

In this chapter, we will report a $Mg(OH)_2$ co-precipitation technique as a Cr(III) extraction method similar to that in Davidson et al., (2020) with a different procedure and more thorough investigations into its robustness. We will discuss the optimal conditions of $Mg(OH)_2$ co-precipitation for Cr(III) extraction (i.e. equilibration time after double spike addition), and compare the results from frozen samples and those processed at sea. We will also discuss the uncertainties of the Cr(III) and Cr(VI) isotope data. A Chelex-extracted Cr(III) profile in the Eastern Tropical North Pacific will also be presented to investigate the possible reasons for the discrepancy between Cr(III) data acquired from $Mg(OH)_2$ co-precipitation and Chelex.

## 2.2 Methods

### 2.2.1 Chemical and Materials

#### 2.2.1.1 Reagents

Samples were handled under clean conditions (i.e. class 100 clean laminar flow benches, positive-pressure clean labs with recirculating fume hoods. High purity water was deionized, run through an ultrapure cartridge and then distilled in a borosilicate glass still (Barnstead Mega-Pure). All acids were either quadruply-distilled in Vycor glass to remove contaminants, or purchased as high purity acids (Optima™). Reagent grade ammonium hydroxide ($NH_3 \cdot H_2O$) was purified via isothermal distillation three times (i.e. vapor phase transfer of ammonia from a

concentrated 16 M solution into distilled water). Blanks for acids and ammonium hydroxide were both checked for each batch before use on a quadrupole ICP-MS (PlasmaQuand2+).

Hydrogen peroxide ($H_2O_2$, Suprapur. 30% (v/v)) was purchased from Merck KGaA. It was stored in a dark cold room to minimize decomposing. Ammonium persulfate (APS) salt was purchased from Sigma-Aldrich (BioXtra, 98.0%). Its solution was freshly prepared before each use.

The anion exchange resin AG 1-X8 (200 - 400 mesh size, chloride form) was purchased from Eichrom. It was cleaned with methanol (1 hour), 1 M NaOH (1 hour), 1 M HCl (2-3 days), and another 1 M HCl (2-3 days) with 3-5 times of distilled water rinses between each cleaning. Chelex-100 resin was purchased from Bio-Rad. Clean Chelex-100 resin was converted to ammonium form with ammonium hydroxide, with several distilled water rinses until the pH of the effluent was lower than 9.

PFA teflon vials (Savillex) and high density polyethylene (HDPE) bottles were leached with 1M HCl (reagent grade) in a 60°C oven overnight, followed by 0.06M HCl (high purity) in the 60°C oven overnight. 12mL chromatographic columns (HDPE) and 2mL mini columns (hand-made from heat-shrink tubing) were leached in 1M HCl in the 60°C oven overnight, followed by several distilled water rinses before each use.

Low Trace Metal Seawater (LTMSW) was made by filtering $Mg(OH)_2$-precipitated seawater with cleaned 0.2μm Nuclepore filter membranes. The precipitation step was used to co-precipitate and remove the original trace metal in the seawater. The LTMSW was then acidified to pH ~8 with concentrated HCl for method tests.

#### 2.2.1.2 Standards

All standards were double-bagged and kept in a glass jar with a small amount of water to minimize evaporation and changes in concentration.

The Cr isotopic standard reference material, SRM 979, was acquired from the National Institute of Standards and Technology (NIST) in the form of a hydrated chromium (III) nitrate, $Cr(NO_3)_3 \cdot 9H_2O$. This chromium salt was dissolved in 2% (v/v) $HNO_3$. The absolute isotopic abundance ratios for SRM 979 were established by Shields et al. (1966).

The $^{50}Cr$-$^{54}Cr$ double spike was prepared from $^{50}Cr$ and $^{54}Cr$ enriched metal powders. The details of the preparation process are described in Moos and Boyle (2019). The Cr of the double

spike is in the form of Cr(III) in 2% $HNO_3$.The isotopic composition of the final double spike solution is: 57.65% $^{50}$Cr, 0.14% $^{52}$Cr, 0.10% $^{53}$Cr, and 42.10% $^{54}$Cr, according to optimal composition calculation (Rudge et al., 2009). The double spike was cleaned with the third column of the sample purification procedure (see 2.2.2.1) to remove traces of Fe.

### 2.2.2 Procedures for total dissolved Cr isotope analysis

#### 2.2.2.1 Pre-concentration and chromatography

The total dissolved Cr isotope analysis procedure was described in detail in Moos and Boyle (2019). Briefly, seawater samples were acidified with concentrated HCl to pH ~1.9 after being shipped back to MIT. Lowering the pH reduces Cr(VI) to Cr(III). To accelerate this process, samples were put in a 60°C oven for 7 to 14 days. After that, a $^{50}$Cr-$^{54}$Cr double spike was added to samples (0.5~1L) in 1 L separatory funnels with a roughly 1:1 double spike/sample Cr ratio. This mixture was put on a shaker table overnight for sample Cr(III) and double spike Cr(III) to reach equilibrium. Cr was then pre-concentrated using a $Mg(OH)_2$ co-precipitation method by adding concentrated $NH_3 \cdot H_2O$. Once white precipitates were observed, the funnels would be kept upright overnight, allowing the precipitates to grow and settle by gravity. The precipitates were collected into 50mL centrifuge tubes three times. After centrifuging and siphoning, the precipitates were dissolved in HCl. The pH of the solution was adjusted to reach a $[H^+]$ of 0.02M for the next step.

A three-step chromatography was conducted to remove all of the matrix and isobaric ions. All three chromatography columns use AG1X8 anion exchange resin. The first column is designed to remove major seawater matrix cations. This is done by oxidizing sample Cr(III) to Cr(VI) with ammonium persulfate (APS, $(NH_4)_2S_2O_8$) (1h, 110°C) before loading it onto the first column, and reducing it back to Cr(III) by 2M $HNO_3$ + 2% (v/v) $H_2O_2$ while it is adsorbed on the resin, which would release Cr(III) from the resin. The second column is aimed at removing polyatomic sulfur interferences, which comes from both the seawater itself and the degradation from the APS in the previous step. This is a crucial step because $^{32}S^{16}O^1H^+$ at mass 49 is an isobaric interference for $^{49}$Ti, which would be used to correct for $^{50}$Ti on $^{50}$Cr. The third mini-column was to remove traces of Fe. This is achieved by dissolving the dried-down samples in 6M HCl. In the strong acidic medium, Fe would complex with $Cl^-$ to form $FeCl_4^-$, which has a high affinity to the anion exchange resin, whereas Cr(III) would pass through. After the second

and the third column, dried-down samples were digested with aqua regia to decompose resin residues. The final samples would be dissolved in 2% (v/v) $HNO_3$ and ready for MC-ICP-MS analysis.

#### 2.2.2.2 MC-ICP-MS analysis

All Cr isotope measurements were made on an IsoProbe MC-ICP-MS. The Cr isotope analytical method used in this thesis was developed by Moos and Boyle (2019). Typical operating conditions are listed in Table 2.1.

Briefly, a 'peak-jump' mode was applied in the Cr isotope analysis on IsoProbe MC-ICP-MS. Each sample run includes ten cycles; each cycle includes three sequences with an axial mass jump in the third sequence. Faraday cup configurations and other conditions for each sequence is listed in Table 2.2 (adapted from Table 2 in Moos and Boyle, 2019). Sequence 2, a shorter version of sequence 1, was used to correct $^{56}Fe$ in sequence 3 for any effect induced by a shorter recording time (2s). The corrected $^{56}Fe$ and other raw data recorded in sequence 1 was then used in data reduction.

Mass spectrometry is specially tuned for polyatomic sulfur interferences (i.e. $^{32}S^{16}O^{1}H^{+}$ on mass 49, $^{34}S^{16}O^{+}$ on mass 50, $^{34}S^{16}O^{1}H^{+}$ on mass 51). An APS (100mM) + Cr SRM (1μM) mixture was used for fine-tuning to minimize the mass 49 to mass 52 ratio. This tuning step could significantly lower the polyatomic sulfur interferences.

Each sample was bracketed by two SRM-DS mixtures with the same sample Cr to DS ratio and similar signal level (within 10%). Offsets in $\delta^{53}Cr_{SRM}$ were observed for different SRM to DS ratios in SRM-DS mixtures (see 2.3.2). Therefore, it is necessary to match this ratio between samples and their bracketing standards.

The $\delta^{53}Cr$ data was calculated by iteration on each isotope correction and instrumental mass fractionation ($\beta$) in an Excel spreadsheet (Moos and Boyle, 2019). The [Cr] concentration was calculated by averaging the results from the single isotope dilution formula using corrected $^{50}Cr$ and $^{54}Cr$:

$$C_{sample} = \frac{f_{spike}}{f_{natural}} \times C_{spike} \times \left(\frac{V_{spike}}{V_{sample}}\right) \times \left(\frac{R_{true,\,sample} - R_{true,\,spike}}{R_{natural} - R_{true,\,sample}}\right)$$

$C_{sample}$: the Cr concentration of the sample,

$f_{spike}$: the fraction of $^{50}Cr$ (or $^{54}Cr$) in the double spike,

$f_{natural}$: the fraction of $^{50}Cr$ (or $^{54}Cr$) in Cr with natural isotopic abundances,

$C_{spike}$: the Cr concentration of the spike,

$V_{spike}$: the spike volume,

$V_{sample}$: the sample volume,

$R_{true,\ sample}$: the measured $^{52}Cr/^{50}Cr$ (or $^{52}Cr/^{54}Cr$) ratio of the sample-spike mixture after all corrections,

$R_{true,\ spike}$: the measured $^{52}/^{50}Cr$ (or $^{52}Cr/^{54}Cr$) ratio of the double spike after all corrections,

$R_{natural}$: the $^{52}Cr/^{50}Cr$ (or $^{52}Cr/^{54}Cr$) ratio of Cr with natural isotopic abundances.

The recovery was calculated from the $^{54}Cr$ signals of the bracketing SRM-DS and the sample-DS mixtures.

### 2.2.3 Procedures for Cr(III) and Cr(VI) isotope analysis

#### 2.2.3.1 Cr(III) isotope analysis

The Cr(III) isotope method is largely the total dissolved Cr method without sample acidification, so that Cr(VI) would not be converted to Cr(III) or be pre-concentrated. Although the basic premise of the Cr(III) method is simple, there are some details that need to be tested to obtain accurate Cr(III) isotope data.

Cr(III) isotope analysis was conducted on both freshly collected samples processed at sea and frozen samples. Samples were processed in a clean van on research vessels. Filtered seawater samples were transferred into 1L separatory funnels and spiked with ~2nmol double spike within hours of sampling from Niskin bottles. Sample-double spike equilibration was allowed for 0.5 - 12 hours (see 2.3.4) before adding ammonium hydroxide to induce $Mg(OH)_2$ precipitation. Funnels were kept upright in the clean van for the precipitates to settle by gravity. Three aliquots of 50mL precipitates with seawater were collected in 50mL centrifuge tubes. The precipitates for each sample were dissolved in HCl and combined in the lab. From this step on, the procedure would be the same as that for total dissolved Cr analysis.

Frozen samples were stored in either -80°C or -20°C freezers on ship and in the lab to preserve Cr redox species. Samples were taken out from the freezers to thaw at room temperature on a shaker table, minimizing the time for thawing. Immediately after complete thawing, 2 nmol of the double spike was added into the sample bottles. They were placed on a shaker table for the sample Cr(III) and double spike Cr(III) to equilibrate for 0.5 to 12 hours. Then the spiked

seawater samples were transferred to 1L separatory funnels, and proper amounts of ammonium hydroxide were added. Precipitates are collected on the next day. Subsequent steps are the same as that for the total dissolved Cr analysis.

#### 2.2.3.2 Cr(VI) isotope analysis

Cr(VI) isotope ratios were measured from seawater samples where their Cr(III) had been extracted by $Mg(OH)_2$ co-precipitation. The Cr(III)-extracted seawater samples were filtered through clean 0.4μm Nuclepore® filter membranes to remove any $Mg(OH)_2$ precipitate. They were then acidified with concentrated HCl to pH 1.9. Putting them in a 60°C oven for 14 days accelerates the reduction of Cr(VI) to Cr(III). They can then be treated as acidified seawater following the same procedure as that for the total dissolved Cr analysis.

### 2.2.4 Cr(III) extraction by Chelex-100 resin

To compare different Cr(III) extraction methods, Simone Moos extracted Cr(III) from eight samples collected from cruise NH1410 station 13F using chelex-100 resin (Figure 2.1). The data will be compared to two nearby stations - one at P2 and the other in Rue et al. (1997). $Mg(OH)_2$ co-precipitation was applied to samples from P2, whereas Chelex resin as a Cr(III) extraction technique was applied by Rue et al. (1997). We followed the Chelex procedure described in Rue et al. (1997). 5g Chelex-100 resin was added to 2L unacidified seawater samples at natural pH at sea. The resin was collected on a filter back in the lab in a month and digested overnight with 7.5M $HNO_3$ with two additional $H_2O$ rinses. Double spike was added to this Cr(III) solution. The filtrate was acidified to pH 2 and sat for years before Cr(VI) analysis. Both the extracted Cr(III) and Cr(VI) were then purified and analyzed on an IsoProbe MC-ICP-MS as described in Moos and Boyle, 2019.

## 2.3 Results and discussions

### 2.3.1 Blanks and reproducibility

One quality control seawater sample from the surface Atlantic Ocean has been measured repeatedly with each batch of samples since November, 2017. The external reproducibility of $\delta^{53}Cr$ and [Cr] is 1.02 ± 0.12‰ (2SD, n=25) and 3.21 ± 0.12 (SD, n=25), respectively. The external reproducibility of low-Cr (i.e. Cr(III) or Cr(VI)) analysis was also determined using the

same quality control seawater with a sample Cr to double ratio of 0.3. The resulting reproducibility of $\delta^{53}$Cr and [Cr] is 1.10 ± 0.25‰ (2SD, n=5) and 3.24 ± 0.04 nmol/kg (SD, n=5), respectively. The higher uncertainty of the $\delta^{53}$Cr of the low-Cr quality control sample is due to lower signal levels on masses 52 and 53. In this case, the signal level at mass 53 is lower than 0.1 volt.

Procedural Cr blanks were on the order of 0.02 nmol, which is comparable to that in Moos and Boyle (2019). Considering a typical Cr amount for total dissolved Cr analysis (2 nmol), the blank is negligible. Therefore, Cr data of total dissolved Cr was not corrected for blank. As for Cr(III) and Cr(VI) analysis, the Cr amount in the analyte varies from 0.44 to 1.66 nmol. The blank accounts for less than 5% of sample Cr. Therefore, no correction for Cr(III) or Cr(VI) was performed.

However, the Cr blank of the chelex extraction is 0.47 ± 0.02 nmol (SD, n=2), with the resin blank $\delta^{53}$Cr averaging at 1.37 ± 0.21‰ (2SD, n=2). This blank contributes to 41~235% of the sample Cr. Therefore, Chelex extracted Cr(III) data was corrected for procedural blank by mass balance.

**2.3.2 Varying SRM to DS ratios in the SRM-DS standard mixtures**

Each sample was bracketed by two SRM-DS standard mixtures when analyzed on MC-ICP-MS. The sample $\delta^{53}$Cr was reported as a relative value to the bracketing SRM-DS standard mixtures. The optimal ratio of Cr/DS in the sample-DS (or SRM-DS) mixtures is 1:1 to minimize error propagation in double spike technique data reduction (Rudge et al., 2009). For total dissolved Cr analysis, the optimal ratio can be easily achieved. However, for Cr(III) and Cr(VI) isotope analysis, the natural abundance could be too low to reach this ratio. Therefore, we ran SRM-DS standard mixtures of varying SRM/DS ratios (from 0.25 to 1.5, Table 2.3) bracketed by SRM-DS mixtures with a 1:1 ratio to test whether there are offsets among different SRM/DS ratios. This test is designed to evaluate to what extent the bracketing SRM/DS ratio needs to match its sample/DS ratio. The measurements show that when the SRM/DS ratio ranges from 0.75 to 1.50, the $\delta^{53}Cr_{SRM}$ (-0.02±0.06‰, n=3, 2SD) is within the error of a 1:1 SRM-DS mixture. However, as the SRM/DS decreases from 0.50 to 0.25, the $\delta^{53}Cr_{SRM}$ leans toward negative values with larger errors (Figure 2.2). Similar observations were also reported in Schoenberg et al. (2008) and Moos and Boyle (2019). Therefore, it is necessary to match the

Cr/DS ratio of the sample and its bracketing SRM-DS mixtures when sample/DS ratio is lower than 0.75.

### 2.3.3 The recovery of co-precipitation in the Cr(III) method

$^{53}$Cr(III)-spiked neutral low trace metal seawater (LTMSW) was used to test the recovery of co-precipitation in the Cr(III) method. The equilibration time between $^{53}$Cr(III) addition and co-precipitation in this test was similar to that used for seawater samples (several hours). The precipitates in this test were dissolved in 2% $HNO_3$ without further column chromatography, and measured on a quadrupole ICP-MS (PlasmaQuand2+). The co-precipitation recovery for Cr(III) calculated by single isotope dilution is 99±12% (SD, N=3). It shows that $Mg(OH)_2$ co-precipitation can quantitatively recover Cr(III) from neutral seawater without Cr(III) loss to container walls.

### 2.3.4 The effect of varying equilibration time

The equilibration time discussed in this section is defined as the time interval between double spike addition and the initiation of co-precipitation by ammonium hydroxide. For total dissolved Cr isotope analysis, one-day equilibration time was adequate for the Cr(III) in the sample and that in the DS to equilibrate at pH ~2 (Table 2.4). However, cautions need to be considered when both Cr(III) and Cr(VI) are present in anoxic samples at pH ~8. In 2.3.3, we have demonstrated that within hours of Cr(III) spike addition, Cr(III) can be recovered quantitatively by co-precipitation. However, it still remains unknown whether redox transformations would occur between Cr(III) and Cr(VI) during the sample-DS equilibration time under oxic conditions. Therefore, the goal of this section is to find a proper range of equilibration time, which is long enough for sample Cr(III) and DS Cr(III) to reach equilibrium, whereas short enough to avoid Cr redox transformations.

To find a proper equilibration time window, one seawater sample in the ETNP ODZ (P2, 200m) was analyzed in four splits for Cr(III) isotopes with varying equilibration time (0.5, 4, 8 and 12 hours). The average overall recovery of the four splits is 67±2% (n=4, SD) (Table 2.5 and Figure 2.3). And the average overall recovery for all Cr(III) isotope analyses is 61±11% (N=49, SD), which is comparable to the total dissolved Cr method (65%, Moos and Boyle. 2019). The averages of the [Cr(III)] and $\delta^{53}$Cr(III) of the four splits are 1.67±0.12 nmol/kg (n=4, SD) and

0.20±0.09‰ (n=4, SD), respectively. The consistent recovery of the four splits and the similar recovery to total Cr method demonstrates no Cr(III) loss at natural seawater pH within 12 hours. The consistent recovery, [Cr(III)] and $\delta^{53}$Cr(III) data of the four splits also indicates no redox transformations occurring within 12 hours.

### 2.3.5 Frozen samples vs. Shipboard Cr(III) extraction

[Cr(III)] and $\delta^{53}$Cr(III) data of three depths at station P2 (RR1805) were acquired from freshly collected samples processed at sea and frozen ones (Table 2.6 and Figure 2.4). Both [Cr(III)] and $\delta^{53}$Cr(III) data from shipboard processed and frozen samples agree with each other. It shows that frozen samples can preserve Cr redox species effectively. This is not consistent with a previous study showing that Cr(VI) and total dissolved Cr is lower, whereas Cr(III) is higher in frozen samples than shipboard-processed samples using catalytic cathodic stripping voltammetry (Boussemart et al., 1992). Compiling all Cr(III) analyses done in both ways, we find the recovery of shipboard-processed and frozen samples are 57±9% (n=10, SD) and 63±11% (n=39, SD), respectively. This shows that freezing seawater does not lead to lower recovery, which means no loss of Cr(III) in frozen samples. The discrepancy between the two studies might result from different methods used (CSV vs. $Mg(OH)_2$ co-precipitation), different reducing conditions of the seawater used (oxic vs. anoxic) and thus different Cr redox species compositions and properties (i.e. the amount of Cr(III) and organically-complexed Cr(III)). However, the exact explanation for this discrepancy is still unclear.

### 2.3.6 Calculated vs. measured Cr(VI) isotope data at station P2

Seven samples at station P2 were analyzed and calculated for Cr(VI) concentration and isotopic composition (Table 2.7 and Figure 2.5). Calculations were done using total dissolved Cr and Cr(III) data assuming mass balance. The uncertainties of the calculated Cr(VI) data were propagated from that of the total dissolved Cr and Cr(III) data of the same sample. Calculated Cr(VI) data has relatively large propagated error (2SD: 0.29‰ to 1.22‰) depending on Cr(VI) concentrations.

The measured Cr(VI) also has lower recovery (41±11%, SD, n=11) than that of the Cr(III) and total dissolved Cr. This might result from Cr loss to container walls in basic media because of the difficulty in nucleating precipitates after previous precipitation for Cr(III)

analysis. The measured Cr(VI) has an average internal error of 0.12±0.07‰ (SD, n=11). This average internal error is higher than that of the $\delta^{53}$Cr(III) (0.07±0.03‰, SD, n=49). A negative correlation was observed between the measured Cr(VI) internal standard error and the sample Cr amount (Figure 2.6). The correlation is reasonable - as less Cr is present in the sample, the noise/signal level would be larger, which leads to higher internal error for $\delta^{53}$Cr(VI) measurements.

### 2.3.7 Comparison between $Mg(OH)_2$ co-precipitation and Chelex extraction

Figure 2.7 shows the [Cr(III)] and [Cr(VI)] profiles at station 13F and in Rue et al. (1997), which agree with each other. Consistent Cr profiles between 13F and in Rue et al. (1997), and between 2T and P2 (Moos et al., 2020) show that spatial variability for stations in the same proximity of the coast is negligible. Therefore, it is legitimate to compare Cr profiles among the four stations.

Figures 2.8 and 2.9 show the Cr concentration and isotopic composition of different Cr species at 13F and P2 using two Cr(III) extraction methods. Chelex extraction yields 1/2 to 1/3 of the Cr(III) extracted by $Mg(OH)_2$ co-precipitation. However, the chelex extracted Cr(III) has almost the identical $\delta^{53}$Cr as that extracted by $Mg(OH)_2$ co-precipitation. The Cr(VI) from the filtrate of the chelex extracted seawater is higher in concentration, but lighter in isotopes than that by $Mg(OH)_2$ co-precipitation. Despite these differences, the total dissolved Cr concentration and isotope profiles at 13F calculated by mass balance is identical to those measured at P2.

As we have shown previously, $Mg(OH)_2$ co-precipitation can extract Cr(III) quantitatively. In contrast, chelex is only able to extract a fraction of the Cr(III) present in anoxic seawater. We hypothesize that the Cr(III) fraction not seen by chelex might be organically bound Cr(III). These Cr(III) complexes may be thermodynamically stronger than Chelex-Cr(III) complexes, or have such slow dissociation kinetics that the Cr(III) is inaccessible to the Chelex. This could also explain why the radioactive (inorganic) $^{51}$Cr test done in Rue et al. (1997) shows an almost quantitative recovery. If it were the case, the inorganic Cr(III) would have the same isotopic composition as the total Cr(III) (potentially inorganic and organically bound Cr(III)), which indicates no isotopic fractionation between the inorganic and organically bound Cr(III)

pools. Equilibration time among Cr(III) species and double spike was not discussed here because the double spike was added after chelex extraction.

### 2.4 Conclusions

A new Cr(III) and Cr(VI) isotope method for seawater was presented. It was adapted from a seawater total dissolved Cr isotope method using $Mg(OH)_2$ co-precipitation (Moos and Boyle, 2019). We have shown a quantitative recovery of Cr(III) by $Mg(OH)_2$ co-precipitation on neutral seawater samples. Sample Cr(III) - double spike equilibration time between 0.5 to 12 hours neither causes Cr(III) loss onto container walls nor leads to Cr redox transformations. Their Cr(III) concentration and isotope values are within the error of each other. Frozen samples also give the same Cr(III) concentration and isotope composition as those processed at sea. Cr(III) analysis may be more practical on frozen samples. When Cr(III) isotopes are measured on MC-ICP-MS, it is recommended to match the Cr to double spike ratio of the samples and their bracketing SRM/DS mixtures for a Cr/DS ratio lower than 0.75 for accuracy purposes. Finally, we compared our $Mg(OH)_2$ co-precipitation with Chelex-100 resin as Cr(III) extraction methods. The [Cr(III)] using Chelex-100 resin is lower than that by $Mg(OH)_2$ co-precipitation, but is consistent with Rue et al. (1997) using the same procedure. The discrepancy between the methods is hypothesized to be due to the organically bound Cr(III) that could be co-precipitated, but not bound by chelex. This offers us some new insights into Cr(III) complexes that could potentially exist in the ocean but have been neglected due to analytical restrictions.

## Figures and Tables

**Table 2.1 Typical IsoProbe operating conditions for Cr isotope analysis**

| | |
|---|---|
| **Nebulizer** | MicroMist glass nebulizer |
| **Aspiration rate** | ~45 uL/min |
| **Desolvator** | APEX |
| **Cool gas flow** | 13 L/min |
| **Intermediate gas flow** | 0.75 L/min |
| **Neb gas 1** | 0.79 L/min |
| **Neb gas 2** | 2.30 L/min |
| **Sample matrix** | 2% (v/v) $HNO_3$ |
| **Axial mass** | 50.5 (54.4 after peak jump) |

**Table 2.2 Faraday cup configurations and conditions for each sequence in one cycle on MC-ICP-MS (adapted from Table 2 in Moos and Boyle, 2019)**

| **Sequence** | **Durations (s)** | **Axial mass** | **Faraday cups** | | | | | |
|---|---|---|---|---|---|---|---|---|
| | | | **L2** | **Axial** | **H1** | **H2** | **H3** | **H5** |
| 1 | 20 | 50.5 | $^{49}Ti$ | $^{50}Cr$, $^{50}Ti$, $^{50}V$ | $^{51}V$ | $^{52}Cr$ | $^{53}Cr$ | $^{54}Cr$, $^{54}Fe$ |
| 2 | 2 | 50.5 | | $^{50}Cr$, $^{50}Ti$, $^{50}V$ | | $^{52}Cr$ | $^{53}Cr$ | $^{54}Cr$, $^{54}Fe$ |
| 3 | 2 | 54.42 | | | | $^{56}Fe$ | | |

**Figure 2.1 Sampling sites for Cr(III) extraction method comparison**

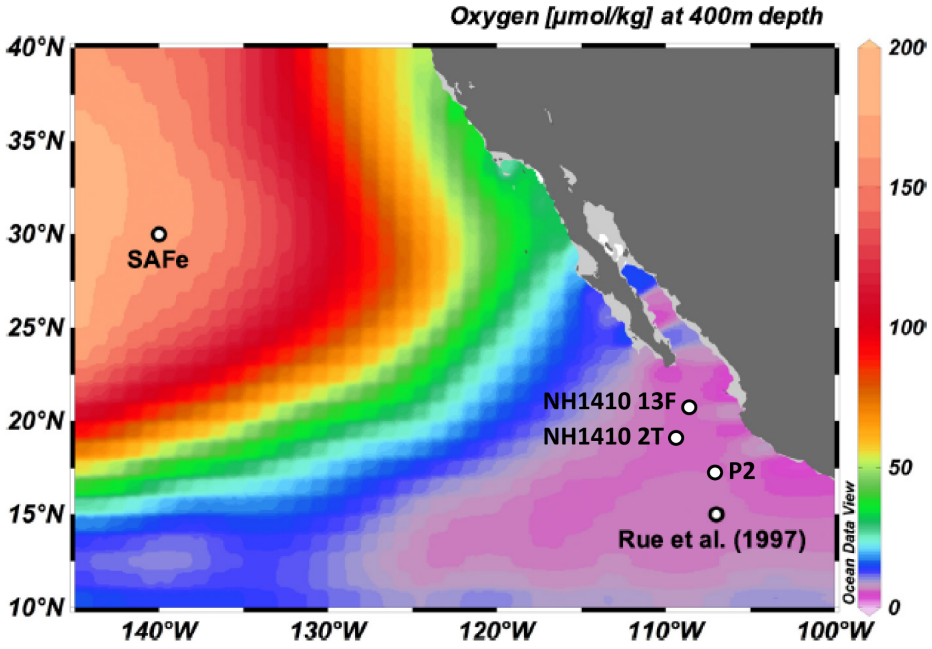


**Table 2.3 $\delta^{53}$Cr of Cr SRM 979 in SRM-DS standard mixtures with varying SRM/DS ratios**

| SRM/DS ratio | 0.25 | 0.35 | 0.50 | 0.75 | 1.00 | 1.50 |
|---|---|---|---|---|---|---|
| $\delta^{53}$Cr | -0.27 | -0.19 | -0.12 | -0.04 | -0.03 | 0.02 |
| 2SE | 0.09 | 0.05 | 0.04 | 0.03 | 0.03 | 0.03 |

**Figure 2.2 $\delta^{53}$Cr of Cr SRM 979 in SRM-DS standard mixtures with varying SRM/DS ratios**

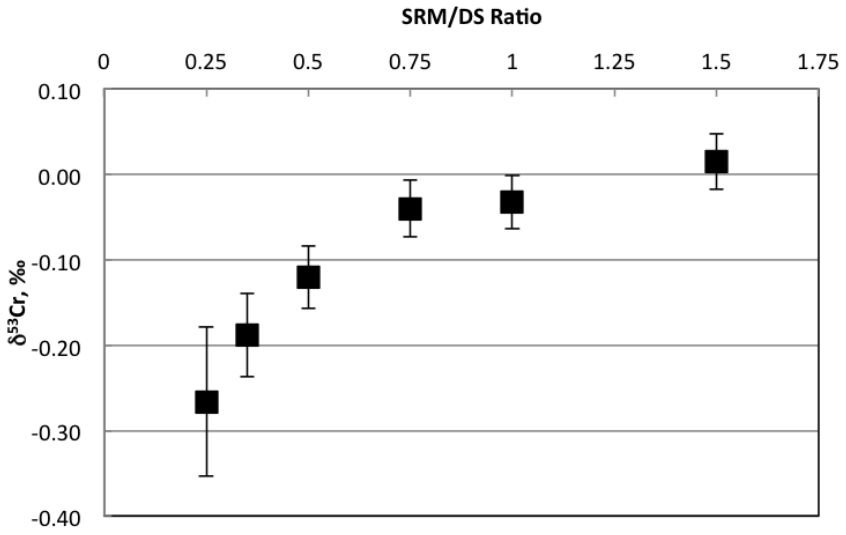

**Table 2.4 [Cr] and $\delta^{53}$Cr data of the in-house quality control sample with varying isotope equilibration time**

| Equilibrium time (d) | [Cr] (nmol/kg) | $\delta^{53}$Cr (‰) |
|---|---|---|
| **0 (20 min)** | 3.37 | 0.93 |
| **1** | 3.37 | 1.01 |
| **2** | 3.37 | 1.02 |
| **3** | 3.35 | 1.00 |

**Table 2.5 [Cr(III)] and $\delta^{53}$Cr(III) data of one sample (P2, 200m) with varying isotope equilibration time**

| Equilibration time (h) | [Cr(III)] (nmol/kg) | SD (External) | $\delta^{53}$Cr(III) (‰) | 2SE (External) | Recovery |
|---|---|---|---|---|---|
| **0.5** | 1.54 | 0.12 | 0.18 | 0.12 | 64% |
| **4** | 1.72 | 0.12 | 0.09 | 0.12 | 69% |
| **8** | 1.59 | 0.12 | 0.21 | 0.12 | 68% |
| **12** | 1.81 | 0.12 | 0.30 | 0.12 | 66% |
| **Average** | 1.67 | | 0.20 | | 67% |
| **SD** | 0.12 | | 0.09 | | 2% |

**Figure 2.3 a) [Cr(III)] and b) $\delta^{53}$Cr(III) data of one sample (P2, 200m) with varying isotope equilibration time**

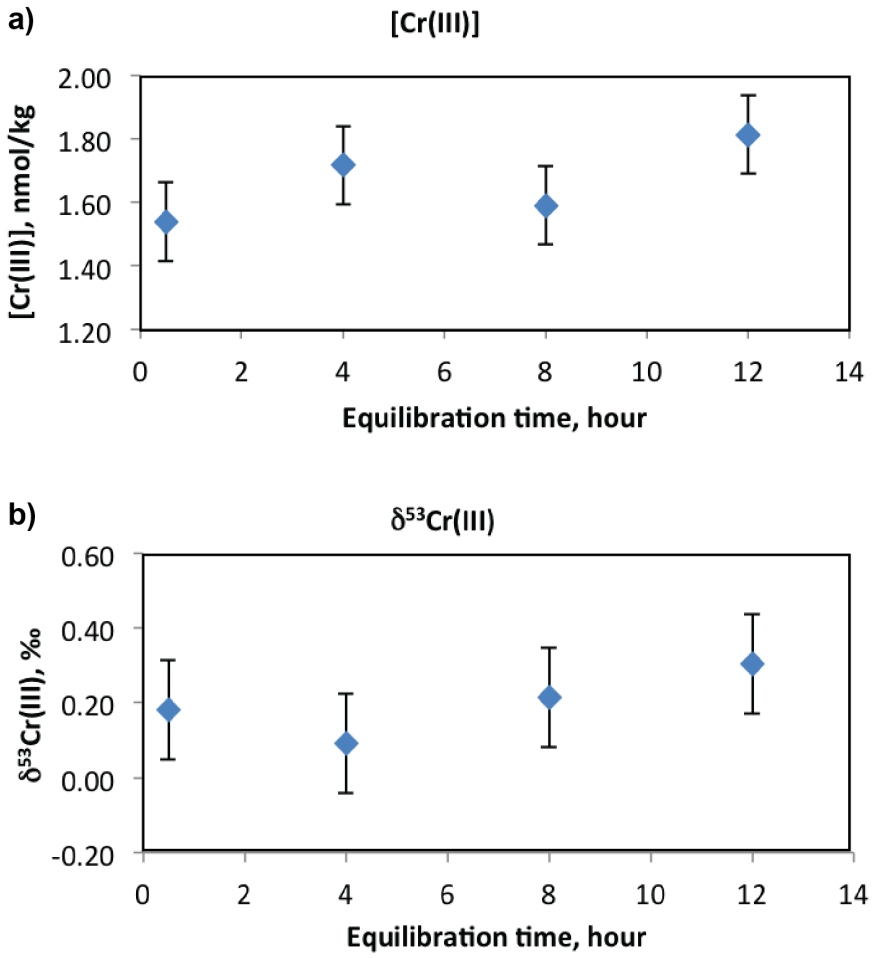

**Table 2.6 [Cr(III)] and $\delta^{53}$Cr(III) data of three samples (of station P2) processed at sea and from frozen samples**

| Depth (m) | Shipboard processing | | | | Frozen | | | | Average (n=2, SD) | |
|---|---|---|---|---|---|---|---|---|---|---|
| | Eq time (h) | [Cr(III)] (nmol/kg) | $\delta^{53}$Cr(III) (‰) | Recovery | Eq time (h) | [Cr(III)] (nmol/kg) | $\delta^{53}$Cr(III) (‰) | Recovery | [Cr(III)] (nmol/kg) | $\delta^{53}$Cr(III) (‰) |
| **150** | 3.5 | 1.60 | 0.16 | 54% | 3.5 | 1.59 | 0.08 | 67% | 1.60±0.01 | 0.12±0.06 |
| **250** | 0.5 | 1.79 | 0.31 | 52% | 0.5 | 1.72 | 0.46 | 66% | 1.76±0.05 | 0.39±0.10 |
| **350** | 1.25 | 1.46 | 0.11 | 53% | 1.25 | 1.37 | -0.08 | 71% | 1.41±0.06 | 0.02±0.13 |

**Figure 2.4 a) [Cr(III)] and b) $\delta^{53}$Cr(III) data of three samples (of station P2) processed at sea and from frozen samples**

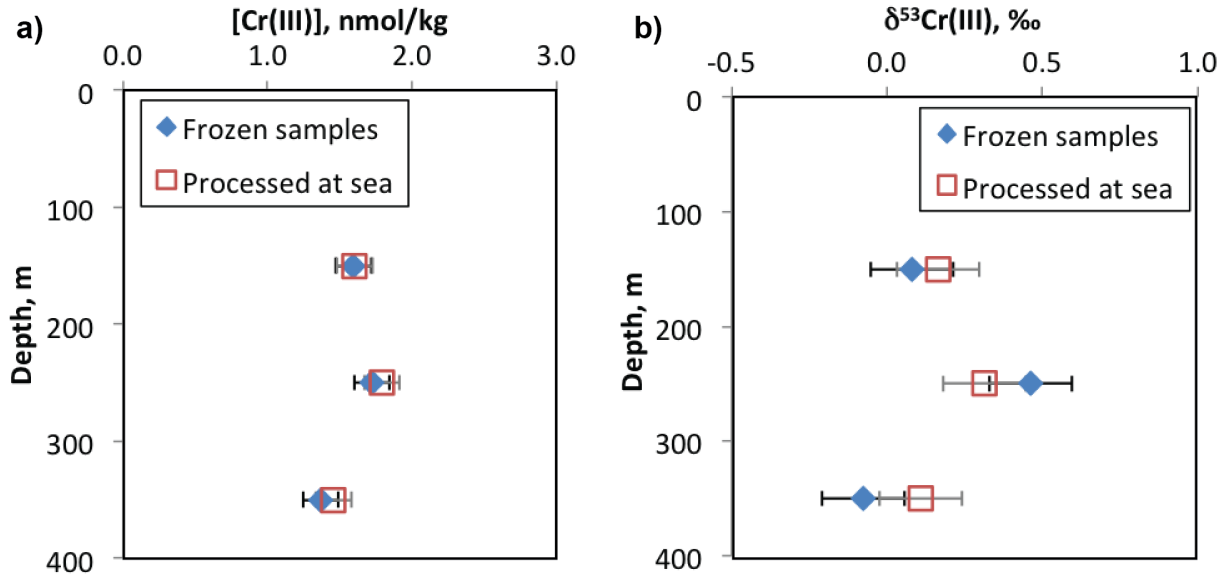

**Table 2.7 [Cr(VI)] and $\delta^{53}$Cr(VI) data of calculated and measured Cr(VI) at station P2. The uncertainties of the calculated [Cr(VI)] and $\delta^{53}$Cr(VI) were calculated by error propagation; the uncertainties of the measured [Cr(VI)] and $\delta^{53}$Cr(VI) are internal or external uncertainties, whichever is larger.**

| Depth (m) | Calculated Cr(VI) | | | | Measured Cr(VI) | | | | |
|---|---|---|---|---|---|---|---|---|---|
| | [Cr(VI)] (nmol/kg) | SD | $\delta^{53}$Cr(VI) (‰) | 2SD | [Cr(VI)] (nmol/kg) | SD | $\delta^{53}$Cr(VI) (‰) | 2SD | Recovery |
| **100** | 2.10 | 0.18 | 1.44 | 0.32 | 1.96 | 0.12 | 1.65 | 0.12 | 23% |
| **150** | 1.30 | 0.18 | 2.29 | 0.73 | 1.03 | 0.12 | 2.89 | 0.13 | 36% |
| **175** | 1.20 | 0.18 | 2.16 | 0.77 | 0.76 | 0.12 | 3.20 | 0.22 | 43% |
| **200** | 1.04 | 0.18 | 2.75 | 1.05 | 0.95 | 0.12 | 2.23 | 0.12 | 48% |
| **250** | 0.90 | 0.18 | 2.79 | 1.22 | 0.96 | 0.12 | 2.98 | 0.17 | 56% |
| **350** | 1.84 | 0.18 | 1.69 | 0.43 | 1.47 | 0.12 | 2.49 | 0.19 | 54% |
| **500** | 2.46 | 0.18 | 1.43 | 0.29 | 2.28 | 0.12 | 1.68 | 0.12 | 51% |

**Figure 2.5 [Cr(VI)] and $\delta^{53}$Cr(VI) profiles of calculated and measured Cr(VI) at station P2**

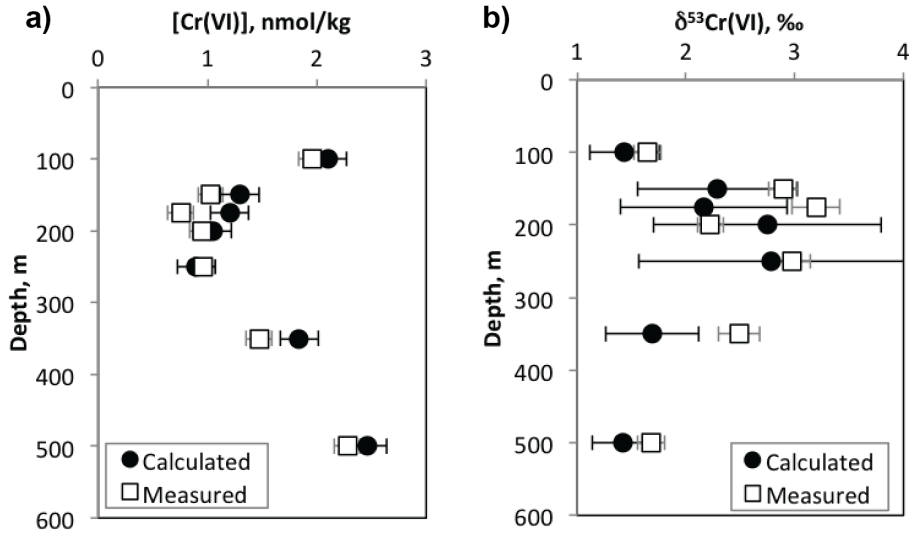

**Figure 2.6 The correlation between the $\delta^{53}$Cr(VI) internal error and the sample Cr(VI) amount**

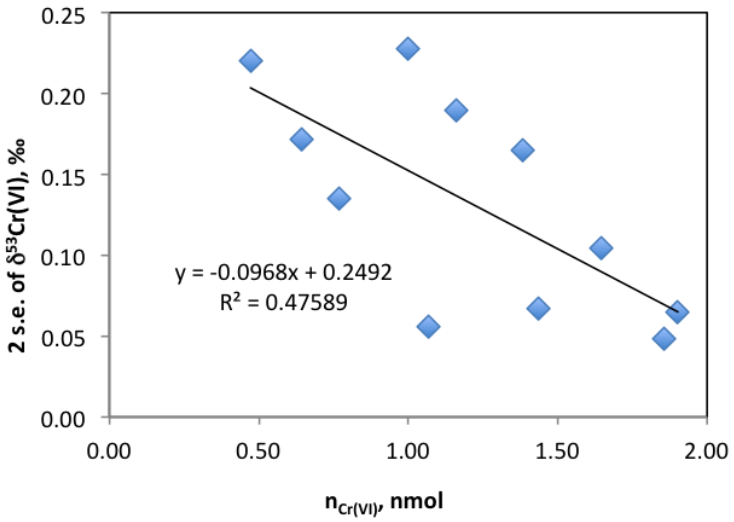

**Table 2.8 Cr(III) concentration and isotope data of station 13F (cruise NH1410) using chelex-100 extraction method**

| Depth | Corrected Cr(III) | | Cr(VI) | | Calculated (Cr(III)+Cr(VI)) | |
|---|---|---|---|---|---|---|
| m | [Cr] (nmol/kg for seawater; ng for blanks) | $\delta^{53}$Cr (‰) | [Cr] (nmol/kg) | $\delta^{53}$Cr (‰) | [Cr] (nmol/kg) | $\delta^{53}$Cr (‰) |
| Blank-1 | 0.48 | 1.30 | | | | |
| Blank-2 | 0.46 | 1.45 | | | | |
| 10 | 0.12 | 0.63 | 2.60 | 1.15 | 2.72 | 1.13 |
| 100 | | | 1.74 | 1.57 | | |
| 200 | 0.49 | 0.12 | 1.97 | 1.50 | 2.46 | 1.22 |
| 300 | | | 2.07 | 1.54 | | |
| 350 | 0.59 | 0.09 | 2.15 | 1.54 | 2.73 | 1.23 |
| 400 | 0.47 | 0.08 | 2.34 | 1.53 | 2.80 | 1.29 |
| 600 | 0.34 | -0.36 | 2.88 | 1.29 | 3.22 | 1.11 |
| 800 | 0.26 | -0.47 | 3.36 | 1.10 | 3.62 | 0.98 |

**Figure 2.7 [Cr(III)] and [Cr(VI)] profiles of NH1410 station 13F and Rue et al. (1997) determined by chelex-100 extraction method**

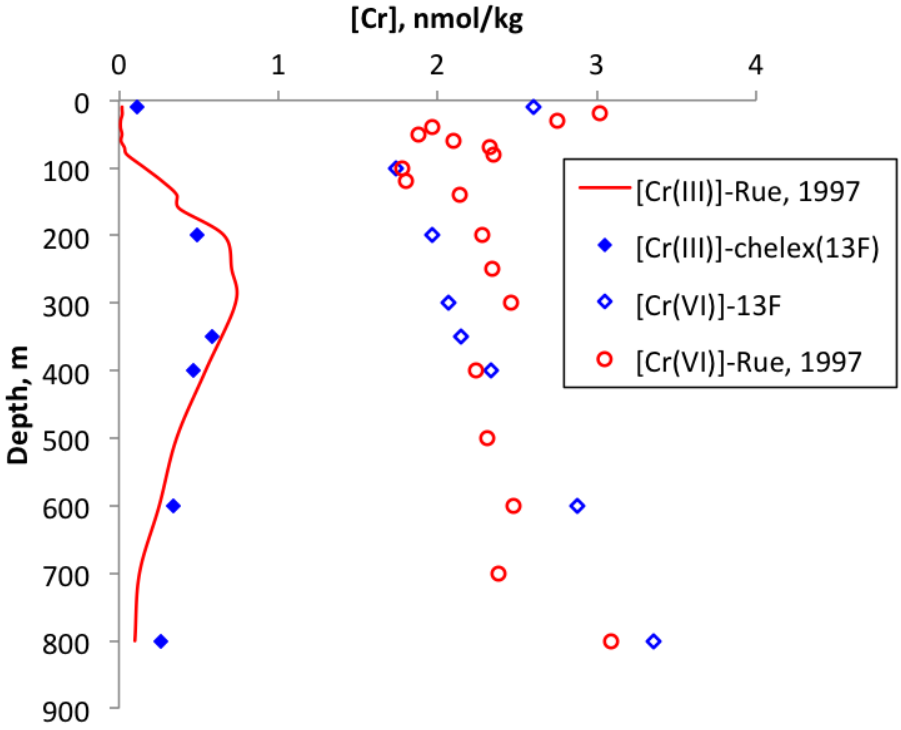

**Figure 2.8 a) [Cr(III)] and b) [Cr(VI)] and [$Cr_{tot}$] profiles of station 13F (NH1410) using chelex-100 extraction method, and station P2 (RR1805) using $Mg(OH)_2$ co-precipitation method**

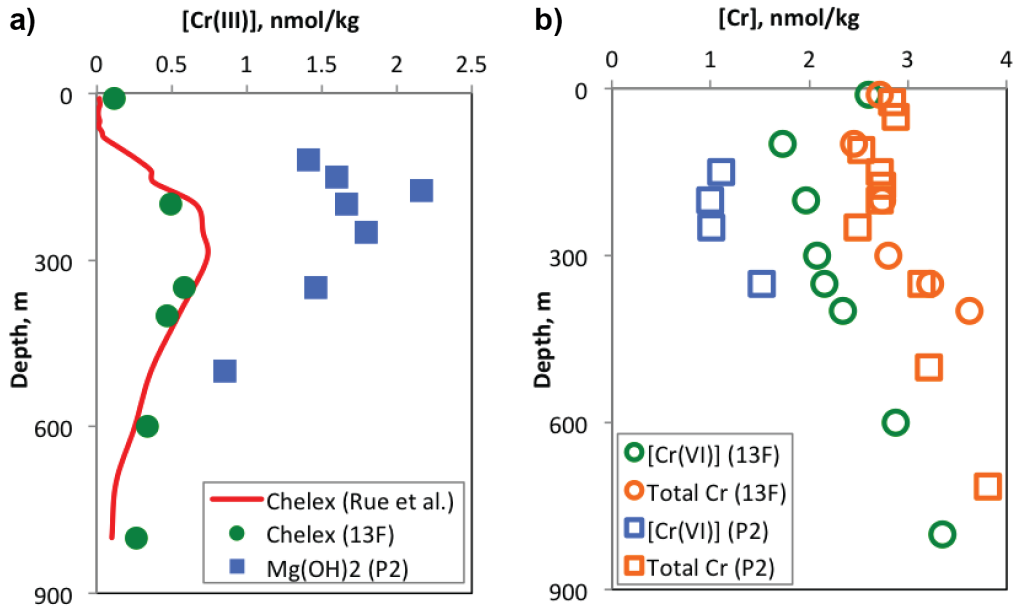


**Figure 2.9 The $\delta^{53}Cr$ profiles of Cr(III), Cr(VI), and total dissolved Cr at station 13F (NH1410) using chelex-100 extraction method, and station P2 (RR1805) using $Mg(OH)_2$ co-precipitation method**

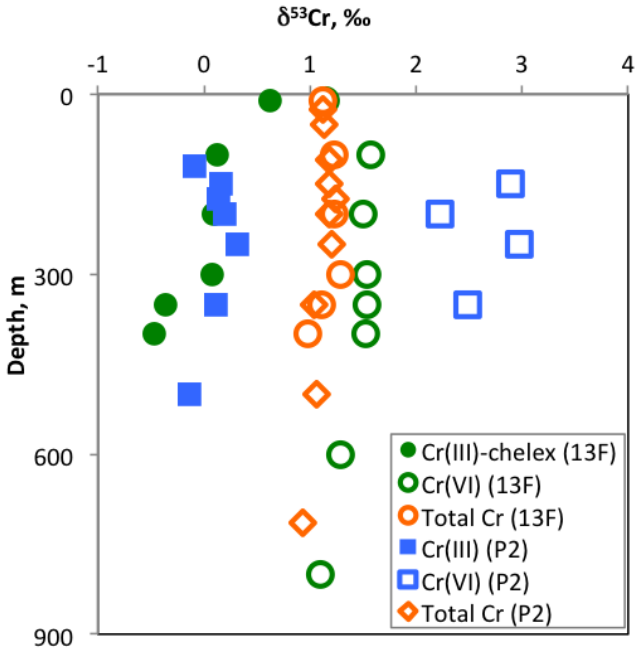

**References**


Bonnand, P., James, R. H., Parkinson, I. J., Connelly, D. P., & Fairchild, I. J. (2013). The chromium isotopic composition of seawater and marine carbonates. *Earth and Planetary Science Letters*, *382*, 10-20.

Bruggmann, S., Scholz, F., Klaebe, R. M., Canfield, D. E., & Frei, R. (2019). Chromium isotope cycling in the water column and sediments of the Peruvian continental margin. *Geochimica et Cosmochimica Acta*, *257*, 224-242.

Boussemart, M., van den Berg, C. M., & Ghaddaf, M. (1992). The determination of the chromium speciation in sea water using catalytic cathodic stripping voltammetry. *Analytica Chimica Acta*, *262*(1), 103-115.

Cranston, R. E., & Murray, J. W. (1978). The determination of chromium species in natural waters. *Analytica Chimica Acta*, *99*(2), 275-282.

Crowe, S. A., Døssing, L. N., Beukes, N. J., Bau, M., Kruger, S. J., Frei, R., & Canfield, D. E. (2013). Atmospheric oxygenation three billion years ago. *Nature*, *501*(7468), 535-538.

Davidson, A. B., Semeniuk, D. M., Koh, J., Holmden, C., Jaccard, S. L., Francois, R., & Crowe, S. A. (2020). A Mg (OH) 2 coprecipitation method for determining chromium speciation and isotopic composition in seawater. *Limnology and oceanography: methods*, *18*(1), 8-19.

D'Arcy, J., Babechuk, M. G., Døssing, L. N., Gaucher, C., & Frei, R. (2016). Processes controlling the chromium isotopic composition of river water: Constraints from basaltic river catchments. *Geochimica et Cosmochimica Acta*, *186*, 296-315.

Ellis, A. S., Johnson, T. M., & Bullen, T. D. (2002). Chromium isotopes and the fate of hexavalent chromium in the environment. *Science*, *295*(5562), 2060-2062.

Ellis, A. S., Johnson, T. M., & Bullen, T. D. (2004). Using chromium stable isotope ratios to quantify Cr (VI) reduction: lack of sorption effects. *Environmental science & technology*, *38*(13), 3604-3607.

Farkaš, J., Chrastný, V., Novák, M., Čadkova, E., Pašava, J., Chakrabarti, R., ... & Bullen, T. D. (2013). Chromium isotope variations (δ53/52Cr) in mantle-derived sources and their weathering products: Implications for environmental studies and the evolution of δ53/52Cr in the Earth's mantle over geologic time. *Geochimica et Cosmochimica Acta*, *123*, 74-92.

Frei, R., Gaucher, C., Poulton, S. W., & Canfield, D. E. (2009). Fluctuations in Precambrian atmospheric oxygenation recorded by chromium isotopes. *Nature*, *461*(7261), 250-253.

Frei, R., Poiré, D., & Frei, K. M. (2014). Weathering on land and transport of chromium to the ocean in a subtropical region (Misiones, NW Argentina): a chromium stable isotope perspective. *Chemical Geology*, *381*, 110-124.

Goring-Harford, H. J., Klar, J. K., Pearce, C. R., Connelly, D. P., Achterberg, E. P., & James, R. H. (2018). Behaviour of chromium isotopes in the eastern sub-tropical Atlantic Oxygen Minimum Zone. *Geochimica et Cosmochimica Acta*, *236*, 41-59.

Janssen, D. J., Rickli, J., Quay, P. D., White, A. E., Nasemann, P., & Jaccard, S. L. (2020). Biological control of chromium redox and stable isotope composition in the surface ocean. *Global biogeochemical cycles*, *34*(1), e2019GB006397.

Moos, S. B., & Boyle, E. A. (2019). Determination of accurate and precise chromium isotope ratios in seawater samples by MC-ICP-MS illustrated by analysis of SAFe Station in the North Pacific Ocean. *Chemical Geology*, *511*, 481-493.

Moos, S. B., Boyle, E. A., Altabet, M. A., & Bourbonnais, A. (2020). Investigating the cycling of chromium in the oxygen deficient waters of the Eastern Tropical North Pacific Ocean and the Santa Barbara Basin using stable isotopes. *Marine Chemistry*, *221*, 103756.

Murray, J. W., Spell, B., & Paul, B. (1983). The contrasting geochemistry of manganese and chromium in the eastern tropical Pacific Ocean. In *Trace metals in sea water* (pp. 643-669). Springer, Boston, MA.

Nasemann, P., Janssen, D. J., Rickli, J., Grasse, P., Frank, M., & Jaccard, S. L. (2020). Chromium reduction and associated stable isotope fractionation restricted to anoxic shelf waters in the Peruvian Oxygen Minimum Zone. *Geochimica et cosmochimica acta*, *285*, 207-224.

Paulukat, C., Døssing, L. N., Mondal, S. K., Voegelin, A. R., & Frei, R. (2015). Oxidative release of chromium from Archean ultramafic rocks, its transport and environmental impact–A Cr isotope perspective on the Sukinda valley ore district (Orissa, India). *Applied Geochemistry*, *59*, 125-138.

Rickli, J., Janssen, D. J., Hassler, C., Ellwood, M. J., & Jaccard, S. L. (2019). Chromium biogeochemistry and stable isotope distribution in the Southern Ocean. *Geochimica et cosmochimica acta, 262*, 188-206.

Rotaru, M., Birck, J. L., & Allègre, C. J. (1992). Clues to early solar system history from chromium isotopes in carbonaceous chondrites. *Nature*, *358*(6386), 465-470.

Rudge, J. F., Reynolds, B. C., & Bourdon, B. (2009). The double spike toolbox. *Chemical Geology*, *265*(3-4), 420-431.

Rue, E. L., Smith, G. J., Cutter, G. A., & Bruland, K. W. (1997). The response of trace element redox couples to suboxic conditions in the water column. *Deep Sea Research Part I: Oceanographic Research Papers*, *44*(1), 113-134.

Semeniuk, D. M., Maldonado, M. T., & Jaccard, S. L. (2016). Chromium uptake and adsorption in marine phytoplankton–Implications for the marine chromium cycle. *Geochimica et Cosmochimica Acta*, *184*, 41-54.

Scheiderich, K., Amini, M., Holmden, C., & Francois, R. (2015). Global variability of chromium isotopes in seawater demonstrated by Pacific, Atlantic, and Arctic Ocean samples. *Earth and Planetary Science Letters, 423*, 87-97.

Schoenberg, R., Zink, S., Staubwasser, M., & von Blanckenburg, F. (2008). The stable Cr isotope inventory of solid Earth reservoirs determined by double spike MC-ICP-MS. *Chemical Geology*, *249*(3-4), 294-306.

Shields, W. R., Murphy, T. J., Catanzaro, E. J., & Garner, E. L. (1966). Absolute isotopic abundance ratios and the atomic weight of a reference sample of chromium. *Journal of research of the National Bureau of Standards. Section A, Physics and chemistry*, *70*(2), 193.

Sun, Z., Wang, X., & Planavsky, N. (2019). Cr isotope systematics in the Connecticut River estuary. *Chemical Geology*, *506*, 29-39.

Wang, X., Reinhard, C. T., Planavsky, N. J., Owens, J. D., Lyons, T. W., & Johnson, T. M. (2016). Sedimentary chromium isotopic compositions across the Cretaceous OAE2 at Demerara Rise Site 1258. *Chemical Geology*, *429*, 85-92.

Wang, X., Glass, J. B., Reinhard, C. T., & Planavsky, N. J. (2019). Species‐dependent chromium isotope fractionation across the eastern tropical North Pacific oxygen minimum zone. *Geochemistry, Geophysics, Geosystems*, *20*(5), 2499-2514.

Wu, W., Wang, X., Reinhard, C. T., & Planavsky, N. J. (2017). Chromium isotope systematics in the Connecticut River. *Chemical Geology*, *456*, 98-111.

# Chapter 3 Total chromium and trivalent chromium isotopes in the Eastern Tropical North Pacific oxygen deficient zone

## 3.1 Introduction

Oxygen deficient zones (ODZs) are active sites for redox cycling of various redox species, including chromium. A few studies have measured Cr redox species in the ETNP ODZ and observed Cr reduction signals. Murray et al. (1983) found Cr(III) maximum and Cr(VI) minima in the upper core of the ODZ along an east-west transect off the coast of Baja Mexico in the eastern North Pacific at 22°N. This transect was located at the fringe of the intense ETNP ODZ with its oxygen level always above 2 μmol/kg. Rue et al. (1997) investigated Cr(III) and Cr(VI) inside the ETNP ODZ where the oxygen level is below 5 μmol/kg from 110 to 600m. They observed the same feature as Murray et al. (1983) in the upper core of the ODZ (300m). Both studies indicate partial reduction of Cr(VI) to Cr(III) followed by scavenging of the particle-reactive Cr(III).

Recently, chromium isotopes have been used to study the Cr cycling in the ETNP ODZ. It is based on several studies showing that isotopically light Cr(VI) is preferentially reduced by various reducing agents with different isotopic effects (Sikora et al., 2008; Zink et al., 2010; Dossing et al., 2011; Basu and Johnson, 2012; Kitchen et al., 2012; Bauer et al., 2018). Moos et al. (2020) investigated the isotopic composition of total dissolvable Cr in the ETNP ODZ, and observed Cr depletion (by up to 0.8 nmol/kg) with 0.1-0.2 ‰ heavier Cr isotope ratios compared to the oxic SAFe station in the northeastern Pacific Ocean. The co-occurrence of heavier nitrogen isotope signals at the same station implies microbial reduction of Cr. These features are even more intense in the Santa Barbara Basin, in which case the Fe(II) diffused from the underlying reducing sediments is hypothesized to be the responsible reductant.

Attempts have been made to measure the Cr isotopes of different redox species. Wang et al. (2019) reported Cr(III) and Cr(VI) isotopes using a Chelex extraction method. However, their total Cr concentration is not consistent with previous studies in the same region, especially the high surface concentration up to 5.08 nmol/L. Therefore, reliable Cr isotopes of different redox

species in the ETNP ODZ are still unavailable prior to this study, which hinders our understanding of the Cr cycling and associated isotopic effects in anoxic environments.

In this chapter, we will demonstrate Cr concentrations and isotopic compositions of total dissolved Cr, Cr(III) and Cr(VI) in the water column of the ETNP ODZ. We will discuss the isotopic fractionation of Cr reduction based on these data and Rayleigh fractionation model. Our data also sheds some light on the Cr scavenging process and the accompanied isotopic partitioning by comparing ODZ data to an oxic reference station SAFe. The temporal and spatial variability of the redox cycling of Cr in the ETNP ODZ will also be discussed.

### 3.1.1 Oceanographic settings

The study sites in this chapter are located in the ETNP ODZ. In this region, coastal upwelling that brings up abundant nutrients fuels the productivity in the surface, and rich sinking organic materials consequently consume the oxygen in the subsurface. Thermal stratification and poor ventilation also help maintain the suboxic conditions in the ETNP. The circulation in the ETNP ODZ and off Mexico has been studied thoroughly (Wyrtki, 1967; Fiedler and Talley, 2006; Kessler, 2006; Evans et al., 2020; Portela et al., 2016; Gangopadhyay et al., 2011). In the surface, the equatorward California Current Water (CCW) influx controls the northern part of the ODZ (Wyrtki, 1967). This water mass has low salinity, low temperature and high oxygen. Further south, the surface water between 23°N and 17°N is formed by heating and evaporation of the California Current Water (Garfield et al., 1983). In the subsurface, a salinity maximum is a characteristic of Subtropical Subsurface Water (StSsW, also known as 13CW) with extremely low oxygen. Deeper down to 1000m, the Pacific Intermediate Water, characterized by a salinity minimum, sets the lower boundary of the ODZ.

The locations of the stations in this chapter are summarized in Table 3.1 and Figure 3.1. Station 23 is off the west coast of Baja California Mexico at the northern fringe of the ODZ, where its oxygen level is never below 2 μM. Station P3 is located at the mouth of the Gulf of California which is controlled by complex and dynamic currents and mesoscale eddies (i.e. Lavin et al., 2003). Station P1 is an onshore station near the west coast of Mexico. The “Coring station” is on the continental margin slope, with fully anoxic bottom waters down to the bottom at 460m. Stations P2 and 15 are offshore stations near the heart of the ETNP ODZ.

### 3.2 Seawater sampling and Processing

#### 3.2.1 Seawater Sampling

Samples in this chapter were collected from cruises R/V Roger Revelle 1804 and 1805 from April to May, 2018 and R/V Kilo Moana 19-20 in September, 2019. Samples above 750m from both cruises were collected in 5 L acid-cleaned Teflon-coated external-spring "Niskin-type" bottles (Ocean Test Equipment) on a powder-coated trace metal clean rosette (Sea-Bird Electronics). After the recovery of the rosette, the Niskin-like bottles were carried into a laminar-flow clean van, pressurized with nitrogen, and filtered through either 0.2μm AcroPak® capsule filters or 0.4μm Nuclepore® membrane filters. Samples deeper than 1000m were collected by regular internal spring closure Niskin bottles, and filtered through 0.2μm AcroPak® capsule filters. Samples between 300m to 500m were collected in both sampling systems to evaluate the contamination levels of the regular Niskin bottles at stations P1, P2 and P3 on both cruises.

#### 3.2.2 Cr sample processing

For total dissolved Cr analysis, samples were acidified to pH 1.9 in the lab. Then the acidified samples were put in a 60°C oven for 10 days to accelerate Cr(VI) to Cr(III) conversion. As for Cr(III) analysis, we used both unacidified fresh samples processed at sea and unacidified frozen samples processed within hours of thawing in the laboratory. As has been shown in chapter 2, the two types of samples give identical Cr(III) concentration and isotope data. These samples were quantitatively spiked with typically ~2 nmol of the $^{50}$Cr-$^{54}$Cr double spike, equilibrated for 6 hours and co-precipitated with ammonium hydroxide.

#### 3.2.3 Other oceanographic parameters

Temperature, salinity and oxygen data were collected with a CTD system attached to a SEABird rosette. Al Devol (University of Washington) measured nitrite concentration at sea. Kenneth Bolster and Jim Moffett (University of Southern California) measured Fe(II) concentration at sea.

### 3.3 Results and Discussion

#### 3.3.1 Total dissolved Cr data from six stations (P1, P2, P3, coring station, 15 and 23)

All of the stations see a general pattern of a [Cr] increase and $\delta^{53}Cr$ decrease from the surface to 1500m (Figures 3.2 and 3.3). However, within the ODZ from 100m to 700m, a [Cr] minimum and $\delta^{53}Cr$ maximum appear at close depths in the upper core of the ODZ (Figure 3.3). Deeper than 1500m the water column shows homogeneous [Cr] and $\delta^{53}Cr$ values (Figure 3.2). The trends of [Cr] and $\delta^{53}Cr$ at each station are summarized below from onshore to offshore stations.

At the coring station in the upper 400m, [Cr] ranges from 2.33 to 2.68 nmol/kg, and $\delta^{53}Cr$ ranges from 1.18 to 1.34 ‰. The [Cr] minimum and $\delta^{53}Cr$ maximum in this depth range are observed at 100m and 75m, respectively. However, the heaviest $\delta^{53}Cr$ at the station (1.85 ‰) is seen in its anoxic bottom at 450m, with the [Cr] being 2.34 nmol/kg, as low as that at 100m. At station P1, from the surface to 1500m, [Cr] ranges from 2.29 to 4.54 nmol/kg, and $\delta^{53}Cr$ ranges from 0.69 to 1.32 ‰. Its [Cr] minimum and $\delta^{53}Cr$ maximum are both observed at 125m. At station P2 in the upper 1000m, [Cr] ranges from 2.49 to 4.14 nmol/kg, and $\delta^{53}Cr$ ranges from 0.80 to 1.24 ‰. Its [Cr] minimum and $\delta^{53}Cr$ maximum are observed at 250m and 175m, respectively. Deeper than 1500m, [Cr] and $\delta^{53}Cr$ have averages of 4.95 ± 0.08 nmol/kg (n=5, SD) and 0.63 ± 0.06 ‰ (n=5, 2SD), respectively. At station 15, from 100 to 1000m, [Cr] ranges from 2.69 to 4.23 nmol/kg, and $\delta^{53}Cr$ ranges from 0.76 to 1.26 ‰. Its [Cr] minimum and $\delta^{53}Cr$ maximum appear at 200m and 150m, respectively. At station P3 in the upper 1000m, [Cr] ranges from 2.26 to 4.11 nmol/kg, and $\delta^{53}Cr$ ranges from 0.85 to 1.28 ‰. Its [Cr] minimum and $\delta^{53}Cr$ maximum are observed at 140m and 110m, respectively. Deeper than 1500m, [Cr] and $\delta^{53}Cr$ have averages of 4.75 ± 0.11 nmol/kg (n=4, SD) and 0.65 ± 0.10 ‰ (n=4, 2SD), respectively. At station 23, from the surface to 500m, [Cr] ranges from 2.62 to 3.06 nmol/kg, and $\delta^{53}Cr$ ranges from 0.98 to 1.14 ‰. Its [Cr] minimum and $\delta^{53}Cr$ maximum are both observed at 150m.

#### 3.3.2 Cr(III) and Cr(VI) data from P1, P2 and P3

Station P2 has the highest sampling resolution for Cr(III) analysis. Out of the thirteen samples that were analyzed for Cr(III), ten of them were in the ODZ (100-725m) from cruises RR1805 (April 2018) and KM1920 (September 2019). Both the Cr(III) concentration and isotope profiles agree between the two cruises with no evident seasonal variability (Table 3.3 and Figure

3.4). Therefore, in the following discussion, Cr(III) data from the two cruises will be discussed together.

Inside the ODZ, the Cr(III) concentration ranges from 0.42 to 1.66 nmol/kg, which accounts for 11% to 64% of the total dissolved Cr at the same depth (Table 3.4 and Figure 3.5). The Cr(III) maximum appears in the upper ODZ (~200m). The Cr(III) isotopic composition ranges from -0.14 to +0.52 ‰ inside the ODZ, with the heaviest isotope signature also seen at 200m. Outside the ODZ (25m, 70m and 1000m), the average Cr(III) concentration is 0.24 ± 0.06 nmol/kg (SD, n=3), with an average isotope composition of -0.03‰ ± 0.02‰ (SD, n=2).

At station P3, seven samples were analyzed for Cr(III) while four samples were analyzed for Cr(VI) inside the ODZ from 140m to 600m. [Cr(III)] ranges from 0.46 to 1.10 nmol/kg and $\delta^{53}$Cr(III) ranges from -0.47 to +0.51‰. The highest [Cr(III)] and heaviest $\delta^{53}$Cr(III) were both observed at 190m. This depth is also where we see the lowest [Cr(VI)] and heaviest measured $\delta^{53}$Cr(VI), which are 1.04 nmol/kg and 2.95‰, respectively.

At station P1, [Cr(III)] ranges from 0.98 to 1.41 nmol/kg and $\delta^{53}$Cr(III) ranges from -0.15‰ to +0.27‰ between 150m and 500m.

### 3.3.3 Cr species data compared with other literature

Prior to this study, there were three published datasets of Cr species in the ETNP ODZ, one of which includes isotope analysis (Murray et al., 1983; Rue et al., 1997; Wang et al., 2019). Murray et al. (1983) investigated a transect close to station 23. Our total dissolved Cr concentration agrees with theirs in the same season (September - October). Both Rue et al. (1997) and Wang et al. (2019) investigated Cr species in the center of the ETNP ODZ, adjacent to our stations P1, P2 and 15. However, our Cr(III) concentration and isotope data differ from both datasets. Rue et al. (1997) reported a Cr(III) maximum of 0.73 nmol/kg at 300m, which is about half the amount of Cr(III) determined with our co-precipitation method. But their total dissolved Cr concentration calculated from Cr(III) and Cr(VI) largely agree with our measured data. As in Wang et al. (2019), from 30m to 300m, the Cr(III) concentration ranges from 1.98 to 2.55 nmol/L, with its isotopic composition ranging from 1.09 to 1.15 ‰. In the same depth range, their Cr(VI) concentration ranges from 2.51 to 2.84 nmol/L with Cr(VI) isotope compositions ranging from 1.55 to 1.93 ‰. Adding up the Cr(III) and Cr(VI) numbers gives a total dissolved Cr concentration larger than 4.5 nmol/L (as high as 5.08 nmol/L) in the upper

300m. This high total dissolved Cr concentration is not consistent with other published surface Cr concentration in the same area (Rue et al., 1997; Murray et al., 1983; Moos et al., 2020) or other parts of the global ocean (Jeandel and Minster, 1987; Cranston and Murray, 1978; Scheiderich et al., 2015; Goring-Hartford et al., 2018; Moos and Boyle, 2019; Rickli et al., 2019; Naseman et al., 2020; Moos et al., 2020; Janssen et al., 2020).

Rue et al. (1997) and Wang et al. (2019) both used slightly different Chelex-100 solid phase extraction methods to extract Cr(III), but found different Cr(III) concentrations. We also analyzed eight samples from a nearby station (NH1410, station 13F) using the same method and procedure as described in Rue et al. (1997) (see 2.3.7). Our Cr(III) concentrations agree with their data, but differ from Wang et al. (2019). Chapter 2 and Davidson et al. (2020) have demonstrated the robustness of $Mg(OH)_2$ co-precipitation as a Cr(III) extraction technique. Therefore, we believe that there is some analytical characteristic of the chelex method that underestimates Cr(III) data, and that our Cr species data is more reliable.

### 3.3.4 The isotopic fractionation of Cr reduction in the ETNP ODZ

#### 3.3.4.1 Global Cr array

Most of the published Cr isotope data fits into a global linear relationship between logarithmic seawater chromium concentration (log[Cr]) and its stable isotope ratio ($\delta^{53}Cr$) (Scheiderich et al., 2015; Goring-Hartford et al., 2018; Moos and Boyle, 2019; Rickli et al., 2019; Naseman et al., 2020; Moos et al., 2020; Janssen et al., 2020). This linear relationship was proposed to reflect biological uptake/regeneration processes that resemble cumulative Rayleigh fractionation with a factor of -0.8 ‰. Some outliers from this linear relationship seem to be linked to freshwater dilution (Scheiderich et al., 2015) and strong reduction followed by scavenging occurring in close proximity to reducing sediments (Goring-Harford et al., 2018; Moos, 2019).

Most of the Cr isotope data in the ETNP ODZ from this study fall on this global Cr array (Figures 3.6 and 3.7). The only outlier is from a bottom sample at the coring station on the slope ([Cr]=2.34 nmol/kg, $\delta^{53}Cr$=1.85 ‰), which was taken 5 m above the seafloor. Similar patterns of a drawdown in [Cr] and enrichment in heavier Cr isotopes is also seen on the ETSP ODZ shelf (Nasemann et al., 2020). Similar to bottom samples of Chukchi Shelf in the Arctic Ocean (Moos, 2019), these isotopically heavy samples also may be linked to strong Cr reduction by Fe(II)

diffusing from reducing sediments followed by scavenging onto newly formed iron oxyhydroxide.

#### 3.3.4.2 Cr reduction fractionation factor

The fractionation factor of Cr reduction in the ODZ was calculated assuming a closed-system ($Cr(VI)_{depletion} = Cr(VI)_{initial} - Cr(VI)_{observed}$) Rayleigh fractionation model:

$$\frac{R_{sw}}{R_{sw}^{0}} = f^{\alpha-1},$$

where $R_{sw}^{0}$ is the initial $^{53}Cr/^{52}Cr$ of Cr(VI), $R_{sw}$ is the $^{53}Cr/^{52}Cr$ of the remaining Cr(VI) after Cr(VI) reduction, $f$ is the fraction of Cr(VI) remaining in seawater, and α is the isotopic fractionation factor of Cr(VI) reduction. For our purposes, SAFe station (30°N, 140°W) in the northeastern Pacific was chosen as the oxic counterpart where the initial Cr(VI) at each density layer is coming from. The Cr concentration and isotopic composition of total dissolved Cr at SAFe station is reported in Moos and Boyle (2019). At the SAFe station where dissolved oxygen is never below 20 μmol/kg in the upper 700m, it is reasonable to expect that Cr(III) is negligible (Cranston and Murray, 1978; Rue et al., 1997; Murray et al., 1983). Therefore, we have

$$[Cr]_{SAFe}=[Cr(VI)]_{SAFe} \text{ and } \delta^{53}Cr_{SAFe}=\delta^{53}Cr(VI)_{SAFe}.$$

The [Cr(VI)] and $\delta^{53}Cr(VI)$ used in $f$ and $R_{sw}$ were either measured directly or calculated from the differences between the Cr(III) at ODZ stations and the total dissolved Cr at the same density at SAFe station (Moos and Boyle, 2019). Rearranging the equation above, we have

$$\alpha = \frac{ln(\frac{R_{sw}}{R_{sw}^{0}})}{ln(f)} + 1.$$

In a permil (‰) space, fractionation factor can be expressed as

$$\varepsilon\ (‰) = (\alpha - 1) \times 1000\ (‰) = \frac{ln(\frac{R_{sw}}{R_{sw}^{0}})}{ln(f)} \times 1000\ (‰)$$

Given the uncertainties of the datapoints on x and y axes, we applied York linear regression to our datasets (York et al., 2004). It takes the weight of different datapoints into consideration. This was done on a data analysis and graphing software OriginLab© (version OriginPro 2021b).

From the calculated Cr(VI) data at station P2 from 70m to 1000m, we determined the fractionation factor of Cr(VI) reduction to be -1.29 ± 0.04 ‰ (2SE) in the ETNP ODZ (Figure 3.8). The fractionation factor derived from measured Cr(VI) (-1.68 ± 0.07 ‰, 2SE) is slightly larger than that from calculated Cr(VI) data. We will use the fractionation factor of -1.29 ± 0.04 ‰ in subsequent discussion because the calculated P2 Cr(VI) dataset covers the widest range of Cr reduction extent (*f*), thus giving a more accurate fractionation factor (Figure 3.8). The Cr species data at stations P1 and P3 also follows the same linear regression with the same Cr reduction fractionation factor.

This isotopic fractionation (-1.29 ± 0.04 ‰) is larger than that inferred from the global (presumed biological) $\delta^{53}$Cr-log[Cr] slope (-0.8‰). This difference is real despite the fact that our data also fall on the global biogenic relationship. The contradiction can be understood by realizing that a large fraction of the ODZ total dissolved Cr consists of both Cr(III) and Cr(VI), with lighter Cr(III) balancing the heavier Cr(VI). ODZ [Cr] and light Cr isotope depletion occurs because only a fraction of the generated light Cr(III) is removed onto sinking particles. The net consequence of this preferential Cr reduction of lighter Cr(VI) and partial scavenging of the generated lighter Cr(III) is that the reduction signal in the total dissolved Cr is suppressed, making the total dissolved Cr data fall on that seemingly less fractionated global relationship.

Figure 3.9 illustrates this pathway stepwise at the ODZ Cr(III) maximum. First, ~ 83% of the Cr(VI) in seawater entering the ODZ from the oxic ocean is converted to Cr(III) (with a presumed constant isotope fractionation) that makes the Cr(VI) progressively heavier along a Rayleigh fractionation path. Meanwhile isotopically light Cr(III) accumulates and becomes slightly heavier as the source Cr(VI) evolves. Second, although there seems to be an isotope partitioning associated with Cr scavenging, that fractionation effect is small and may vary from basin to basin (see 3.3.6 and 4.3.1.2). For simplicity, in this figure, we assume that dissolved and scavenged Cr(III) have identical isotopic compositions. Only a moderate fraction (~36%) of the generated Cr(III) is scavenged by sinking particles, leaving behind significant dissolved Cr(III) in the total dissolved Cr pool. The end result depends on the fraction of the original Cr(VI) that is reduced, the fraction of Cr(III) scavenged and the isotopic partitioning between scavenged and dissolved Cr(III).

Despite the Cr in the ODZ going through unique redox processes, its total dissolved Cr is consistent with global datasets on the $\delta^{53}$Cr - log[Cr] space. To explain this seemingly

"coincidence", we first need to understand what the linear $\delta^{53}$Cr - log[Cr] relationship implies. A previous study on Si isotope systematics (Reynolds et al., 2006) points out that a linear correlation between logarithmic concentration and isotopic composition does not necessarily translate to a single fractionation process, but may involve a composite of processes (surface uptake, regeneration, thermocline ventilation, and ocean mixing and circulation). A similar argument for Cr isotope systematics was also proposed in Nasemann et al. (2020); they proposed that the global apparent fractionation factor, which also applies to ETSP ODZ dataset, represents a net effect of reduction, scavenging and other processes in the ODZ. The ETNP ODZ Cr data in this study corroborates this statement - the fractionation factor we determined (-1.29 ± 0.04 ‰) reflects the Cr(VI) reduction process in the ODZ, whereas the one derived from the global $\delta^{53}$Cr-log[Cr] plot (-0.8‰) reflects a complex signal arising from reduction and surface biological uptake, followed by scavenging and regeneration in the deep ocean.

The fact that the ETNP ODZ Cr data falls on the global Cr array indicates that the Cr cycling in this anoxic setting is in line with the global Cr cycling in spite of the unique reduction process. However, it is still not evident why the extent of reduction and the fraction of Cr(III) remaining in the water column result in a total dissolved $\delta^{53}$Cr-log[Cr] pathway matching the oxic ocean biological removal and regeneration relationship. To reach such a "coincidence", some factors play critical roles: the isotopic fractionation of Cr(VI) reduction, the scavenging fraction of Cr(III), the isotopic fractionation of Cr(III) scavenging, etc. A particle maximum in the ETNP ODZ is observed at the same depth where we see maximum Cr reduction and removal, which may indicate that this factor may interplay with the reduction and scavenging process (Garfield et al., 1983).

### 3.3.5 Possible mechanisms of Cr reduction

Various abiotic and biotic processes could potentially reduce Cr(VI), including organic matter (Scheiderich et al., 2015; Kitchen et al., 2012), ferrous Fe (Bauer et al., 2018; Basu and Johnson, 2012; Dossing et al., 2011; Kitchen et al., 2012), magnetite (Ellis et al., 2002), hydrogen peroxide (Zink et al., 2010) and nitrate-reducing bacteria such as *Shewanella oneidensis* (Sikora et al., 2008). Bauer et al. (2019) compiled the isotopic fractionation factor of Cr reduction by different reductants in experimental settings (Table 1.1). The fractionation factor varies from -1.50‰ to -5.0‰. However, the Cr concentrations used in these experiments are

usually a few orders of magnitude higher than seawater levels. In this part, we will base our discussion on ancillary data and our incubation experiment (see Appendix 2).

#### 3.3.5.1 Cr reduction by Fe(II)?

Reduced iron (Fe(II)) has long been considered a potential reducing agent for Cr(VI) in the environment. Different forms of reduced iron (dissolved and solid phase Fe(II), goethite, siderite, green rust, FeS) can reduce Cr(VI) with a negative isotopic fractionation effect ranging from -1.5‰ to -4.2‰ (Bauer et al., 2018; Basu and Johnson, 2012; Dossing et al., 2011; Kitchen et al, 2012). Specifically, the Cr isotope fractionation during reduction of Cr(VI) by aqueous Fe(II) is found to be -1.5‰ at seawater pH (Dossing et al., 2011). Studies of the kinetics of this reaction have also shown that it could occur on a timescale of minutes to months in natural environments (Sedlak and Chan, 1997; Pettine et al., 1998).

In the core of the ODZ where oxygen is below the CTD detection limit, an accumulation of dFe(II) was observed in ETNP, ETSP and Arabian Sea ODZs (Bolster et al., 2018; Cutter et al., 2018; Moffett et al., 2007). In the ETNP ODZ, from Bolster et al. (2018) and the Fe(II) data collected on cruises RR1805 and KM1920, an Fe(II) maximum was also observed in the upper core of the ODZ at the same depth as the Cr(III) maximum, secondary nitrite maximum and intermediate particle maxima (Garfield et al., 1983). This co-occurrence was also seen in the ETSP ODZ (Whitmire et al., 2009; Chapter 4).

However, shipboard incubation experiments (see Appendix 2) show that Fe(II) loss during the incubation is one order of magnitude lower than Cr(III) gain. The rate constant of Cr(VI) reduction by Fe(II) is 0.008 $nM^{-1} \cdot d^{-1}$ at incubation conditions (13°C, seawater pH and ionic strength) using the rate constant formula in Pettine et al. (1998). This number is one order of magnitude lower than that calculated by incubation Cr data ($0.066 \pm 0.012$ $(nmol/kg)^{-1} \cdot d^{-1}$, SD, n=3). Therefore, Fe(II) was not the major reductant for Cr reduction in the ODZ.

#### 3.3.5.2 Microbial-mediated Cr reduction?

Another possible mechanism responsible for Cr reduction in the ODZ is through microbial mediation. This hypothesis derives from the correlation of Cr profiles and nitrogen system profiles (N*, N isotopes and N species) in the ETNP ODZ (Moos et al., 2020). Firstly, from the same cruises where we collected our Cr data, nutrients including nitrite were measured.

At stations P2 and P3, the secondary nitrite maximum (SNM) appears at 180m and between 180m to 300m, respectively, with tens-of-meters temporal fluctuations during the cruise (Figure 3.10). These depths coincide with [Cr(III)] maxima, which were at 200m and 190m at P2 and P3, respectively. The N* profile at P3 also shows a minimum at 300m, which implies maximal denitrification. A study of N isotopes in the same ETNP ODZ region also demonstrates similar depth of SNM and N deficit as P2, as well as the heaviest $\delta^{15}N_{NO3-}$ signal coming from denitrification (Fuchsman et al., 2018). A particle maxima and high bacterial activities indicates active microbial activities, possibly from denitrifiers (Garfield et al., 1983; Ohnemus et al., 2017 and 2018). Therefore, the maximum Cr(III) in the same depth range might be linked to the activities of denitrifiers.

Secondly, microbial Cr reduction at the μM-level by *Shewanella oneidensis* strain MR-1 has shown a negative isotopic fractionation effect of -4.11‰ and -1.75‰ depending on the concentration of reducing agents and reaction rates (Sikora et al., 2008). Although this isotopic fractionation effect is greater than what we have observed, the fractionation factor might vary depending on different microbes, levels of substrates, and thus the reaction rates in oceanic settings compared to in cultures (Bryan et al., 1983).

However, our shipboard incubations (see Appendix 2) indicate that particles are not involved in Cr reduction on the timescale of days. Although microbes may not reduce Cr(VI) directly, their metabolites (i.e. soluble enzymes) in the dissolved phase could play a role here. Saito et al. (2020) observed abundant nitrite oxidoreductase in the ETNP ODZ. This enzyme may be involved in accidental catalysis of other redox-sensitive metals such as Cr.

#### 3.3.5.3 Other possible mechanisms

If we assume a pseudo-first order reaction for Cr reduction, the responsible reductant should have a significant concentration difference between ~200m and 300m according to incubation results. One of the candidates could be nitrite. Nitrite profiles at stations P2 and P3 show a two-fold difference at 200m and 300m (Figure 3.10). At station P2, the nitrite concentrations at 180m (SNM) and 300m are 2.51 nmol/kg and 0.91 nmol/kg, respectively. If nitrite were the reducing agent, it would produce a Cr(III) gain of 0.18 nmol/kg, which is within our analytical error. A sedimentary correlation between $\delta^{53}Cr$ and $\delta^{15}N$ also indicates possible coupling between Cr cycling and denitrification (Gueguen et al., 2016). Therefore, at this stage,

the mechanism of Cr reduction in the ODZs still remains unclear. We ruled out Fe(II) and denitrifiers as the reducing agent for day-term reduction. The hypothesis of nitrite being the reductant needs to be verified with future experiments.

### 3.3.6 Scavenging

#### 3.3.6.1 ODZ Cr data compared to SAFe station

Previous measurements of Cr(III), Cr(VI) and particulate Cr concentrations in the ODZ imply that Cr(VI) in the ODZ is reduced to Cr(III), which is then scavenged by particles (Murray et al., 1981; Rue et al., 1997). Here, I used a similar approach as in Moos et al., (2020) and compared the ODZ Cr profiles with that of the SAFe station (30°N, 140°W), an oxic counterpart in the North Pacific (Moos and Boyle, 2019). Briefly, the ODZ Cr profiles were compared to SAFe data at the same potential density ($\sigma_\theta$), which was determined from polynomial fitting in Moos et al., 2020, to correct for different upwelling strengths at each station (Figure 3.11). And the amount of the scavenged Cr and its isotopic composition are calculated as the difference between the ODZ and SAFe Cr data by mass balance.

#### 3.3.6.2 Inter-station variability of Cr scavenging in the ETNP ODZ

From Figure 3.11, there are some common features in [Cr] and $\delta^{53}$Cr for all the stations with respect to SAFe station. First, all stations see a Cr depletion in the upper core of the ODZ within potential density ($\sigma_\theta$) layers of 26.0~26.5 kg/m$^3$. These density layers are also where the $\delta^{53}$Cr maximum appears at all stations. Second, there is an inshore-offshore trend for both Cr depletion and heaviest $\delta^{53}$Cr signals. The inshore and slope stations (P1, P3 and coring station) have greater Cr depletion extent and heavier $\delta^{53}$Cr than the offshore ones (P2, 15 and 23). This feature is evident in both Figures 3.11 and 3.12. For inshore stations, the Cr depletion and $^{53}$Cr enrichment signals are stretched into the lower part of the ODZ, deeper than offshore stations. Given the sample level of Cr(III) at P1 and P2 (Figure 3.5), these trends may imply that Cr scavenging is more pronounced, and the cycling of Cr(III) is faster in regions closer to the coast.

However, there are some distinct features at stations 23 and P3. At these two stations, although the Cr depletion in the upper core of the ODZ is evident which stretches down to 600m, the heavier $\delta^{53}$Cr is not as clear as other stations. Specifically, P3 only sees an obvious heavier $\delta^{53}$Cr signal between 110m and 140m, whereas deeper down in the ODZ, the $\delta^{53}$Cr profile

overlaps with the $\sigma_\theta$-adjusted SAFe profile. At station 23, however, the $\delta^{53}Cr$ profile overlaps with the $\sigma_\theta$-adjusted SAFe profile in the upper 200m, but shows a heavier-than-SAFe signal between 300m and 500m. It is worth noting that in the upper 500m of station 23 where we analyzed for Cr, the $O_2$ concentration is never below 8 μmol/kg, which is higher than the suboxia criteria of 2 μmol/kg. Besides, station 23 is located to the west of Baja California peninsula with distinctly different water masses from other ODZ stations. In the upper 500m, the equatorward California Current is controlling station 23, with its low-salinity core positioned at 160m (Gangopadhyay et al., 2011). This can be seen from the T-S diagram (Figure 3.13), where station 23 has a salinity minimum as low as 33.5 at 40m. This salinity minimum is shallower than the California Current core probably as a result of interactions with coastal upwelling. It is also fresher than other stations down to 500m. Therefore, it is likely that the fresher California Current contains lower Cr but a similar or lighter $\delta^{53}Cr$ signal than SAFe station. Below 300m where it is less affected by California Current, the heavier signal starts to be evident. In this case, SAFe station could no longer be treated as its source water.

Similarly, at P3, a prominent Cr depletion in the upper 600m is not accompanied with heavier $\delta^{53}Cr$. This might result from the differences between P3 and other ODZ stations. First, it is also affected by the equatorward California Current, but the influence is restricted within the upper 100m. This can be seen on the T-S diagram where it shows a salinity minimum as low as 34.0, higher than station 23 but lower than other ODZ stations. Second, although it is fully anoxic (oxygen <2 μmol/kg) from 140 to 600m, its maximal Cr(III), nitrite and Fe(II) levels are all lower than P2 (Figure 3.10; Fe(II) data not shown here). This might indicate that the biotic/abiotic redox processes occurring at P3 are less active than that at P2. Third, it is also located in a highly dynamic zone at the southern tip of the Baja California peninsula and at the outer mouth of the Gulf of California. This "transition zone" (Lavin et al., 2003) is where three water masses (Tropical Surface Water, California Current Water, and Gulf of Mexico Water) intermingle among themselves in the top 150-200m. It is also affected by physical processes at different temporal and spatial scales (Checkley et al., 2009; Gangopadhyay et al., 2011; Lavin et al., 2003; Castro et al., 2006; Portela et al., 2016). Variability in oxygen and nitrite profiles from cruises KM1919 and 1920 validates the high spatial and temporal dynamism at station P3 (Figure 3.14).

### 3.3.6.3 Scavenged Cr isotopic composition calculated by mass balance

From mass balance, we can calculate the amount and the isotopic composition of the Cr that has been scavenged from the ODZ water column using the following equation:

$$[Cr]_s \times \delta^{53}Cr_s + [Cr]_{ODZ} \times \delta^{53}Cr_{ODZ} = [Cr]_{SAFe,\sigma_\theta} \times \delta^{53}Cr_{SAFe,\sigma_\theta}.$$

In this equation, the subscripts *s*, *ODZ* and *SAFe* denote the scavenged Cr, ODZ Cr and SAFe Cr at a certain potential density $\sigma_\theta$, respectively. The calculated data is summarized in Table 3.5 and plotted in Figure 3.15. The propagation of uncertainty gives a $[Cr]_s$ standard deviation of 0.17 nmol/kg. Therefore, only $[Cr]_s$ above 0.17 nmol/kg will be included and discussed here. As for $\delta^{53}Cr_s$, the standard deviation depends on all the other terms in the equation, ranging from 0.35‰ to 1.78‰.

Maximal Cr scavenging appears at $\sigma_\theta$ between 26.0 to 26.5 kg/m$^3$, along with the isotopically heaviest scavenged Cr. Except the bottom sample at the coring station where its scavenged Cr is 1.15 nmol/kg, the scavenged Cr in the water column reaches up to 0.90 nmol/kg. The weighted average of the scavenged $\delta^{53}Cr$ is +0.5 ± 0.4‰ (SD, n=55). This number might be biased toward the heavier side, because samples with larger Cr scavenging with heavier $\delta^{53}Cr_s$ have larger weights. However, it shows that the scavenged Cr is lighter than the total dissolved Cr at the same depths. When we compare the isotopic composition of the scavenged Cr and Cr(III) measured at the same depth at P2, their difference averages +0.4 ± 0.4‰ ($\Delta\delta^{53}Cr_{scavenged\text{-}Cr(III)}$, weighted, SD, n=10). This indicates that slightly heavier Cr(III) is preferentially scavenged.

## 3.4 Conclusions

We measured concentrations and isotopic compositions of total dissolved Cr, Cr(III) and Cr(VI) in the ETNP ODZ. A Cr(III) maximum up to 1.66 nmol/kg in the upper core of the ODZ indicates Cr(VI) reduction occurs in the anoxic waters. The Cr(III) is isotopically lighter than Cr(VI) by ~2‰. The lighter Cr(III) and heavier Cr(VI) verify that Cr reduction would preferentially take lighter Cr(VI). An isotopic fractionation associated with Cr reduction in the ETNP ODZ was determined to be -1.29 ± 0.04 ‰. We also observed Cr depletion in the upper 1000m when comparing ODZ stations to an oxic reference station SAFe. This implies Cr scavenging followed by Cr reduction. And the scavenging of Cr is more intense at inshore

stations than that of offshore ones. No apparent temporal variability of Cr(III) and total dissolved Cr was observed.

## Figures and Tables

**Table 3.1 Sampling stations and their locations and cruises in the ETNP ODZ**

| Station | Latitude and longitude | Cruise | Distance from ODZ coast (km) |
|---|---|---|---|
| Coring station | 21.3 ºN, 105.7 ºW | RR1804-5 | 45 |
| P1 | 20.2 ºN, 106.0 ºW | RR1804-5 | 40 |
| P2 | 17.0 ºN, 107.0 ºW | RR1804-5, KM1919-20 | 320 |
| 15 | 15.1 ºN, 110.0 ºW | RR1804-5 | 700 |
| P3 | 21.8 ºN, 110.0 ºW | KM1919-20 | 500 |
| 23 | 27.1 ºN, 115.2 ºW | KM1919-20 | 1300 |

**Figure 3.1 A map of ETNP ODZ stations**

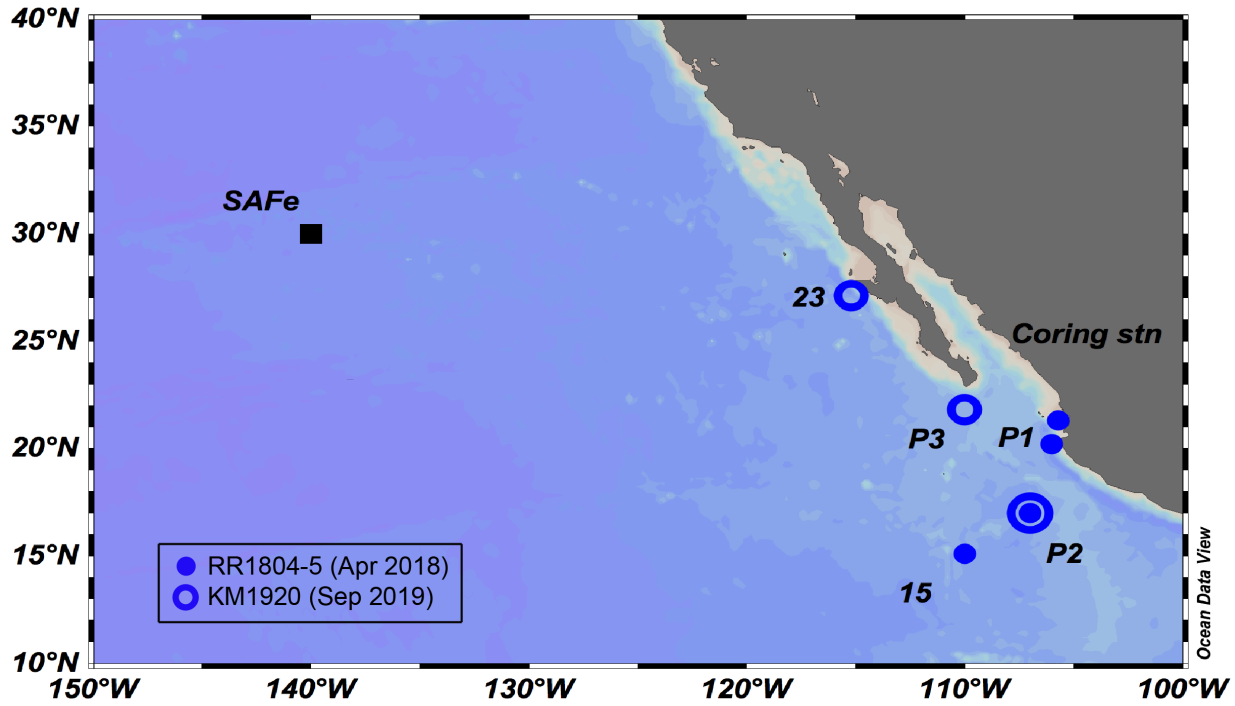

**Table 3.2 Total dissolved Cr concentration and its isotopic composition in the ETNP**

| Station | Depth (m) | CTD Oxygen (μmol/kg) | [Cr] (nmol/kg) | $\delta^{53}$Cr (‰) |
|---|---|---|---|---|
| **Coring station** | 6 | 218.08 | 2.56 | 1.29 |
| | 16 | 135.34 | 2.49 | 1.24 |
| | 26 | 56.96 | 2.57 | 1.27 |
| | 47 | 0.63 | 2.57 | 1.18 |
| | 56 | 0.66 | 2.47 | 1.21 |
| | 76 | 0.67 | 2.44 | 1.34 |
| | 102 | 0.73 | 2.33 | 1.32 |
| | 200 | 0.75 | 2.43 | 1.18 |
| | 300 | 0.81 | 2.68 | 1.24 |
| | 400 | 0.82 | 2.66 | 1.24 |
| | 449 | 0.93 | 2.34 | 1.85 |
| **P1** | 13 | 183.24 | 2.83 | 1.16 |
| | 23 | 108.43 | 2.59 | 1.20 |
| | 38 | 36.41 | 2.58 | 1.16 |
| | 78 | 0.67 | 2.46 | 1.28 |
| | 101 | 0.80 | 2.48 | 1.24 |
| | 126 | 0.81 | 2.29 | 1.32 |
| | 152 | 0.78 | 2.34 | 1.25 |
| | 176 | 0.83 | 2.63 | 1.22 |
| | 302 | 0.85 | 2.77 | 1.21 |
| | 402 | 0.96 | 2.86 | 1.19 |
| | 501 | 0.93 | 3.03 | 1.16 |
| | 702 | 1.11 | 3.51 | 0.98 |
| | 802 | 1.88 | 3.67 | 0.94 |

| | | | | |
|---|---|---|---|---|
| | 902 | 3.05 | 3.70 | 0.88 |
| | 1003 | 7.24 | 3.94 | 0.78 |
| | 1102 | 12.46 | 3.95 | 0.80 |
| | 1202 | 18.35 | 4.66 | 0.69 |
| | 1302 | 26.77 | 4.33 | 0.70 |
| | 1501 | 44.39 | 4.54 | 0.74 |
| **P2** | 25 | 200.85 | 2.84 | 1.12 |
| | 43 | 210.12 | 2.87 | 1.13 |
| | 70 | 106.75 | 2.87 | 1.13 |
| | 100 | 0.85 | 2.53 | 1.18 |
| | 120 | 0.84 | 2.53 | 1.18 |
| | 150 | 0.88 | 2.72 | 1.18 |
| | 175 | 0.95 | 2.74 | 1.24 |
| | 200 | 0.98 | 2.71 | 1.18 |
| | 250 | 1.00 | 2.49 | 1.20 |
| | 300 | 1.04 | 2.52 | 1.17 |
| | 350 | 1.14 | 3.13 | 1.04 |
| | 500 | 1.27 | 3.21 | 1.06 |
| | 725 | 1.56 | 3.81 | 0.93 |
| | 1000 | 11.29 | 4.14 | 0.80 |
| | 1500 | 47.77 | 4.81 | 0.66 |
| | 2000 | 80.61 | 4.95 | 0.66 |
| | 2500 | 101.19 | 5.02 | 0.64 |
| | 3000 | 112.92 | 5.01 | 0.60 |
| | 3500 | 121.00 | 4.97 | 0.61 |
| **Station 15** | 101 | 1.57 | 2.88 | 1.17 |
| | 150 | 0.73 | 2.74 | 1.26 |

| | | | | |
|---|---|---|---|---|
| | 201 | 0.72 | 2.69 | 1.25 |
| | 251 | 0.78 | 2.80 | 1.14 |
| | 301 | 0.80 | 3.14 | 1.06 |
| | 700 | 1.15 | 3.70 | 0.99 |
| | 800 | 2.34 | 3.81 | 0.88 |
| | 1001 | 15.16 | 4.23 | 0.76 |
| **P3** | 65 | 186.06 | 2.67 | 1.04 |
| | 111 | 3.36 | 2.33 | 1.28 |
| | 141 | 0.87 | 2.26 | 1.21 |
| | 192 | 0.78 | 2.32 | 1.06 |
| | 252 | 0.95 | 2.41 | 1.17 |
| | 302 | 0.94 | 2.57 | 1.05 |
| | 325 | 0.94 | 2.62 | 0.95 |
| | 401 | 0.95 | 2.75 | 1.05 |
| | 501 | 1.01 | 2.98 | 1.01 |
| | 599 | 1.33 | 3.05 | 0.88 |
| | 1003 | 7.53 | 4.11 | 0.85 |
| | 1504 | 39.65 | 4.60 | 0.70 |
| | 2001 | 79.95 | 4.74 | 0.69 |
| | 2501 | 98.45 | 4.82 | 0.62 |
| | 2999 | 109.54 | 4.84 | 0.60 |
| **Station 23** | 20 | 222.52 | 3.06 | 0.98 |
| | 50 | 231.18 | 3.06 | 1.05 |
| | 100 | 153.82 | 2.91 | 0.96 |
| | 125 | 92.63 | 2.87 | 1.10 |
| | 150 | 54.68 | 2.62 | 1.14 |
| | 175 | 42.89 | 2.65 | 1.13 |

| | | | | |
|---|---|---|---|---|
| | 200 | 26.52 | 2.74 | 1.05 |
| | 300 | 33.30 | 3.07 | 1.09 |
| | 400 | 16.61 | 3.14 | 1.09 |
| | 500 | 7.76 | 3.36 | 1.08 |

**Figure 3.2 Full water column profiles of a) total dissolved Cr concentration and b) its isotopic composition at stations P1, P2 and P3**

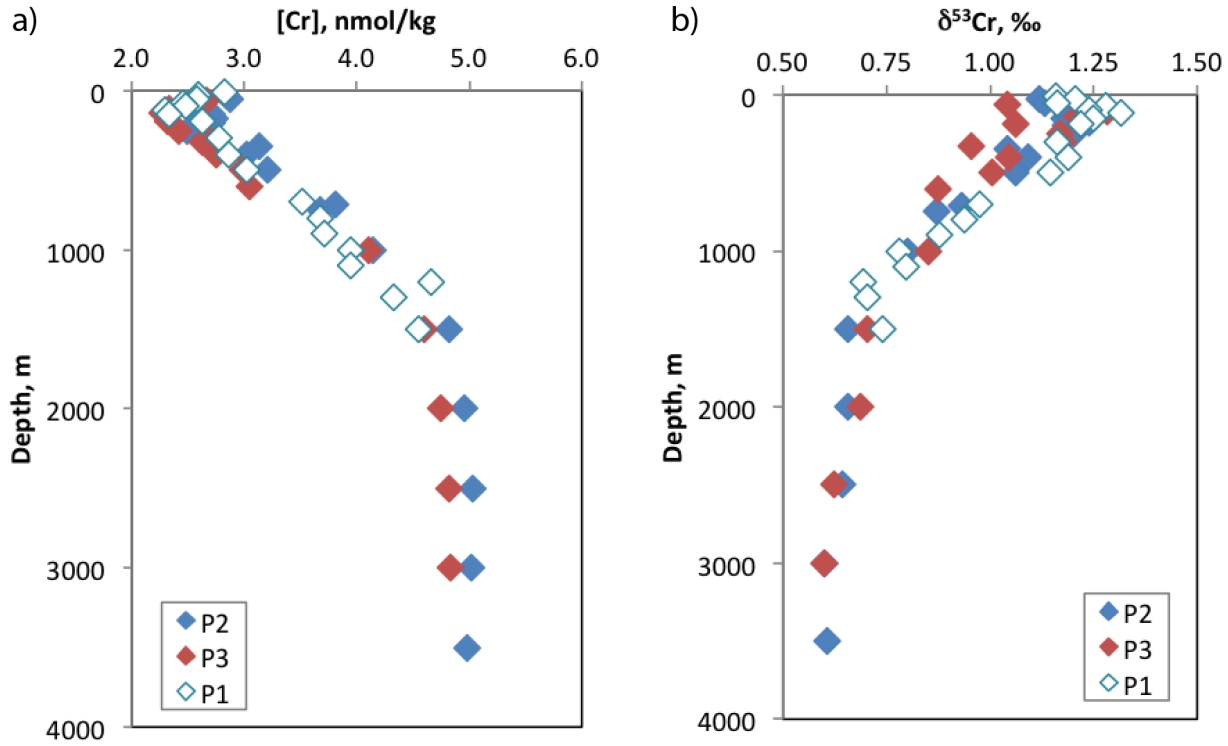

**Figure 3.3 Profiles of a) total dissolved Cr concentration and b) its isotopic composition at stations P1, P2 and P3, coring station, 15 and 23 in the upper 1000m**

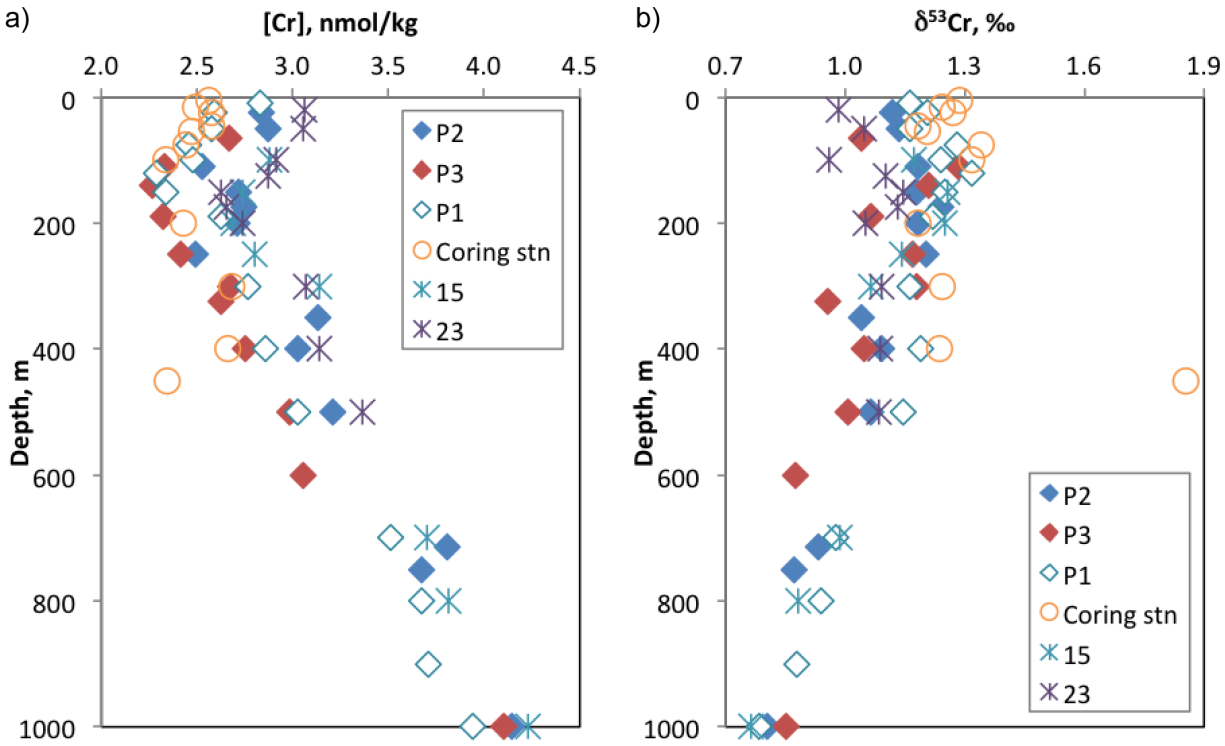

**Table 3.3 Cr(III) concentration and isotope data from RR1805 and KM1920**

| Cruise | Depth (m) | [Cr(III)] (nmol/kg) | $\delta^{53}$Cr(III) (‰) |
|---|---|---|---|
| **RR1805** | 120 | 1.25 | -0.09 |
| | 150 | 1.42 | 0.16 |
| | 175 | 1.54 | 0.52 |
| | 200 | 1.66 | 0.20 |
| | 250 | 1.59 | 0.31 |
| | 350 | 1.29 | 0.11 |
| | 500 | 0.74 | -0.14 |
| **KM1920** | 25 | 0.19 | |
| | 70 | 0.22 | -0.04 |
| | 100 | 0.42 | -0.07 |
| | 150 | 1.20 | 0.29 |
| | 180 | 1.33 | 0.39 |
| | 225 | 1.28 | |
| | 240 | 1.41 | 0.24 |
| | 250 | 1.41 | |
| | 300 | 1.23 | 0.17 |
| | 300 | 1.27 | |
| | 500 | 0.63 | |
| | 600 | 0.52 | |
| | 725 | 0.44 | -0.12 |
| | 1000 | 0.30 | -0.01 |

**Figure 3.4 Cr(III) concentration and isotope profiles of RR1805 and KM1920**

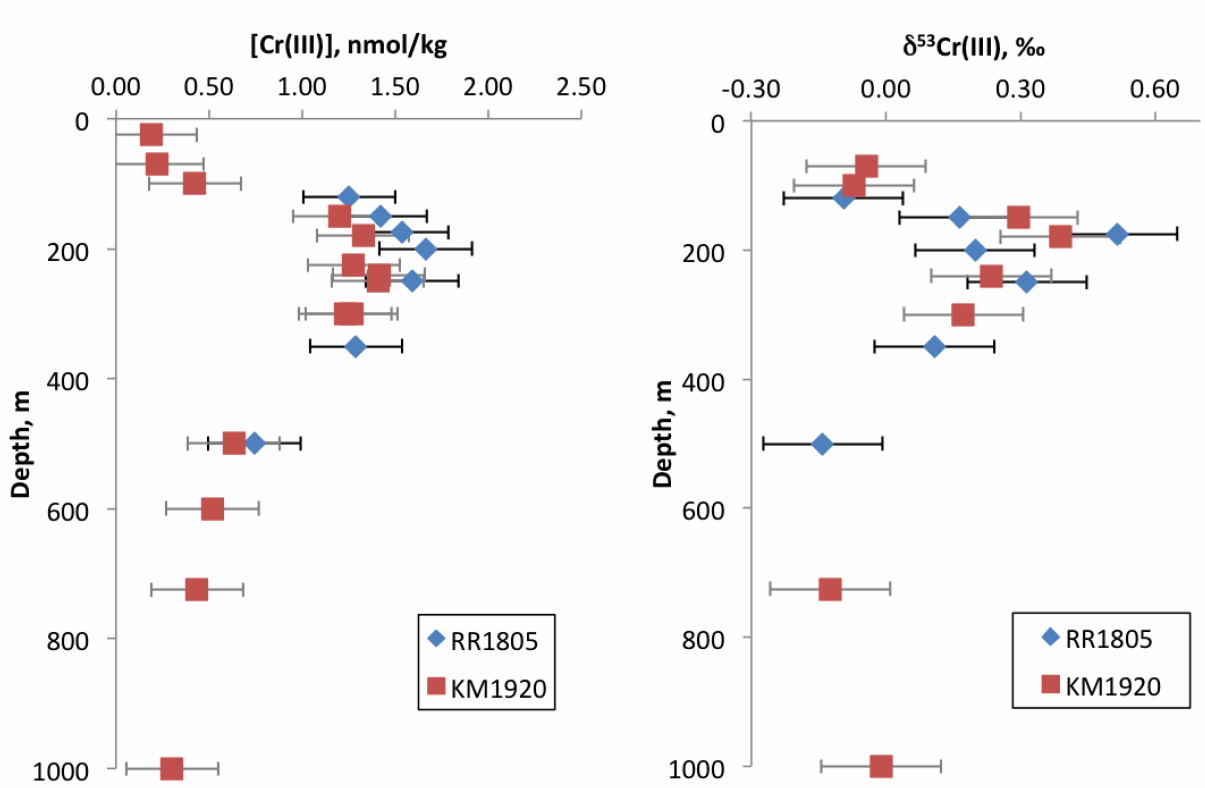

**Table 3.4 Cr concentration and isotopic composition of Cr(III) and Cr(VI)**

| | | | Cr(III) | | Measured Cr(VI) | | Calculated Cr(VI) | |
|---|---|---|---|---|---|---|---|---|
| **Station** | **Depth (m)** | **CTD Oxygen (µmol/kg)** | **[Cr] (nmol/kg)** | **$\delta^{53}$Cr (‰)** | **[Cr] (nmol/kg)** | **$\delta^{53}$Cr (‰)** | **[Cr] (nmol/kg)** | **$\delta^{53}$Cr (‰)** |
| **P2** | 25 | 200.85 | 0.19 | | | | 2.65 | |
| | 70 | 106.75 | 0.22 | -0.04 | | | 2.65 | 1.23 |
| | 100 | 0.85 | 0.42 | -0.07 | 1.96 | 1.65 | 2.10 | 1.44 |
| | 120 | 0.84 | 1.25 | -0.09 | | | 1.27 | 2.44 |
| | 150 | 0.88 | 1.42 | 0.16 | 1.03 | 2.89 | 1.30 | 2.29 |
| | 175 | 0.95 | 1.54 | 0.52 | 0.76 | 3.20 | 1.20 | 2.16 |
| | 200 | 0.98 | 1.66 | 0.20 | 0.95 | 2.23 | 1.04 | 2.75 |
| | 240 | 0.93 | 1.41 | 0.24 | | | 1.07 | 2.48 |
| | 250 | 1.00 | 1.59 | 0.31 | 0.96 | 2.98 | 0.90 | 2.79 |
| | 300 | 1.04 | 1.23 | 0.17 | | | 1.29 | 2.13 |
| | 350 | 1.14 | 1.29 | 0.11 | 1.47 | 2.49 | 1.84 | 1.69 |
| | 500 | 1.27 | 0.74 | -0.14 | 2.28 | 1.68 | 2.46 | 1.43 |
| | 600 | | 0.52 | | | | 2.99 | |
| | 725 | 1.56 | 0.44 | -0.12 | | | 3.37 | 1.07 |
| | 1000 | 11.29 | 0.30 | -0.01 | | | 3.84 | 0.87 |
| **P3** | 140 | 0.87 | 0.66 | 0.32 | 1.46 | 2.05 | 1.60 | 1.58 |
| | 190 | 0.78 | 1.10 | 0.51 | 1.04 | 2.95 | 1.22 | 1.56 |
| | 250 | 0.95 | 1.06 | 0.35 | | | 1.36 | 1.81 |
| | 325 | 0.94 | 0.93 | 0.25 | 1.42 | 2.31 | 1.69 | 1.34 |
| | 400 | 0.95 | 0.82 | -0.11 | | | 1.94 | 1.53 |
| | 500 | 1.01 | 0.63 | -0.47 | 2.43 | 1.57 | 2.36 | 1.40 |
| | 600 | 1.33 | 0.46 | -0.17 | | | 2.59 | 1.06 |
| **P1** | 150 | 0.78 | 1.26 | -0.15 | | | 1.07 | 2.89 |
| | 200 | 0.83 | 1.26 | 0.10 | | | 1.39 | 2.23 |
| | 300 | 0.85 | 1.41 | 0.06 | | | 1.36 | 2.40 |
| | 500 | 0.93 | 0.98 | 0.27 | | | 2.05 | 1.58 |

**Figure 3.5 [Cr] and $\delta^{53}$Cr profiles of different dissolved Cr species in the upper 1000m of stations P1, P2 and P3**

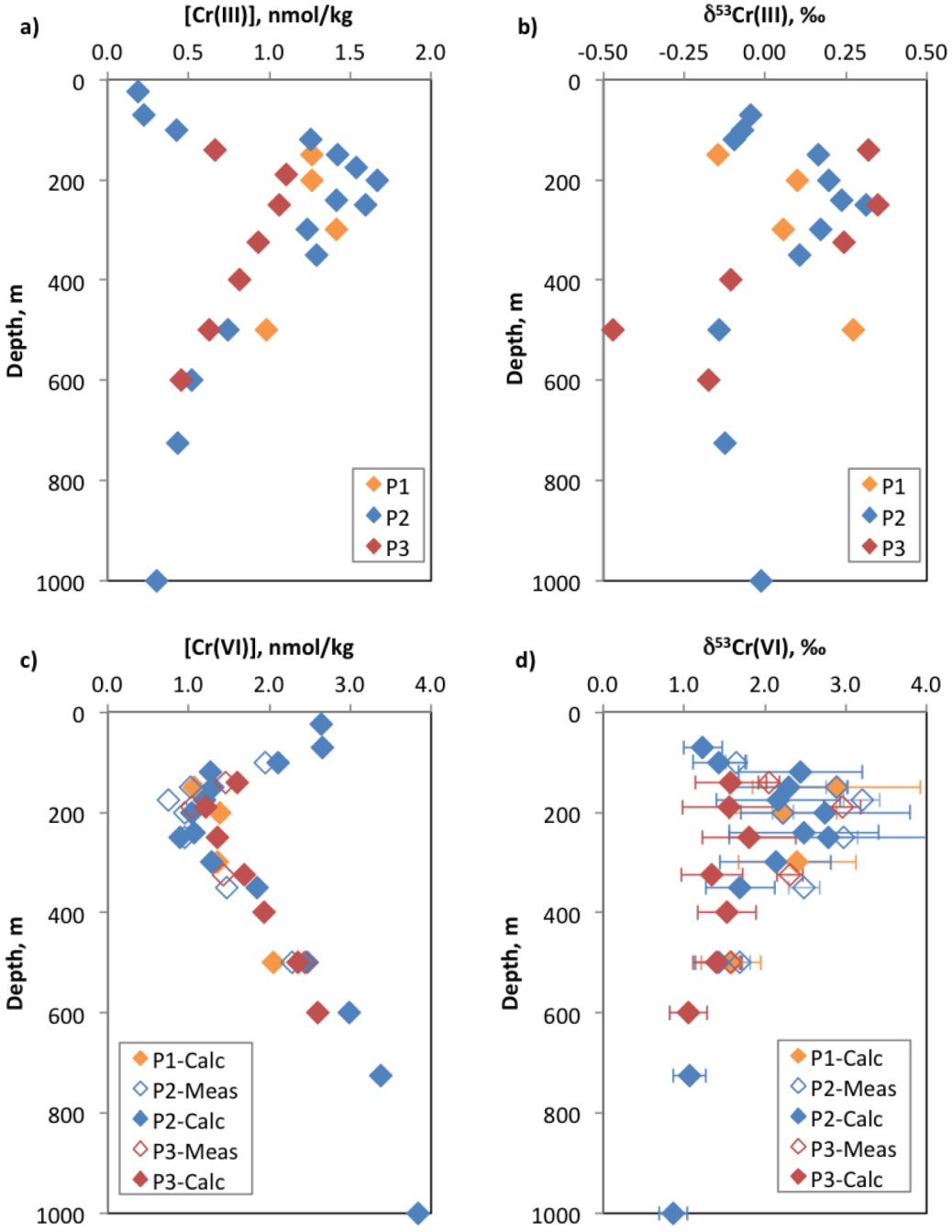

**Figure 3.6 $\delta^{53}$Cr versus ln[Cr] in nmol/kg of all ETNP ODZ stations**

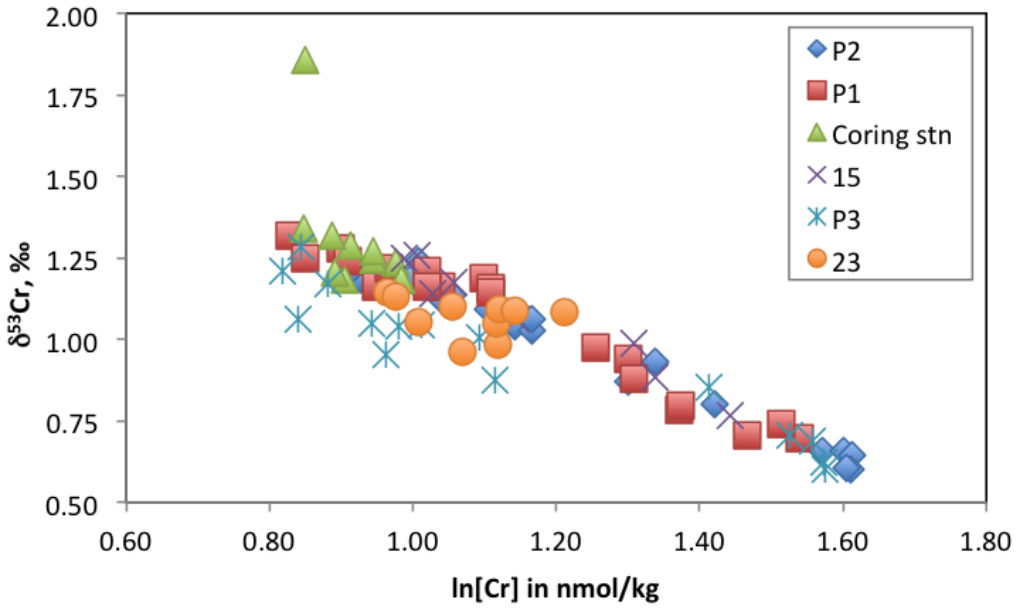


**Figure 3.7 $\delta^{53}$Cr versus ln[Cr] in nmol/kg of ETNP ODZ stations with linear regression**

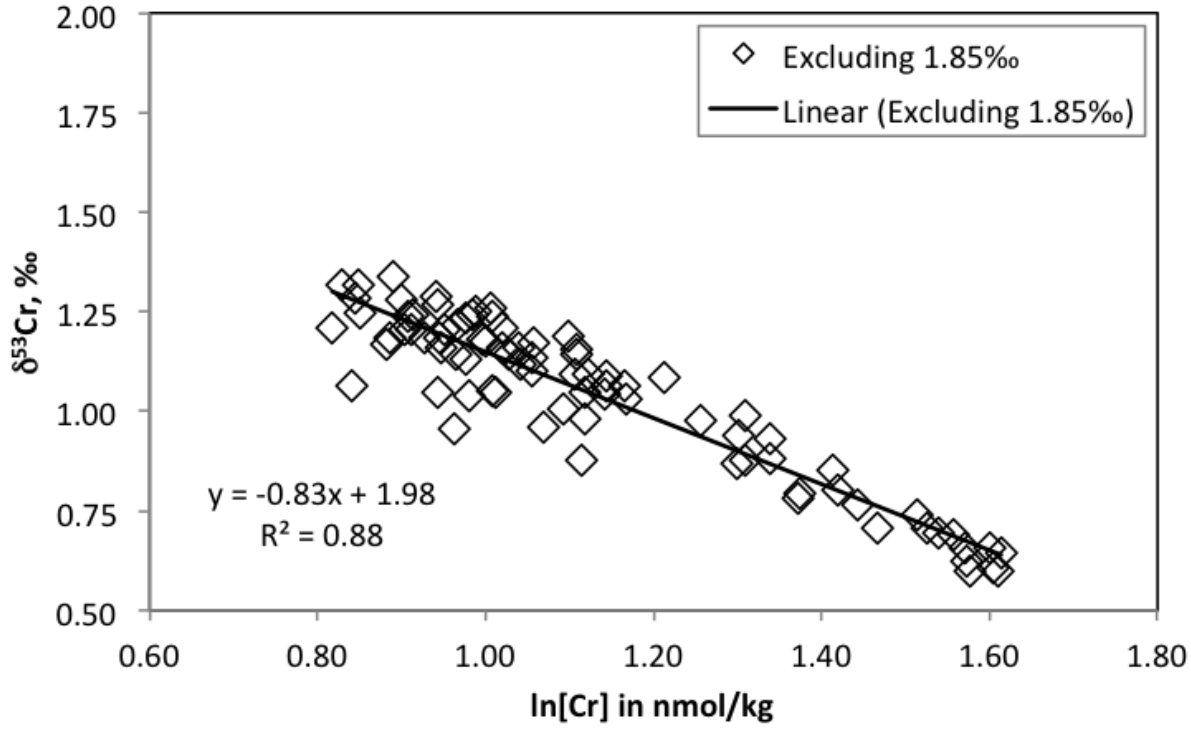

**Figure 3.8 Progressive closed-system conversion of Cr(VI) to Cr(III) with constant fractionation**

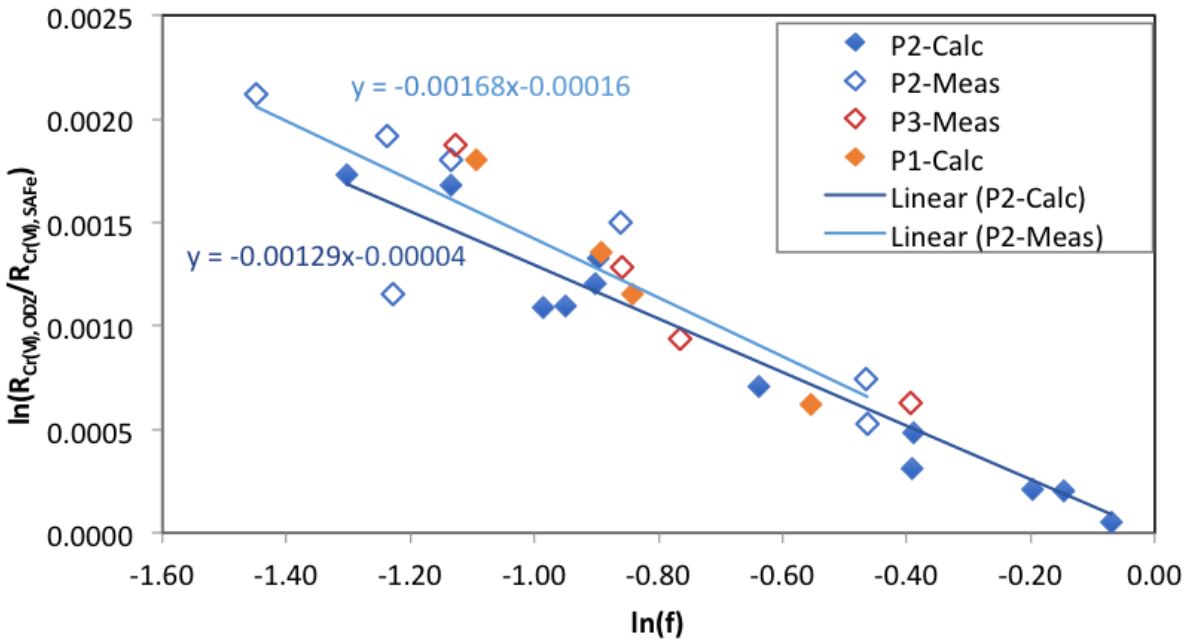

**Figure 3.9 A stepwise illustration of Cr isotope evolution at the Cr(III) maximum of station P2**

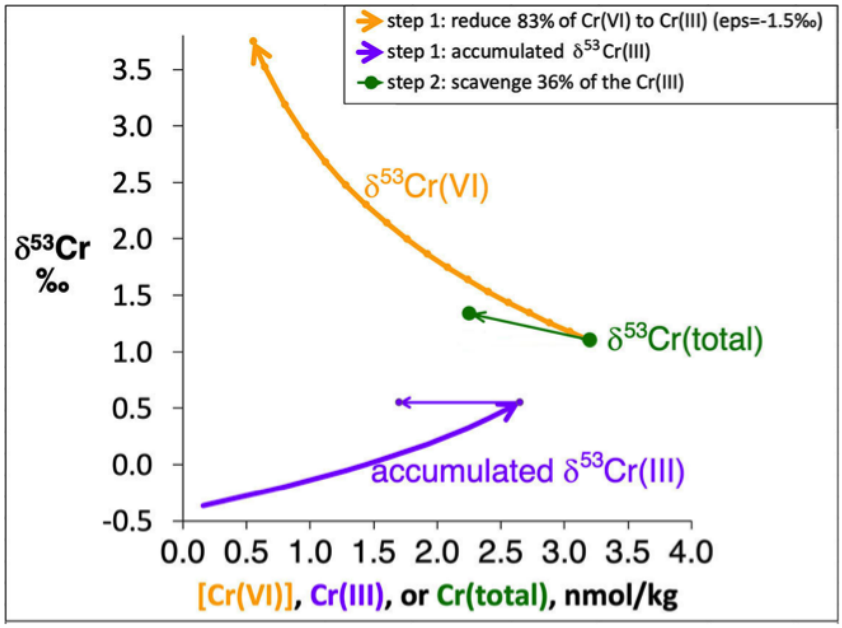

**Figure 3.10 Nitrite profiles at stations P2 and P3 from cruise KM1920**

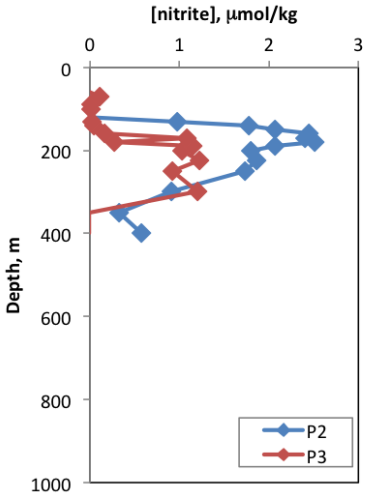

**Figure 3.11 Total dissolved Cr concentration and isotopic composition of ODZ stations (P1, P2, P3, 15, 23, coring station) compared with SAFe station at isopycnal surfaces**

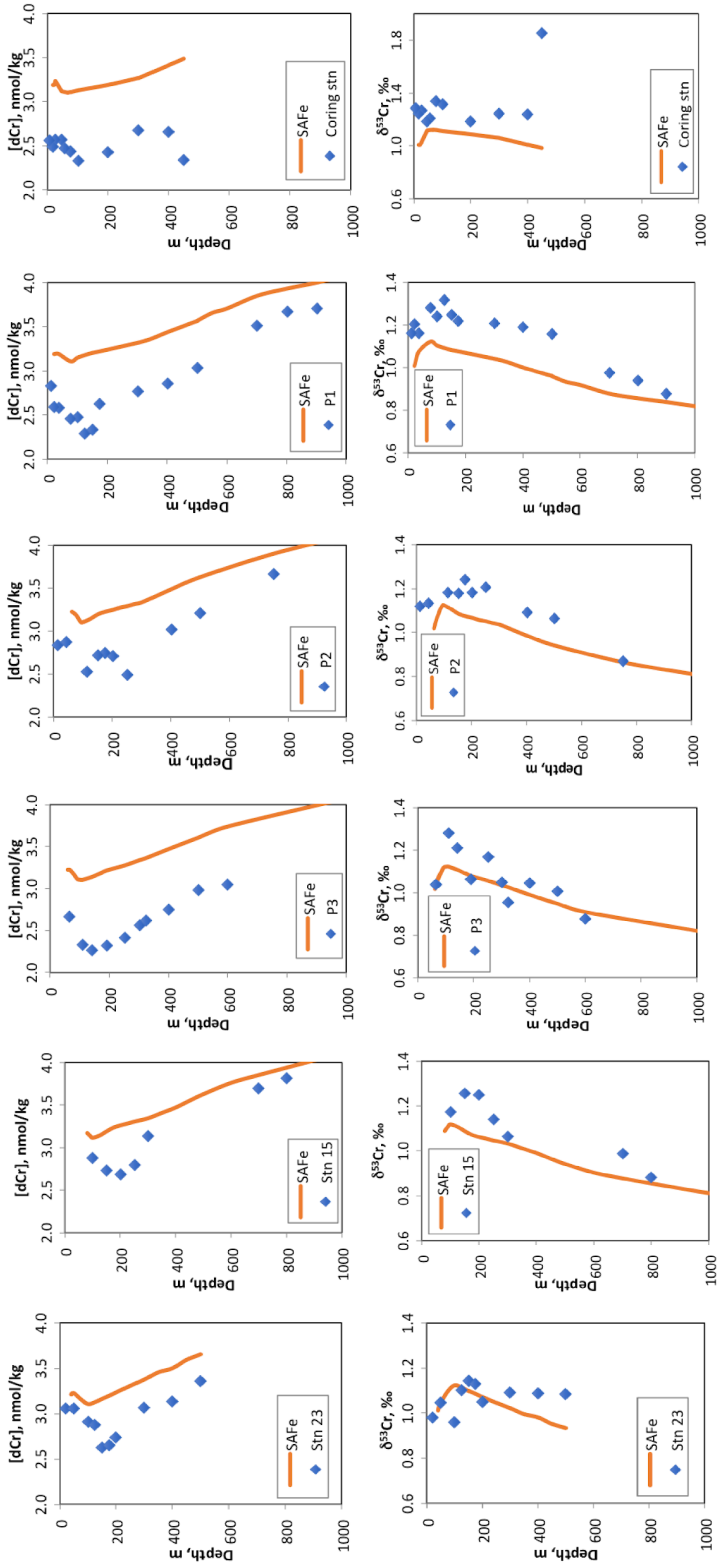

**Figure 3.12 a) Total dissolved Cr concentration and b) isotopic composition of ODZ stations (P1, P2, P3, 15, 23, coring station) against potential density**

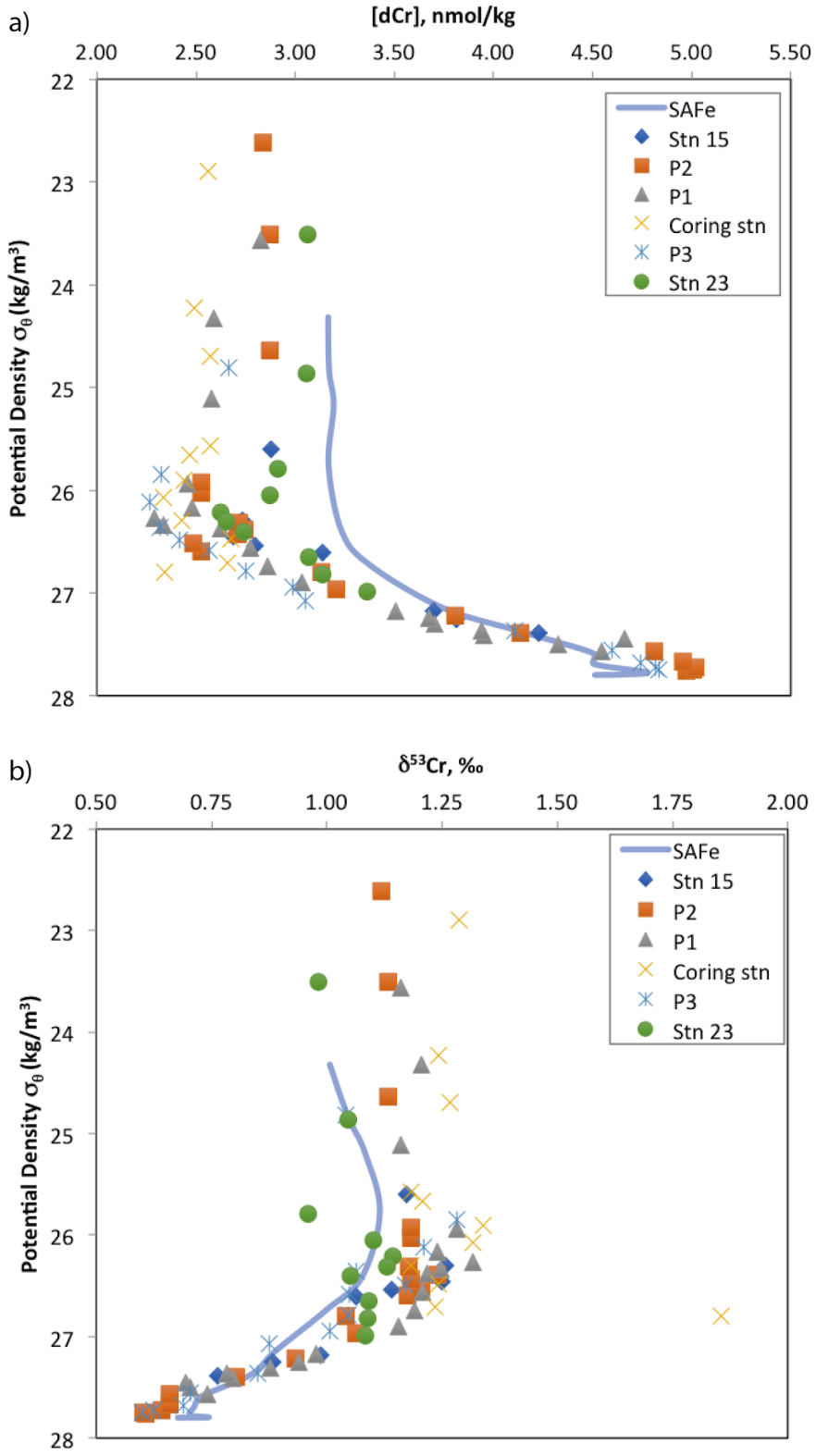

**Figure 3.13 T-S diagram of ODZ stations (P1, P2, P3, 15, 23, coring station)**

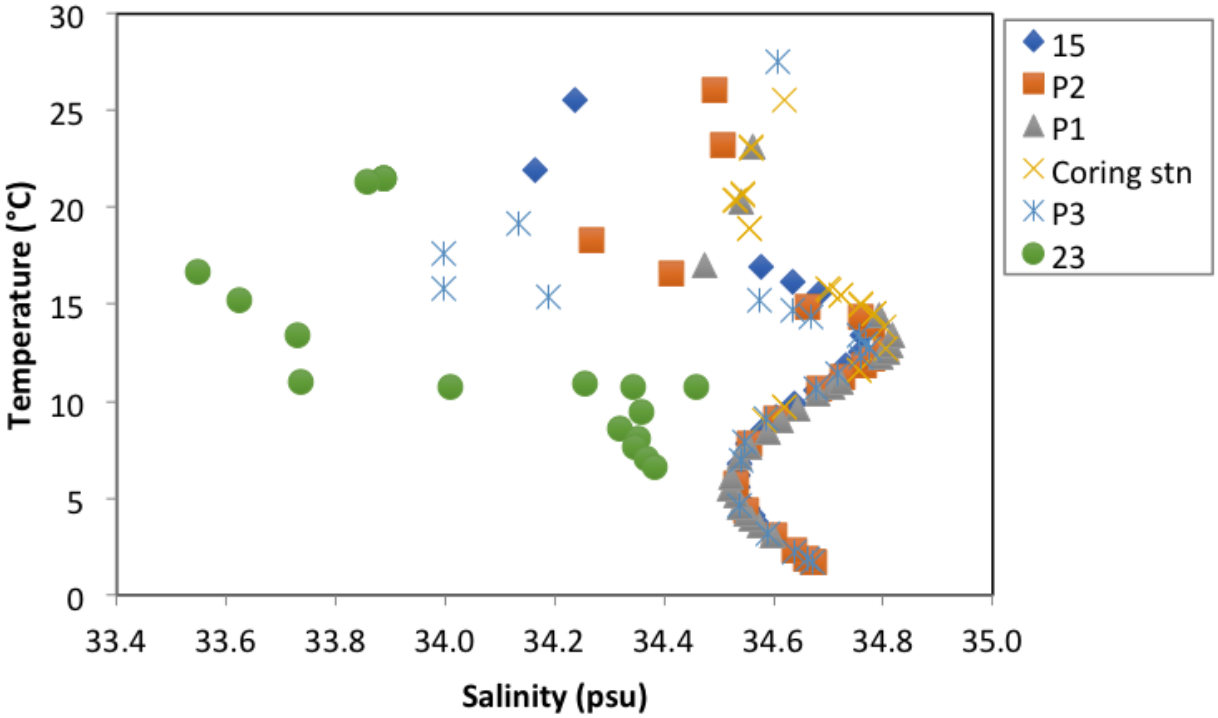


**Figure 3.14 Temporal variability of a) oxygen and b) nitrite profiles at station P3**

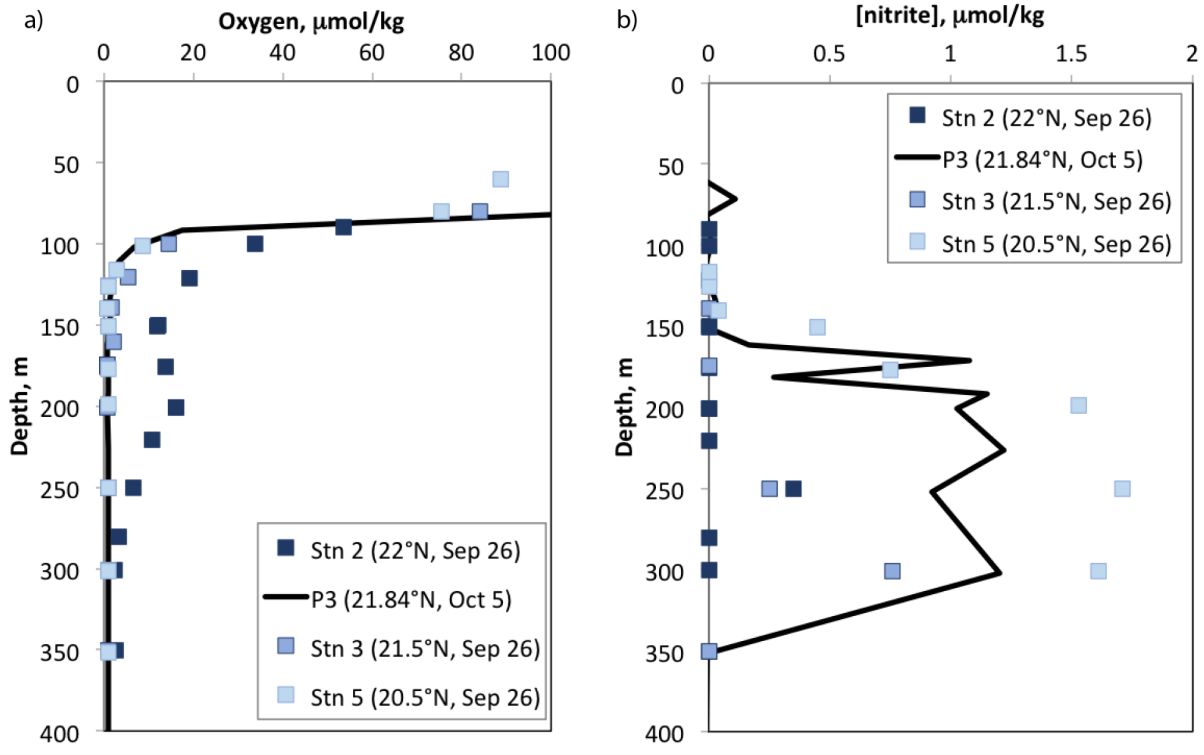

**Table 3.5 [Cr] and $\delta^{53}Cr$ of the calculated scavenged Cr**

| Station | Depth (m) | $[Cr]_{scavenged}$ (nmol/kg) | $\delta^{53}Cr_{scavenged}$ (‰) | Propagated SD of $\delta^{53}Cr_{scavenged}$ |
|---|---|---|---|---|
| P2 | 70 | 0.35 | 0.08 | 0.98 |
| | 100 | 0.58 | 0.85 | 0.63 |
| | 120 | 0.60 | 0.83 | 0.61 |
| | 150 | 0.48 | 0.56 | 0.74 |
| | 175 | 0.48 | 0.14 | 0.72 |
| | 200 | 0.54 | 0.49 | 0.66 |
| | 250 | 0.80 | 0.58 | 0.44 |
| | 300 | 0.81 | 0.60 | 0.44 |
| | 350 | 0.35 | 0.48 | 1.04 |
| | 500 | 0.42 | 0.01 | 0.87 |
| P1 | 25 | 0.60 | 0.16 | 0.56 |
| | 50 | 0.61 | 0.71 | 0.58 |
| | 75 | 0.65 | 0.52 | 0.54 |
| | 100 | 0.67 | 0.60 | 0.53 |
| | 120 | 0.89 | 0.51 | 0.39 |
| | 150 | 0.87 | 0.64 | 0.41 |
| | 190 | 0.60 | 0.45 | 0.59 |
| | 300 | 0.55 | 0.44 | 0.65 |
| | 400 | 0.58 | 0.07 | 0.61 |
| | 500 | 0.54 | -0.06 | 0.68 |
| | 700 | 0.34 | -0.14 | 1.12 |
| | 800 | 0.26 | -0.32 | 1.52 |
| | 900 | 0.29 | 0.35 | 1.37 |
| Stn 15 | 101 | 0.24 | 0.44 | 1.50 |
| | 150 | 0.45 | 0.07 | 0.76 |
| | 201 | 0.58 | 0.19 | 0.60 |
| | 251 | 0.51 | 0.52 | 0.70 |
| | 301 | 0.21 | 0.56 | 1.78 |
| Coring stn | 16 | 0.70 | 0.17 | 0.48 |
| | 26 | 0.66 | 0.08 | 0.52 |

| | | | | |
|---|---|---|---|---|
| | 47 | 0.54 | 0.81 | 0.67 |
| | 56 | 0.64 | 0.79 | 0.56 |
| | 76 | 0.67 | 0.33 | 0.51 |
| | 102 | 0.80 | 0.51 | 0.44 |
| | 200 | 0.76 | 0.78 | 0.47 |
| | 300 | 0.59 | 0.24 | 0.59 |
| | 400 | 0.76 | 0.21 | 0.46 |
| | 449 | 1.15 | -0.79 | 0.35 |
| P3 | 65 | 0.56 | 1.04 | 0.68 |
| | 111 | 0.78 | 0.64 | 0.45 |
| | 141 | 0.87 | 0.85 | 0.41 |
| | 192 | 0.90 | 1.12 | 0.42 |
| | 252 | 0.86 | 0.74 | 0.42 |
| | 302 | 0.77 | 0.99 | 0.49 |
| | 325 | 0.75 | 1.27 | 0.54 |
| | 401 | 0.72 | 0.78 | 0.51 |
| | 501 | 0.62 | 0.67 | 0.60 |
| | 599 | 0.69 | 1.06 | 0.58 |
| Stn 23 | 125 | 0.25 | 1.27 | 1.62 |
| | 150 | 0.54 | 0.88 | 0.69 |
| | 175 | 0.54 | 0.87 | 0.68 |
| | 200 | 0.50 | 1.18 | 0.80 |
| | 300 | 0.31 | 0.33 | 1.17 |
| | 400 | 0.36 | 0.05 | 1.00 |
| | 500 | 0.29 | -0.79 | 1.37 |
| **Weighted Average** | | | 0.51 | |
| **SD** | | | 0.44 | |

**Figure 3.15 a) The concentration and b) isotopic composition of scavenged Cr at ODZ stations (P1, P2, P3, 15, 23, coring station) against potential density**

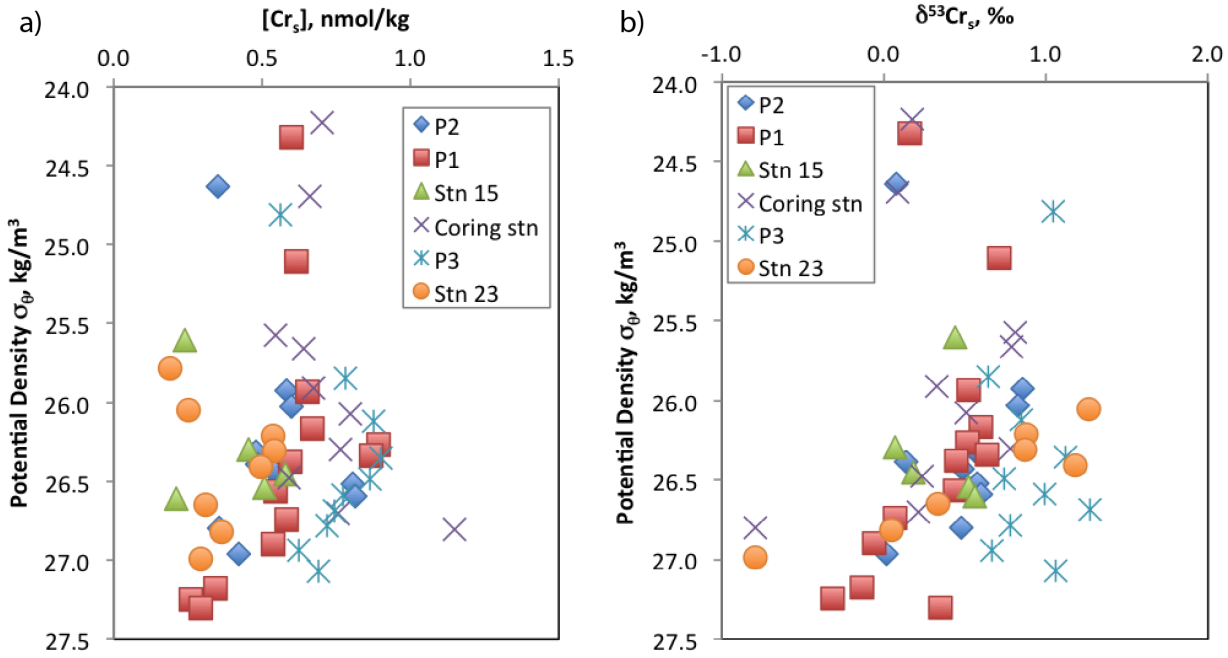


**Figure 3.16 The concentration and isotopic composition of scavenged Cr at ODZ stations (P1, P2, P3, 15, 23, coring station)**

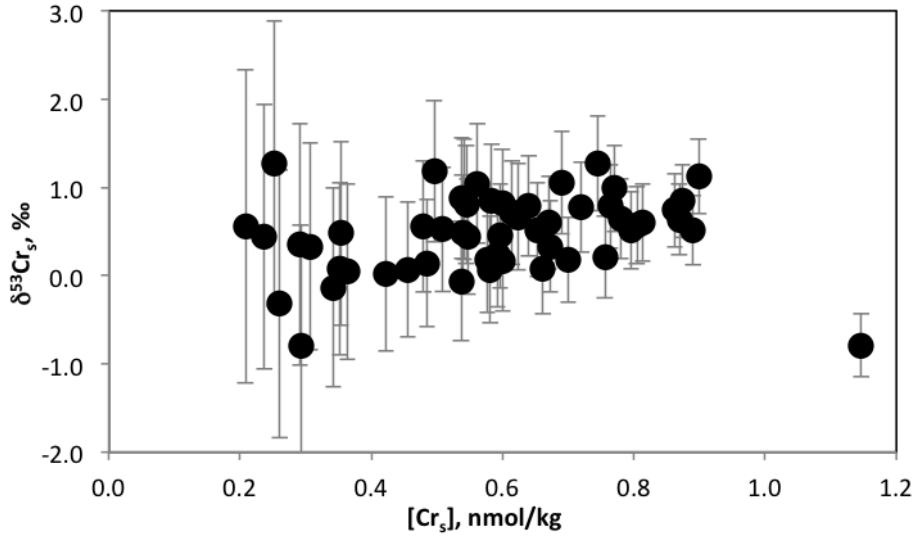

**References**


Basu, A., & Johnson, T. M. (2012). Determination of hexavalent chromium reduction using Cr stable isotopes: isotopic fractionation factors for permeable reactive barrier materials. *Environmental science & technology*, *46*(10), 5353-5360.

Bauer, K. W., Gueguen, B., Cole, D. B., Francois, R., Kallmeyer, J., Planavsky, N., & Crowe, S. A. (2018). Chromium isotope fractionation in ferruginous sediments. *Geochimica et Cosmochimica Acta*, *223*, 198-215.

Bauer, K. W., Cole, D. B., Asael, D., Francois, R., Calvert, S. E., Poulton, S. W., ... & Crowe, S. A. (2019). Chromium isotopes in marine hydrothermal sediments. *Chemical Geology*, *529*, 119286.

Bolster, K. M., Heller, M. I., & Moffett, J. W. (2018). Determination of iron (II) by chemiluminescence using masking ligands to distinguish interferences. *Limnology and Oceanography: Methods*, *16*(11), 750-759.

Bryan, B. A., Shearer, G., Skeeters, J. L., & Kohl, D. H. (1983). Variable expression of the nitrogen isotope effect associated with denitrification of nitrite. *Journal of Biological Chemistry*, *258*(14), 8613-8617.

Castro, R., Durazo, R., Mascarenhas, A., Collins, C. A., & Trasviña, A. (2006). Thermohaline variability and geostrophic circulation in the southern portion of the Gulf of California. *Deep Sea Research Part I: Oceanographic Research Papers*, *53*(1), 188-200.

Checkley Jr, D. M., & Barth, J. A. (2009). Patterns and processes in the California Current System. *Progress in Oceanography*, *83*(1-4), 49-64.

Cranston, R. E., & Murray, J. W. (1978). The determination of chromium species in natural waters. *Analytica Chimica Acta*, *99*(2), 275-282.

Cutter, G. A., Moffett, J. W., Nielsdóttir, M. C., & Sanial, V. (2018). Multiple oxidation state trace elements in suboxic waters off Peru: In situ redox processes and advective/diffusive horizontal transport. *Marine Chemistry*, *201*, 77-89.

Døssing, L. N., Dideriksen, K., Stipp, S. L. S., & Frei, R. (2011). Reduction of hexavalent chromium by ferrous iron: A process of chromium isotope fractionation and its relevance to natural environments. *Chemical Geology*, *285*(1-4), 157-166.

Ellis, A. S., Johnson, T. M., & Bullen, T. D. (2002). Chromium isotopes and the fate of hexavalent chromium in the environment. *Science*, *295*(5562), 2060-2062.

Evans, N., Boles, E., Kwiecinski, J. V., Mullen, S., Wolf, M., Devol, A. H., ... & Moffett, J. W. (2020). The role of water masses in shaping the distribution of redox active compounds in the Eastern Tropical North Pacific oxygen deficient zone and influencing low oxygen concentrations in the eastern Pacific Ocean. *Limnology and Oceanography*, *65*(8), 1688-1705.

Fiedler, P. C., & Talley, L. D. (2006). Hydrography of the eastern tropical Pacific: A review. *Progress in Oceanography*, *69*(2-4), 143-180.

Fuchsman, C. A., Devol, A. H., Casciotti, K. L., Buchwald, C., Chang, B. X., & Horak, R. E. (2018). An N isotopic mass balance of the Eastern Tropical North Pacific oxygen deficient zone. *Deep Sea Research Part II: Topical Studies in Oceanography*, *156*, 137-147.

Gangopadhyay, A., Lermusiaux, P. F., Rosenfeld, L., Robinson, A. R., Calado, L., Kim, H. S., ... & Haley Jr, P. J. (2011). The California Current system: A multiscale overview and the development of a feature-oriented regional modeling system (FORMS). *Dynamics of Atmospheres and Oceans*, *52*(1-2), 131-169.

Garfield, P. C., Packard, T. T., Friederich, G. E., & Codispoti, L. A. (1983). A subsurface particle maximum layer and enhanced microbial activity in the secondary nitrite maximum of the northeastern tropical Pacific Ocean. *Journal of marine research*, *41*(4), 747-768.

Goring-Harford, H. J., Klar, J. K., Pearce, C. R., Connelly, D. P., Achterberg, E. P., & James, R. H. (2018). Behaviour of chromium isotopes in the eastern sub-tropical Atlantic Oxygen Minimum Zone. *Geochimica et Cosmochimica Acta*, *236*, 41-59.

Janssen, D. J., Rickli, J., Quay, P. D., White, A. E., Nasemann, P., & Jaccard, S. L. (2020). Biological control of chromium redox and stable isotope composition in the surface ocean. *Global biogeochemical cycles*, *34*(1), e2019GB006397.

Jeandel, C., & Minster, J. F. (1987). Chromium behavior in the ocean: Global versus regional processes. *Global Biogeochemical Cycles*, *1*(2), 131-154.

Kessler, W. S. (2006). The circulation of the eastern tropical Pacific: A review. *Progress in Oceanography*, *69*(2-4), 181-217.

Kitchen, J. W., Johnson, T. M., Bullen, T. D., Zhu, J., & Raddatz, A. (2012). Chromium isotope fractionation factors for reduction of Cr (VI) by aqueous Fe (II) and organic molecules. *Geochimica et Cosmochimica Acta*, *89*, 190-201.

Lavín, M. F., & Marinone, S. G. (2003). An overview of the physical oceanography of the Gulf of California. *Nonlinear processes in geophysical fluid dynamics*, 173-204.

Moffett, J. W., Goepfert, T. J., & Naqvi, S. W. A. (2007). Reduced iron associated with secondary nitrite maxima in the Arabian Sea. *Deep Sea Research Part I: Oceanographic Research Papers*, *54*(8), 1341-1349.

Moos, S. B., & Boyle, E. A. (2019). Determination of accurate and precise chromium isotope ratios in seawater samples by MC-ICP-MS illustrated by analysis of SAFe Station in the North Pacific Ocean. *Chemical Geology*, *511*, 481-493.

Moos, S. B., Boyle, E. A., Altabet, M. A., & Bourbonnais, A. (2020). Investigating the cycling of chromium in the oxygen deficient waters of the Eastern Tropical North Pacific Ocean and the Santa Barbara Basin using stable isotopes. *Marine Chemistry*, *221*, 103756.

Murray, J. W., Spell, B., & Paul, B. (1983). The contrasting geochemistry of manganese and chromium in the eastern tropical Pacific Ocean. In *Trace metals in sea water* (pp. 643-669). Springer, Boston, MA.

Nasemann, P., Janssen, D. J., Rickli, J., Grasse, P., Frank, M., & Jaccard, S. L. (2020). Chromium reduction and associated stable isotope fractionation restricted to anoxic shelf waters in the Peruvian Oxygen Minimum Zone. *Geochimica et cosmochimica acta*, *285*, 207-224.

Ohnemus, D. C., Rauschenberg, S., Cutter, G. A., Fitzsimmons, J. N., Sherrell, R. M., & Twining, B. S. (2017). Elevated trace metal content of prokaryotic communities associated with marine oxygen deficient zones. *Limnology and Oceanography*, *62*(1), 3-25.

Ohnemus, D. C., Lam, P. J., & Twining, B. S. (2018). Optical observation of particles and responses to particle composition in the GEOTRACES GP16 section. *Marine Chemistry*, *201*, 124-136.

Pettine, M., D'ottone, L., Campanella, L., Millero, F. J., & Passino, R. (1998). The reduction of chromium (VI) by iron (II) in aqueous solutions. *Geochimica et cosmochimica acta*, *62*(9), 1509-1519.

Portela, E., Beier, E., Barton, E. D., Castro, R., Godínez, V., Palacios-Hernández, E., ... & Trasviña, A. (2016). Water masses and circulation in the tropical Pacific off central Mexico and surrounding areas. *Journal of Physical Oceanography*, *46*(10), 3069-3081.

Reynolds, B. C., Frank, M., & Halliday, A. N. (2006). Silicon isotope fractionation during nutrient utilization in the North Pacific. *Earth and Planetary Science Letters*, *244*(1-2), 431-443.

Rickli, J., Janssen, D. J., Hassler, C., Ellwood, M. J., & Jaccard, S. L. (2019). Chromium biogeochemistry and stable isotope distribution in the Southern Ocean. *Geochimica et cosmochimica acta, 262*, 188-206.

Rue, E. L., Smith, G. J., Cutter, G. A., & Bruland, K. W. (1997). The response of trace element redox couples to suboxic conditions in the water column. *Deep Sea Research Part I: Oceanographic Research Papers*, *44*(1), 113-134.

Scheiderich, K., Amini, M., Holmden, C., & Francois, R. (2015). Global variability of chromium isotopes in seawater demonstrated by Pacific, Atlantic, and Arctic Ocean samples. *Earth and Planetary Science Letters, 423*, 87-97.

Sedlak, D. L., & Chan, P. G. (1997). Reduction of hexavalent chromium by ferrous iron. *Geochimica et Cosmochimica Acta*, *61*(11), 2185-2192.

Sikora, E. R., Johnson, T. M., & Bullen, T. D. (2008). Microbial mass-dependent fractionation of chromium isotopes. *Geochimica et Cosmochimica Acta*, *72*(15), 3631-3641.

Wang, X., Glass, J. B., Reinhard, C. T., & Planavsky, N. J. (2019). Species‐dependent chromium isotope fractionation across the eastern tropical North Pacific oxygen minimum zone. *Geochemistry, Geophysics, Geosystems*, *20*(5), 2499-2514.

Whitmire, A. L., Letelier, R. M., Villagrán, V., & Ulloa, O. (2009). Autonomous observations of in vivo fluorescence and particle backscattering in an oceanic oxygen minimum zone. *Optics Express*, *17*(24), 21992-22004.

Wyrtki, K. (1967). Equatorial Pacific Ocean1. *Int. J. Oceanol. & Limnol. Vol*, *1*(2), 117-147.

Zhang, Q., Amor, K., Galer, S. J., Thompson, I., & Porcelli, D. (2019). Using stable isotope fractionation factors to identify Cr (VI) reduction pathways: Metal-mineral-microbe interactions. *Water research*, *151*, 98-109.

Zink, S., Schoenberg, R., & Staubwasser, M. (2010). Isotopic fractionation and reaction kinetics between Cr (III) and Cr (VI) in aqueous media. Geochimica et Cosmochimica Acta, 74(20), 5729-5745

# Chapter 4: Chromium isotopes in other oxygen deficient zones: Eastern Tropical South Pacific and Arabian Sea

## 4.1 Introduction

Both the Eastern Tropical South Pacific (ETSP) and the Arabian Sea are large ODZs in the global ocean. High productivity due to strong upwelling are featured in both ODZs (Barber et al., 2001; Kadko et al., 2017). Active nitrogen cycling including denitrification and anaerobic ammonium oxidation (anammox) have been reported (Codispoti and Christensen, 1985; Devol et al., 2006; Ward et al., 2009; Babbin et al., 2017). Some reduced species (e.g. Fe(II), iodide) are also at higher levels than in the oxic oceans (Cutter et al., 2018; Moffett et al., 2007). However, few studies have investigated chromium cycling in these regions.

Nasemann et al. (2020) compared the Cr isotope profiles of shelf, slope and offshore stations along the Peruvian Margin and found pronounced reduction and removal signals ([Cr] depletion with heavier isotopes) confined to the anoxic shelf which is best approximated by a Rayleigh fractionation model. The coincidence of Cr isotope and nitrate/nitrite anomalies indicates a link of Cr cycling with denitrification on the shelf. However, the understanding of Cr redox processes is limited by the only available total dissolved Cr data. It is hard to extract more details about separated processes of Cr that are highly relevant to different Cr redox species.

In this chapter, we investigated the redox cycling of Cr by applying the Cr(III) isotope method to ETSP samples. We determined the fractionation factor of the Cr reduction in the ETSP, and calculated the amount of scavenged Cr and its isotopic composition by comparing ODZ Cr data with that of an oxic reference station. We further examined our Cr reduction fractionation factor and scavenged Cr data with the global Cr array linear relationship. Finally, we will also present two Cr profiles in the Arabian Sea.

## 4.2 Oceanographic settings and seawater sampling

### 4.2.1 Eastern Tropical South Pacific

Eastern Tropical South Pacific (ETSP) is one of the largest biologically productive regions in the global ocean. High primary production is driven by strong upwelling that provides the euphotic zones with abundant nutrients (Pennington et al., 2006; Kadko, 2017). High carbon fluxes consume significant amounts of the available oxygen in the water column, resulting in a pronounced oxygen deficient zone. Near the continental shelf, poleward Peru-Chile Undercurrent (PCUC) prevails between 50 and 150m, and is known to spawn mesoscale eddies that propagate west through the ODZ (Johnson and McTaggart, 2010). The Peruvian ODZ is largely contained within Equatorial Subsurface Water (ESSW). The ESSW blends into Eastern Tropical South Pacific Intermediate Water (ETSPIW) and South Pacific Central Water (SPCW) further to the west (Peters et al., 2018).

Active redox processes have been observed in the ETSP ODZ. The suboxic/anoxic waters with high sinking organic fluxes are fueling diverse microbial activities that control the cycling of nitrogen, such as denitrification, anaerobic ammonia oxidation (anammox) and anaerobic nitrite oxidation (Codispoti and Christensen, 1985; Babbin et al., 2017). Inorganic redox species also undergo unique processes in this ODZ. Accumulations of reduced species, such as Fe(II) and iodide, are reflecting in-situ reduction and horizontal transport influences on their cycling in the ODZ.

ETNP and ETSP ODZs resemble each other in many ways - strong upwelling, high primary and export productivity, and microbial activities. The water masses that shape the two ODZs (ESSW in the ETSP and StSsW in the ETNP) are both branching off from the Equatorial Countercurrent, and unified as 13°C Water (13CW) (Fiedler and Talley, 2006; Kessler 2006; Stramma et al., 2010; Evans et al., 2020). However, the two ODZs also differ from each other in some ways. The ETSP has stronger upwelling than the ETNP (Pennington et al., 2006). The turnover age of the ETSP ODZ waters is 60 years, shorter than that of the ETNP ODZ waters (90 years; Karstensen, 2008).The ETSP is also thinner and more dynamic than the ETNP. Differences are also seen in primary productivity and iodine profiles (Pennington et al., 2006; Evans et al., 2020; Moriyasu et al., 2020).

In this chapter, we present Cr concentration and isotope signatures from three stations in the ETSP ODZ (Table 4.1 and Figure 4.1). Stations 1 and 11 are located in the ODZ. They both

have strong upwelling, but station 1 is closer to the coast with higher productivity (Kadko, 2017). Station 33 is an oxic station within the low productivity oligotrophic waters of the adjacent mid-ocean gyre.

### 4.2.2 Arabian Sea

The Arabian Sea is one of the three major ODZs in the global ocean. Unlike ETNP or ETSP, it is bounded on the north at subtropical latitudes. Therefore, the ventilation is restricted to the oxygen carried in Red Sea Water (RSW) and Persian Gulf Water (PGW) and the subsurface waters transported from the southern hemisphere. The poor ventilation and locally high primary productivity fueled by strong upwelling and high dust deposition result in an oxygen deficient zone in the central/northern Arabian Sea. However, the high primary productivity zone and the intense oxygen deficient zone are geographically separated. The highest primary productivity is observed in the western Arabian Sea because of the intense upwelling along the coast of Somali and Oman, whereas the ODZ is located in the central/eastern Arabian Sea, overlapping with the extent of secondary nitrite maximum. This eastward shift of the ODZ is a consequence of greater ventilation in the west with oxygenated waters (Oslon et al., 1993).

The most prominent feature of the Arabian Sea is that it is subjected to intense monsoon cycling. Its yearly cycle can be divided into the Northeast (NE) and Southwest (SW) monsoons and two intermonsoon periods. The start and end of the monsoon seasons vary from year to year and region to region. But generally, the NE monsoon is from November to February, whereas the SW monsoon is from June to September. There are the strongest winds during the SW Monsoon that could drive the most intense coastal upwelling on the western boundary. Upwelling during the NE Monsoon is maintained by convective mixing. Controlled by the intensity of the upwelling, the primary productivity also shows seasonal variability. Highest primary productivity is observed during the SW monsoon while the lowest is seen during intermonsoon seasons. NE monsoon has an intermediate level of primary productivity (Banse et al., 1986; Morrison et al., 1998 and 1999; Barber et al., 2001). Despite these seasonal changes, there is no seasonality of oxygen within the ODZ. This is because the turnover age of carbon remineralization is longer than a year.

Biotic and abiotic redox processes have also been studied in the Arabian Sea. Denitrification is found as the dominant nitrogen loss process in the Arabian Sea ODZ (Devol et

al., 2006; Ward et al., 2009). High levels of Fe(II) coinciding with secondary nitrite maximum is thought to be related to denitrification (Moffett et al., 2007). Dissolved Mn(II) and iodide also exhibit pronounced subsurface maxima coincident with nitrite in the Arabian Sea (Saager et al., 1989; Lewis and Luther, 2000; Farrenkopf et al., 1997).

In this chapter, we analyzed the Arabian Sea samples from two stations taken in January 1978 during the NE monsoon (Table 4.1 and Figure 4.2). Station 417 is located in the southern part of the ODZ, where its intensity is not as much as the northern part where its ODZ is thicker. Station 419 is sitting to the southwest of the ODZ without suboxic conditions.

### 4.2.3 Seawater sampling

ETSP seawater samples were taken during the GEOTRACES Eastern Pacific Zonal Transect (International GEOTRACES GP16) from October to December, 2013 (Moffett and German, 2018). Filtered samples were collected from the US GEOTRACES trace metal-clean carousel (Cutter and Bruland, 2012) that is equipped with a Seabird CTD. Total dissolved Cr analysis was made on acidified samples. Cr(III) analysis was made on 1L unacidified frozen samples.

Arabian Sea seawater samples were collected from GEOSECS Indian Ocean Expedition in January, 1978. Samples were collected in 30-liter P.V.C. Niskin sample bottles mounted on General Oceanics rosette samplers (GEOSECS Indian Ocean Expedition Volume 5) with epoxy-coated steel inner springs. To ensure the accuracy of Cr measurements after more than forty years of storage, the outside of sample bottles were wiped carefully, and the samples were vacuum-filtered through a 0.4μm Nuclepore filter membrane. To correct for any evaporation during the storage, filtered samples were analyzed for Mg content and calibrated for salinity using a $CO_2$ seawater standard on a flame atomic absorption spectrophotometry (FAAS), assuming the samples and the $CO_2$ standard have the same Mg/Salinity ratio.

## 4.3 Results and Discussion

### 4.3.1 Total dissolved Cr and Cr(III) in the ETSP ODZ

The total dissolved Cr concentration and isotopic composition profiles in the upper 400m do not show much difference between stations 1 and 11 (Table 4.2 and Figure 4.3). Total

dissolved Cr concentration varies from 2.76 nmol/kg to 3.26 nmol/kg and 2.58 nmol/kg to 3.30 nmol/kg at stations 1 and 11, respectively. The isotopic composition of total dissolved Cr at both stations are relatively constant with depth, ranging from 1.00 ‰ to 1.15 ‰. Our data at station 1 agrees with a nearby station (Station 2: 9.922 ºS, 80.224 ºW) in Nasemann et al. (2020).

Cr(III) concentration at station 1 ranges from 0.52 nmol/kg to 1.35nmol/kg between 45m and 376m (Table 4.2 and Figure 4.3). It is difficult to identify a Cr(III) maximum at this station because of low sampling resolution. But the highest [Cr(III)] of measured samples appears at 80m. The Cr isotopic composition of this station ranges from -0.26 ‰ to +0.13 ‰. At station 11, Cr(III) concentration ranges from 0.35 nmol/kg to 1.85 nmol/kg between 110m and 320m, with its isotopic composition from -0.57 ‰ to +0.98‰. Both the [Cr(III)] maximum and the heaviest $\delta^{53}$Cr(III) appear at 220m at station 11.

At the oxic station 33, the total dissolved Cr concentration increases with depth, from 3.07 nmol/kg at 3m to 4.07 nmol/kg at 1000m (Table 4.2). Its isotopic composition gets lighter with depth, from 1.07 ‰ in the surface to 0.72 ‰ at 1000m.

#### 4.3.1.1 Fractionation factor of Cr reduction in ETSP

Similar to ETNP stations, two ETSP ODZ stations were compared to an oxic station on the west end of the transect (station 33; Figures 4.1 and 4.4). Fourth-order polynomial fittings of [Cr] and $\delta^{53}$Cr versus potential density ($\sigma_\theta$) at station 33 allow for this comparison at isopycnal surfaces (Figure 4.5). The ODZ [Cr] is lower than the oxic counterpart by up to 0.57nmol/kg, whereas the ODZ $\delta^{53}$Cr is only up to 0.17‰ heavier than the oxic counterpart (Figure 4.6). The lower [Cr] with heavier $\delta^{53}$Cr in the ETSP ODZ is consistent with that in the ETNP ODZ. It shows that Cr reduction followed by scavenging is also occurring in the ETSP ODZ.

Calculating the [Cr(VI)] and $\delta^{53}$Cr(VI) from Cr(III) and total dissolved Cr by mass balance, we are able to determine the isotope fractionation factor of Cr reduction in the ETSP assuming a Rayleigh fractionation model. Plotting the ETSP Cr(VI) data together with the ETNP data, it is evident that they follow the same linear trendline except one outlier (Figure 4.7). The fractionation factor ($\varepsilon$) derived from ETNP station P2 and ETSP calculated Cr(VI) data is -1.24 ± 0.04‰ (York linear regression by OriginLab©, 2SD), which is within the error of that from ETNP P2 data alone (-1.29 ± 0.04 ‰). This might indicate that ETNP and ETSP have similar Cr reduction mechanisms. This is supported by similar distributions of reduced species in ETNP and

ETSP ODZs. In the ETSP ODZ, Fe(II) maximum, secondary nitrite maximum and particle maxima also coincide with Cr(III) maximum (Cutter et al., 2018; Ohnemus et al., 2017). In 3.3.5, we rule out Fe(II) or microbes as the direct reducing agent for Cr reduction. Nitrite and the catalytic involvement of nitrite oxidoreductase may still be possible candidates.

#### 4.3.1.2 Calculated isotopic composition of scavenged Cr

The scavenged [Cr] and $\delta^{53}Cr$ is calculated by the ETSP ODZ and oxic counterpart Cr data at the same density by mass balance (Table 4.3 and Figure 4.8). The calculated scavenged [Cr] varies from 0.18 to 0.57 nmol/kg (propagated SD: 0.17nmol/kg; mostly station 11 data). It is lower than that in the ETNP where scavenged [Cr] varies from 0.25 to 0.90 nmol/kg (anoxic bottom: 1.15 nmol/kg). This might result from the differences of the station's proximity to the coast. Station 11 is ~1530km from the ETSP ODZ coast, whereas ETNP ODZ stations are 40km to 1300km from the ETNP ODZ coast. In the ETNP ODZ, we have observed a spatial variability of scavenged Cr dependent on the proximity to the coast. Therefore, a relatively low scavenged [Cr] at station 11 1530km from the coast is reasonable. The $\delta^{53}Cr$ of the scavenged Cr in the ETSP ODZ varies from -0.69 to +0.78‰ (propagated SD: 0.58 to 1.78‰).

A weighted average of the calculated scavenged $\delta^{53}Cr$ is 0.3 ± 0.4‰ (SD, n=11). The difference between the calculated scavenged Cr and dissolved Cr(III) is 0.0 ± 0.3‰ (weighted, SD, n=5; Table 4.4). Taking both ETNP and ETSP ODZs into consideration, the weighted average of the scavenged $\delta^{53}Cr$ is 0.5 ± 0.4‰ (SD, n=66), and the average $\delta^{53}Cr$ difference between scavenged Cr and dissolved Cr(III) is 0.3 ± 0.4‰ (SD, n=15; Figure 4.9). These ETNP and ETSP averages lean toward ETNP numbers because of a larger dataset and greater weights due to higher $[Cr]_{scavenged}$ in the ETNP. Although scavenged Cr is statistically heavier than dissolved Cr(III), the isotopic partitioning is small compared with that from Cr reduction. The scavenged Cr is lighter than the total dissolved Cr (~ 1‰ in the core of the ODZ). This is consistent with the regeneration incubation results in Janssen et al. (2021). In their study, scavenged Cr that is oxidatively released from the particles is isotopically lighter than total dissolved Cr, with an enrichment factor ($\Delta\delta^{53}Cr_{particle\text{-}dissolved}$) of -0.66‰. This would give an average $\Delta\delta^{53}Cr_{dissolved\text{-}Cr(III)}$ of ~ 0.96‰ using our weighted average of the calculated scavenged $\delta^{53}Cr$ (0.3 ± 0.4‰). Considering the $\delta^{53}Cr$ of the total dissolved Cr in the core of the ODZs (1.03

‰ ~ 1.34 ‰), the $\delta^{53}$Cr(III) would fall in the range of 0.07 ‰ to 0.38 ‰, which is within our observed $\delta^{53}$Cr(III) range.

#### 4.3.1.3 Relating the isotope effects of Cr reduction and scavenging with global Cr array

Using species-specific Cr isotope data, we are able to tease apart separated processes (i.e. reduction and scavenging) dependent on Cr redox species. These separated processes are difficult to unravel by solely the total dissolved Cr, which comprises both Cr(VI) and Cr(III).

Now we can examine whether the isotope effects of Cr reduction and scavenging we observe agree with the apparent isotopic fractionation of the global Cr array. Consistent with other observations in ODZs and experimental studies, we observed Cr(VI) reduction in the ODZs with a negative isotope fractionation (-1.29 ± 0.04 ‰). The reduction would produce a Cr(III) pool that is isotopically lighter than residual Cr(VI). A fraction of these lighter Cr(III) is scavenged with a slight isotope partitioning between scavenged Cr and Cr(III) ($\Delta\delta^{53}Cr_{scavenged\text{-}Cr(III)}$ ~ 0.3 ± 0.4‰). Therefore, the scavenged Cr(III) is slightly heavier than the dissolved Cr(III). This would attenuate the isotope fractionation seen in the total dissolved Cr data. Hence we see a less fractionated signature than Cr reduction in the total dissolved Cr data (global Cr array).

We further examine this argument quantitatively by adding the isotopic fractionations of Cr reduction (-1.29 ± 0.05‰) and the coarse estimate of the isotope partitioning during scavenging (+0.3 ± 0.4‰). A resultant net effect of -1.0 ± 0.4‰ is within error of the fractionation factor derived from the global Cr array. This demonstrates that the isotope effects we observed for Cr reduction and scavenging in the ODZs are in line with the isotope signatures of the global Cr array.

### 4.3.2 Total dissolved Cr in the Arabian Sea ODZ

In the Arabian Sea, the full water column Cr profiles of both concentration and isotopic composition show a typical nutrient-like Cr profile seen in other ocean basins (Table 4.5 and Figure 4.10). The difference of the Cr profiles between the two stations is negligible generally, despite station 417 being inside the ODZ whereas station 419 is not (Figure 4.11). The Cr concentration increases from 2.92 nmol/kg in the surface water to 4.43 nmol/kg at 1500m. The average Cr concentration deeper than 2000m is 5.07 ± 0.12 nmol/kg (SD, n=3) and 4.55 ± 0.02 nmol/kg (SD, n=2) at stations 417 and 419, respectively. The Cr isotopic composition gets lighter

with increasing depth from 1.19 ‰ in the surface to 0.73 ‰ at 1500m. Deeper than 2000m, the average $\delta^{53}Cr$ is 0.71 ± 0.02 ‰ (SD, n=3) and 0.70 ± 0.04 ‰ (SD, n=2) at stations 417 and 419, respectively.

We did fourth-order polynomial fittings of $\delta^{53}Cr$ and [Cr] versus potential density ($\sigma_\theta$) for station 419 (Figure 4.12). This allows us to compare the ODZ station with a nearby oxic station at isopycnal surfaces. In the core of the ODZ (160 ~ 200m) at isopycnal surfaces, station 417 is only slightly heavier in $\delta^{53}Cr$ by 0.12 to 0.25‰ than station 419, with a [Cr] deficit of 0.16 to 0.21 nmol/kg (Figure 4.13). This reduction - scavenging signal is relatively small because station 417 is located at a less intense ODZ region in the center of the Arabian Sea compared to its northern part. This is also reflected in its thin ODZ core and low levels of nitrite and Fe(II) close to station 417 in the ODZ core (Figure 4.11 and Moffett et al., 2015).

### 4.3.3 Comparisons among three ODZs

All of the total dissolved Cr data in the three ODZs follows the linear correlation of the global Cr array in the $\delta^{53}Cr$-ln[Cr] diagram except one sample at the bottom of the coring station in the ETNP ODZ (Figures 3.7 and 4.14). In all three ODZs, we observed Cr concentration deficit and heavier Cr isotopic compositions in the upper core of the ODZs when comparing them to an oxic reference station in the same ocean basin. This indicates that unique Cr reduction and scavenging processes are occurring in all three ODZs. Isotopically lighter Cr isotopes are preferentially reduced to Cr(III), which is partially scavenged by sinking particles with only a small fractionation. However, the extent of the reduction and scavenging processes differs from station to station, depending on their distance from the coast, the intensity of the ODZ, microbial activities, particle fluxes, etc.

ETNP and ETSP ODZs share some similarities in terms of Cr redox processes. Firstly, Cr(III) is accumulated in the core of the ODZs. The [Cr(III)] maximum in the two ODZs are both within the potential density of 26.0 to 26.5 kg/m$^3$, which coincides with secondary nitrite maximum, [Fe(II)] maximum and local particle maxima. Cr(III) is isotopically lighter than total dissolved Cr. And Cr(III) closer to its concentration maximum has heavier isotope signatures. This fits into a closed-system Rayleigh fractionation model for Cr reduction where its isotopic fractionation factor is determined to be -1.29 ± 0.04 ‰ for both ODZs. Secondly, both ODZs have maximal scavenging signals at the same depth as [Cr(III)] maximum. The calculated

scavenged Cr is isotopically lighter than total dissolved Cr, but is statistically heavier than dissolved Cr(III) by 0.3 ± 0.4‰ (n=15).

However, the difference of the Cr isotopes in ETNP and ETSP ODZs also reflect differences between the two ODZs. As an example, we compare the Cr(III) data at station P2 in the ETNP ODZ and at station 11 in the ETSP ODZ. Station P2 is 320 km from ETNP ODZ coast, whereas station 11 is 1530 km from ETSP ODZ coast. P2 has a thicker ODZ core (100-750m) than station 11 (180-350m). Despite that P2 is in closer proximity to the coast, their [Cr(III)], [Cr(III)]/[$Cr_{tot}$] ratio and $\delta^{53}$Cr(III) profiles are similar to each other (Figure 4.15). With a thinner ODZ core at station 11, its [Cr(III)] decreases faster with depth beneath Cr(III) maximum. At the Cr(III) maximum, however, with almost identical [Cr(III)] and [Cr(III)]/[$Cr_{tot}$] ratio, the $\delta^{53}$Cr(III) at station 11 (0.98‰ and 0.79‰) is heavier than that at P2 by up to 0.5‰. Note that these extremely heavy Cr(III) data points also do not follow the Rayleigh fractionation relationship (Figure 4.7). This might indicate that other processes are also controlling the Cr cycling at the ETSP ODZ core. A possible process might be Cr(III) stabilization by organic complexation. A total ligand maxima and an excess total ligand maximum for Fe were observed at station 11 at the Cr(III) maximum (Figure 3 in Buck et al., 2018).

### 4.3.4 Comparing calculated scavenged Cr isotope data with sedimentary Cr isotope data

Two studies have investigated the $\delta^{53}$Cr of oxic, reducing and anoxic marine sediments (Reinhard et al., 2014; Gueguen et al., 2016). In Gueguen et al. (2016), globally distributed oxic marine sediments have an average bulk $\delta^{53}$Cr of -0.05 ± 0.10‰ (2SD, n=25), indistinguishable from that measured on leach fractions (-0.21‰ to +0.03‰) and bulk silicate earth $\delta^{53}$Cr values (-0.12 ± 0.10‰, Schoenberg et al., 2008). Using our data from the oxic surface waters in the ETNP and ETSP ODZs, the weighted average of the scavenged $\delta^{53}$Cr is +0.16 ± 0.10‰ (2SD, n=6). The scavenged $\delta^{53}$Cr of oxic surface waters has a slightly heavier $\delta^{53}$Cr signature than the detritus component.

Gueguen et al. (2016) found the authigenic fractions (measured on leach fractions) of the Peru Margin sediments have an average $\delta^{53}$Cr of +0.61 ± 0.06‰ (2SD). Similar $\delta^{53}$Cr values in the authigenic fractions (+0.61 ± 0.06‰, 2SD) and in the bulk sediment (+0.59 ± 0.06‰, 2SD) likely indicate large authigenic Cr enrichments. Our weighted average of the calculated scavenged $\delta^{53}$Cr in the ETSP ODZ (+0.3 ± 0.4‰, n=11) are comparable to their authigenic $\delta^{53}$Cr

values. Therefore, during the transport of the scavenged Cr to deeper oxic ocean and burial, the Cr isotopic fractionation related to oxidative release or diagenesis may be subtle.

In the Cariaco Basin, Reinhard et al. (2014) reported authigenic $\delta^{53}Cr$ data calculated from detrital correction and from acid leach. They found the two methods give similar authigenic $\delta^{53}Cr$ signatures (+0.58 ± 0.10‰ from leachates and +0.53 ± 0.21‰ from detrital correction, 2SD) during this interglacial period with an euxinic bottom. They are heavier than the authigenic $\delta^{53}Cr$ of the last glacial period with an oxic bottom (-0.1‰ ~ +0.2‰). Gueguen et al. (2016) reported a similar authigenic $\delta^{53}Cr$ from leachates (+0.38 ± 0.10‰, 2SD and n=7) from core-top samples in the Cariaco Basin. Our calculated scavenged $\delta^{53}Cr$ from the ETNP and ETSP ODZs (+0.5 ± 0.4‰, SD, n=66) are within their authigenic $\delta^{53}Cr$ ranges.

Another common feature observed by the two studies is heavier authigenic $\delta^{53}Cr$ during interglacial periods than glacial periods by 0.2 to 0.6‰ in both the Cariaco Basin and Peru Margin. Interglacial periods are believed to have higher primary productivity and carbon export due to sea level rise and a resulting increase in nutrient exchange (Dean et al., 1999; Lyons et al., 2003). This results in larger authigenic Cr fractions and heavier $\delta^{53}Cr$ in the sediments in the euxinic bottom waters during the interglacial period. In our seawater measurements, dissolved Cr(III) does show heavier $\delta^{53}Cr(III)$ in high [Cr(III)] samples due to Rayleigh fractionation. Therefore, the interglacial-glacial difference may be explained by larger amounts of Cr(III) with heavier $\delta^{53}Cr(III)$ being scavenged and buried with higher primary productivity and a more intense ODZ during the interglacial periods. However, calculated scavenged Cr does not show such a correlation between scavenged $\delta^{53}Cr$ and [Cr] (Figure 4.9). The scattered data and their large uncertainties require direct $\delta^{53}Cr$ measurements on particulates to confirm this hypothesis.

In conclusion, our estimates of the scavenged $\delta^{53}Cr$ are consistent with authigenic Cr isotopic compositions in reducing and anoxic marine sediments. Therefore, instead of recording deepwater $\delta^{53}Cr$, authigenic $\delta^{53}Cr$ may be more likely to preserve a Cr reduction and scavenging signal in the upper anoxic waters. This is supported by a relatively fast Cr reduction rate in the ODZ on the timescale of days (see Appendix 2) . A strong correlation between sedimentary $\delta^{53}Cr$ and $\delta^{15}N$ (Gueguen et al., 2016) indicates that the sediments may preserve $\delta^{53}Cr$ signals from the thermocline as is the case for $\delta^{15}N$ (Thunell et al., 2004).

## 4.4 Conclusions

Cr reduction and scavenging were observed in both ETSP and Arabian Sea ODZs. The Cr(III) maximum appears in the upper ODZ core (26.0~26.5 kg/m$^3$) in the ETSP ODZ. It coincides with secondary nitrite maximum and Fe(II) maximum. The fractionation factor of Cr reduction in the ETSP ODZ is close to that in the ETNP ODZ (-1.29 ± 0.04 ‰). Similar processes are likely to be responsible for Cr reduction in the two ODZs. Scavenged Cr is isotopically lighter than total dissolved Cr, but only slightly heavier than dissolved Cr(III). It shows the same distribution of the scavenged Cr in the ETNP ODZ. The positive isotope partitioning between scavenged Cr and dissolved Cr(III) and the isotopic fractionation of Cr reduction agree with the slope of the global Cr array linear relationship. Calculated scavenged $\delta^{53}$Cr are comparable to sedimentary $\delta^{53}$Cr, indicating marine sediments may reflect local redox processes of Cr in the overlying water column.

## Figures and Tables

**Table 4.1 Sampling stations and their locations in ETSP and Arabian Sea**

| Ocean Basin | Station | Latitude and longitude | Cruise and time |
|---|---|---|---|
| ETSP | 1 | 12.0 ºS, 79.2 ºW | GEOTRACES GP16 (Oct-Dec 2013) |
| | 11 | 12.0 ºS, 94.0 ºW | GEOTRACES GP16 (Oct-Dec 2013) |
| | 33 | 10.9 ºS, 145.0 ºW | GEOTRACES GP16 (Oct-Dec 2013) |
| Arabian Sea | 417 | 13.0 ºN, 64.5 ºE | GEOSECS Indian Ocean Expedition (Jan 1978) |
| | 419 | 4.0 ºN, 56.8 ºE | GEOSECS Indian Ocean Expedition (Jan 1978) |

**Figure 4.1 A map of ETSP ODZ stations**

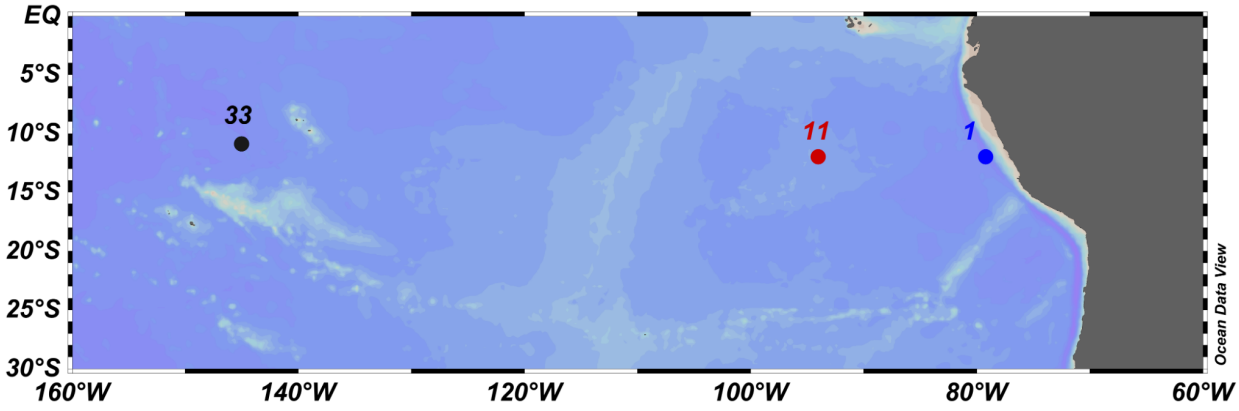

**Figure 4.2 A map of Arabian Sea stations**

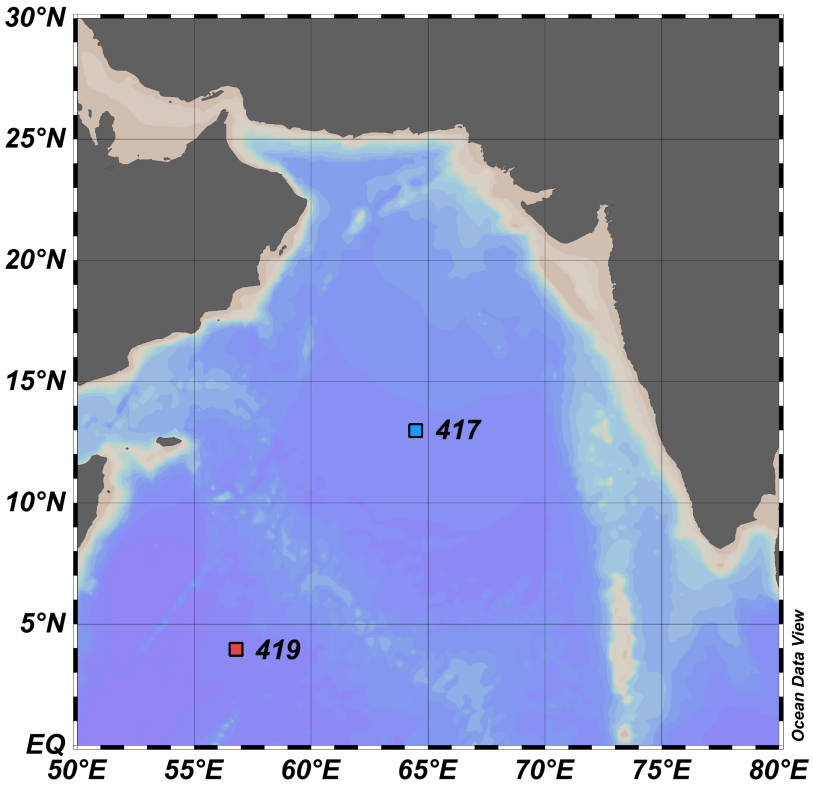

**Table 4.2 Cr concentration and its isotopic composition of total dissolved Cr and Cr(III) at ETSP stations**

| | | | Total dissolved Cr | | Cr(III) | |
|---|---|---|---|---|---|---|
| **Station** | **Depth (m)** | **CTD Oxygen (µmol/kg)** | **[Cr] (nmol/kg)** | **$\delta^{53}$Cr (‰)** | **[Cr] (nmol/kg)** | **$\delta^{53}$Cr (‰)** |
| **1** | 3 | 240.1 | 2.78 | 1.09 | | |
| | 45 | 269.6 | 2.79 | 1.09 | 0.52 | 0.13 |
| | 80 | 1.0 | 2.85 | 1.03 | 1.35 | 0.09 |
| | 131 | 0.9 | 2.93 | 1.13 | | |
| | 181 | 1.0 | 2.89 | 1.12 | | |
| | 235 | 1.2 | 2.76 | 1.13 | | |
| | 300 | 1.4 | 3.05 | 1.05 | | |
| | 376 | | 3.26 | 1.06 | 0.79 | -0.26 |
| **11** | 3 | 224.7 | 3.13 | 1.05 | | |
| | 75 | 253.1 | 3.08 | 1.00 | | |
| | 110 | 218.7 | 3.14 | 1.04 | 0.35 | 0.04 |
| | 180 | 9.4 | 2.77 | 1.09 | 1.45 | 0.50 |
| | 201 | 1.1 | 2.58 | 1.05 | 1.83 | 0.79 |
| | 220 | 1.2 | | | 1.85 | 0.98 |
| | 236 | 1.3 | 2.85 | 1.08 | | |
| | 261 | 1.6 | 2.85 | 1.15 | 1.27 | 0.17 |
| | 320 | 5.3 | 3.30 | 1.12 | 0.77 | -0.57 |
| **33** | 31 | 225.9 | 3.07 | 1.04 | | |
| | 90 | 233.5 | 3.12 | 1.07 | | |
| | 140 | 212.4 | 3.19 | 1.02 | | |
| | 200 | 200.2 | 3.19 | 1.01 | | |
| | 250 | 173.5 | 3.18 | 0.97 | | |
| | 301 | 98.8 | 3.10 | 1.01 | | |
| | 350 | 85.0 | 3.26 | 0.97 | | |
| | 451 | 109.5 | 3.52 | 0.92 | | |
| | 600 | 86.0 | 3.70 | 0.82 | | |
| | 801 | 82.6 | 3.84 | 0.77 | | |
| | 1001 | 118.6 | 4.07 | 0.72 | | |

**Figure 4.3 Profiles of a) Cr concentration and b) isotopic composition of total dissolved Cr and Cr(III) at stations 1 and 11 in the ETSP ODZ**

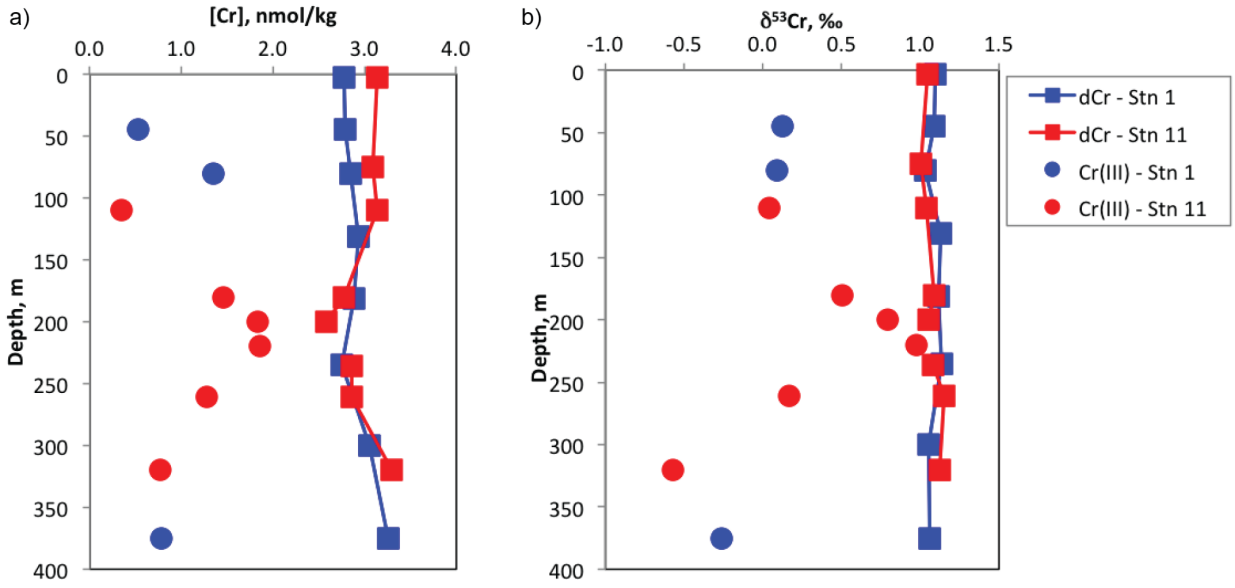


**Figure 4.4 Profiles of a) dissolved oxygen, b) potential density ($\sigma_\theta$) and c) N* in the upper 1000m at stations 1, 11 and 33 in the ETSP ODZ**

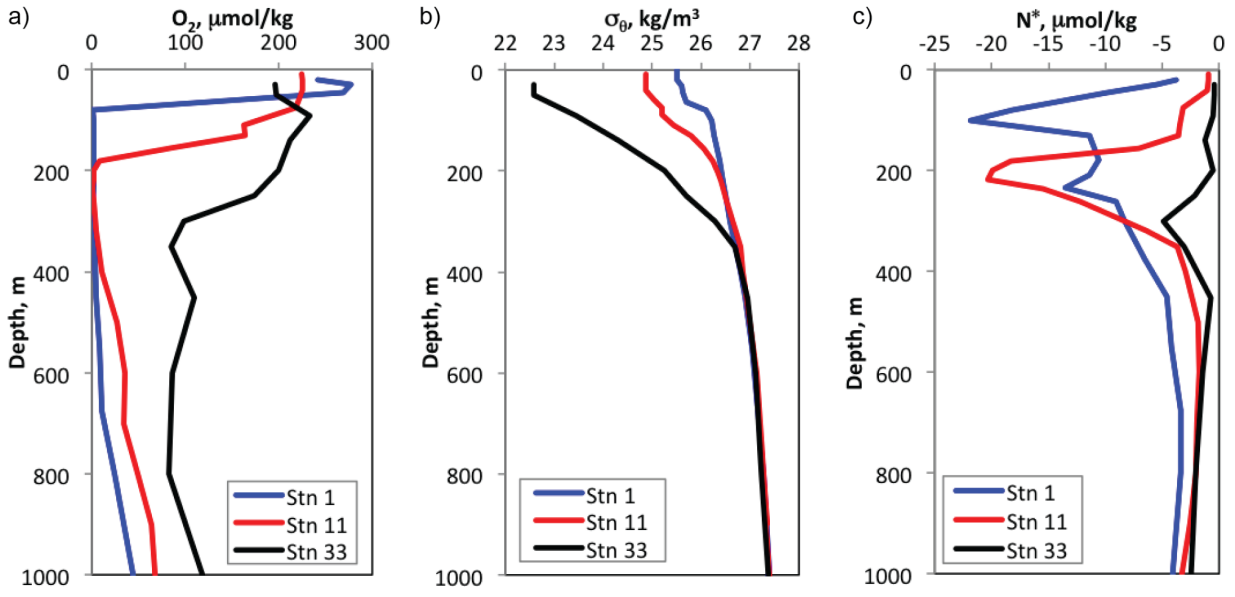

**Figure 4.5 [Cr] and $\delta^{53}Cr$ - $\sigma_\theta$ relationships with 4th-order polynomial fittings at station 33 in ETSP (upper 1000m)**

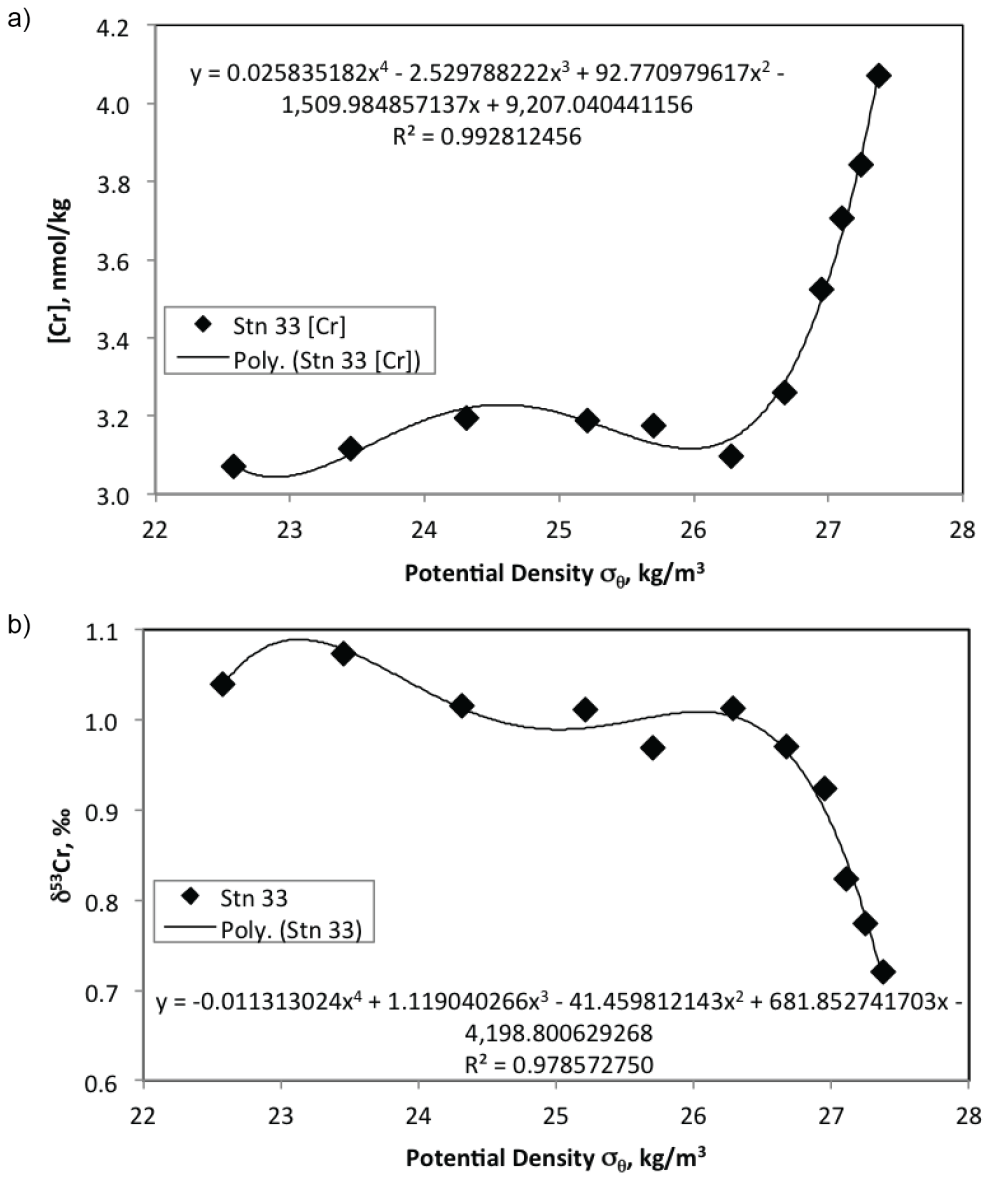

**Figure 4.6 a) Cr concentration and b) isotopic composition of total dissolved Cr and Cr(III) at stations 1 and 11 in the ETSP ODZ against potential density**

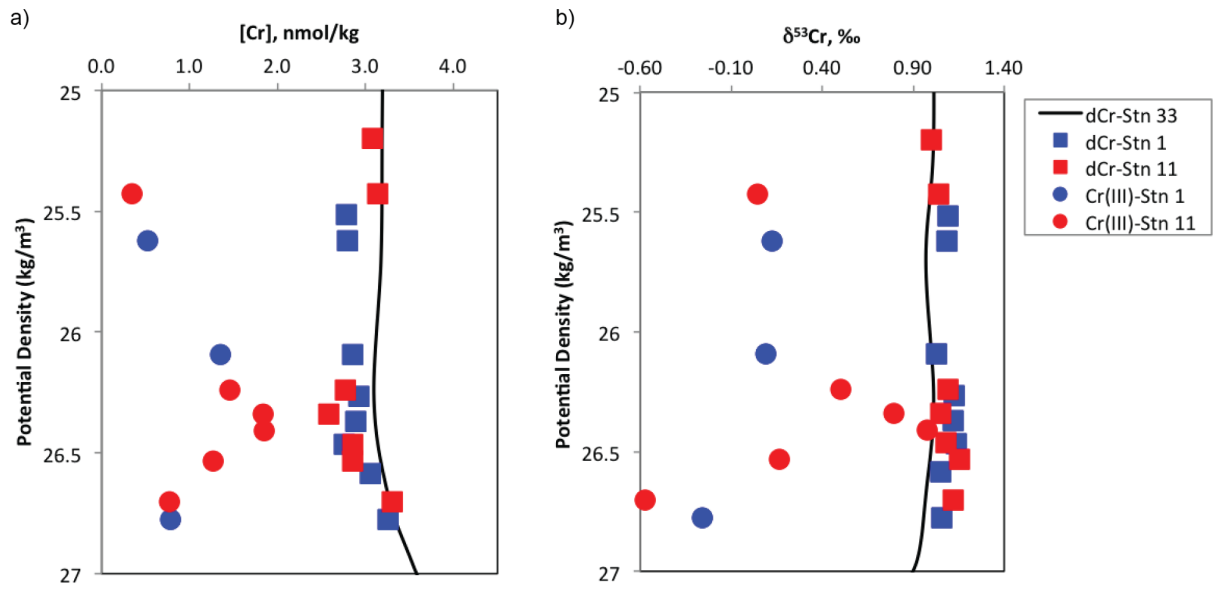

**Figure 4.7 Determination of Cr reduction fractionation factor using ETNP and ETSP data**

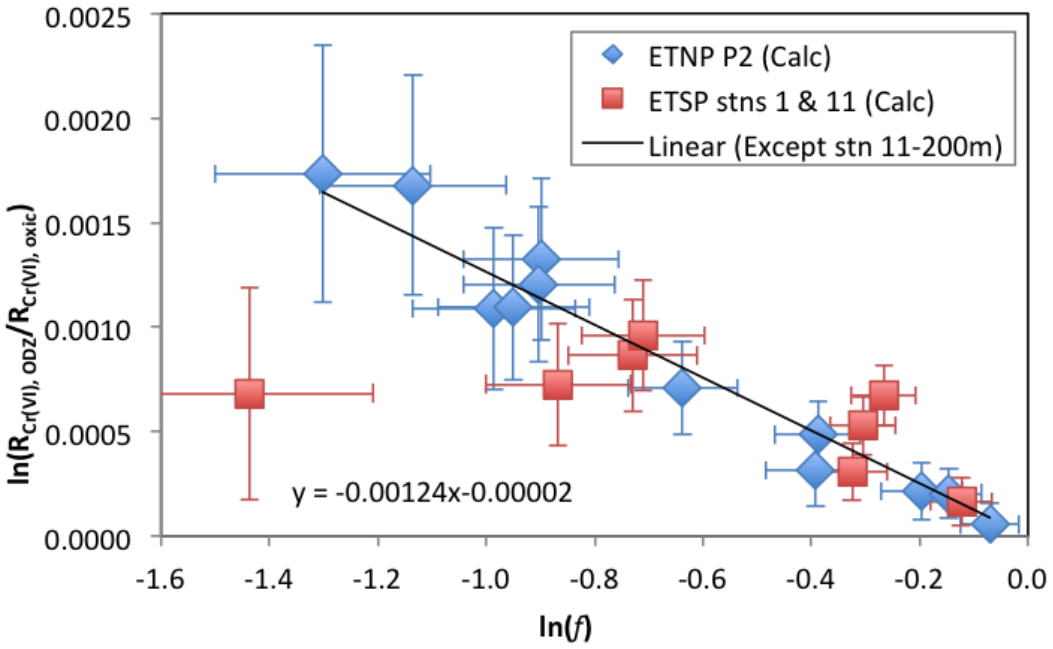


**Table 4.3 [Cr] and $\delta^{53}$Cr of calculated scavenged Cr**

| Station | Depth (m) | $[Cr]_{scavenged}$ (nmol/kg) | $\delta^{53}Cr_{scavenged}$ (‰) | Propagated SD of $\delta^{53}Cr_{scavenged}$ |
|---|---|---|---|---|
| Stn 1 | 3 | 0.37 | 0.29 | 0.85 |
| | 45 | 0.35 | 0.31 | 0.91 |
| | 80 | 0.27 | 0.78 | 1.26 |
| | 131 | 0.21 | -0.69 | 1.60 |
| | 181 | 0.28 | -0.23 | 1.16 |
| | 235 | 0.43 | 0.09 | 0.73 |
| | 300 | 0.18 | -0.28 | 1.78 |
| Stn 11 | 180 | 0.37 | 0.37 | 0.87 |
| | 201 | 0.57 | 0.78 | 0.58 |
| | 236 | 0.33 | 0.26 | 0.95 |
| | 261 | 0.36 | -0.34 | 0.90 |
| **Weighted Average** | | | 0.27 | |
| **SD** | | | 0.42 | |

**Table 4.4 Weighted average of calculated scavenged Cr and its difference from dissolved Cr(III) at the same depth in ETNP and ETSP ODZs (weighted error in SD)**

| | ETNP | ETSP | ETNP + ETSP |
|---|---|---|---|
| $\delta^{53}Cr_{scavenged}$ | 0.5 ± 0.4‰ | 0.3 ± 0.4‰ | 0.5 ± 0.4‰ |
| n | 55 | 11 | 66 |
| $\Delta\delta^{53}Cr_{scavenged\text{-}Cr(III)}$ | 0.4 ± 0.4‰ | 0.0 ± 0.3‰ | 0.3 ± 0.4‰ |
| n | 10 | 5 | 15 |

**Figure 4.8 a) The concentration and b) isotopic composition of calculated scavenged Cr against potential density at stations 1 and 11 in the ETSP ODZ**

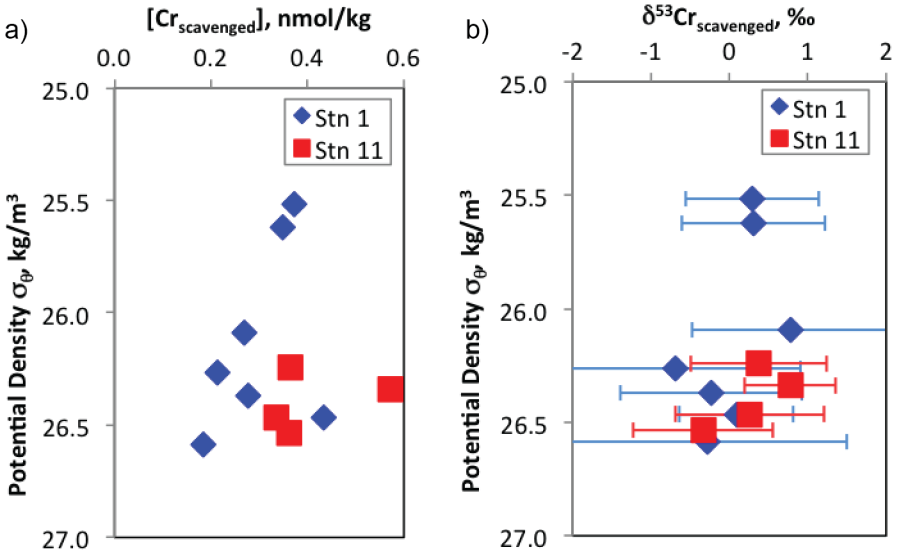

**Figure 4.9 Scavenged $\delta^{53}Cr$ versus [Cr] of ETNP and ETSP**

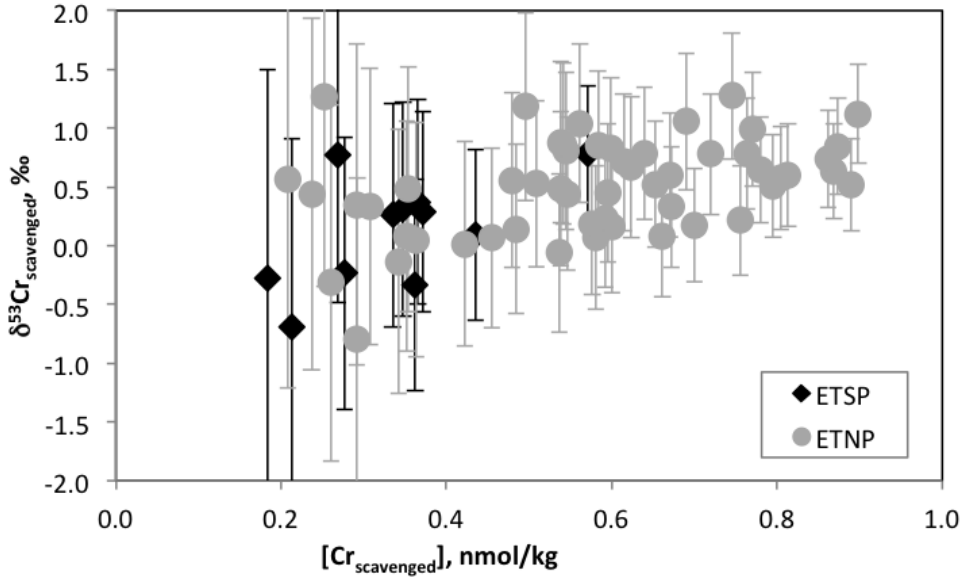

**Table 4.5 Total dissolved Cr concentration and its isotopic composition in Arabian Sea**

| Station | Depth (m) | $[O_2]$ (µmol/kg) | [Cr] (nmol/kg) | $\delta^{53}Cr$ (‰) |
|---|---|---|---|---|
| **417** | 9 | 195 | 2.92 | 1.10 |
| | 54 | 195 | 3.00 | 1.08 |
| | 104 | 40 | 2.95 | 1.09 |
| | 146 | 3 | 3.17 | 0.90 |
| | 166 | 2 | 2.93 | 1.19 |
| | 206 | 3 | 2.94 | 1.15 |
| | 235 | 3 | 3.47 | 0.99 |
| | 306 | 9 | 3.54 | 0.93 |
| | 466 | 18 | 3.24 | 1.06 |
| | 698 | 16 | 3.47 | 0.93 |
| | 1096 | 26 | 3.92 | 0.75 |
| | 1394 | 43 | 4.43 | 0.73 |
| | 1976 | 96 | 5.15 | 0.73 |
| | 3019 | 141 | 5.12 | 0.69 |
| | 3922 | 153 | 4.93 | 0.70 |
| **419** | 5 | 206 | 2.98 | 1.05 |
| | 116 | 124 | 3.15 | 0.93 |
| | 166 | 101 | 3.14 | 0.94 |
| | 217 | 74 | 3.10 | 1.03 |
| | 283 | 77 | 3.13 | 0.93 |
| | 316 | 91 | 3.14 | 0.91 |
| | 404 | 79 | 3.50 | 0.94 |
| | 475 | 92 | 3.38 | 0.84 |
| | 694 | 41 | 3.62 | 0.92 |
| | 1048 | 45 | 4.01 | 0.85 |
| | 1507 | 80 | 4.26 | 0.79 |
| | 2993 | 156 | 4.56 | 0.72 |
| | 4626 | 186 | 4.53 | 0.67 |

**Figure 4.10 Full water column profiles of a) Cr concentration and b) isotopic composition of total dissolved Cr at stations 417 and 419 in the Arabian Sea**

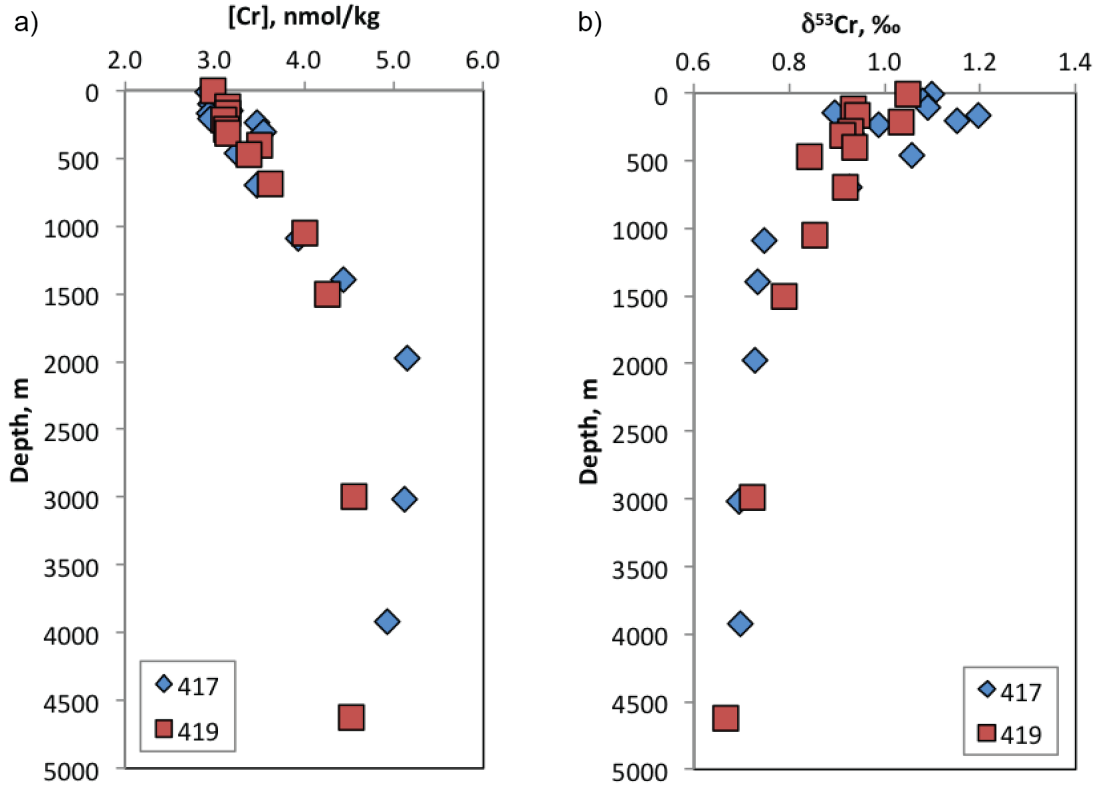


**Figure 4.11 Full water column profiles of a) dissolved oxygen, b) potential density ($\sigma_0$) and c) N* at stations 417 and 419 in the Arabian Sea**

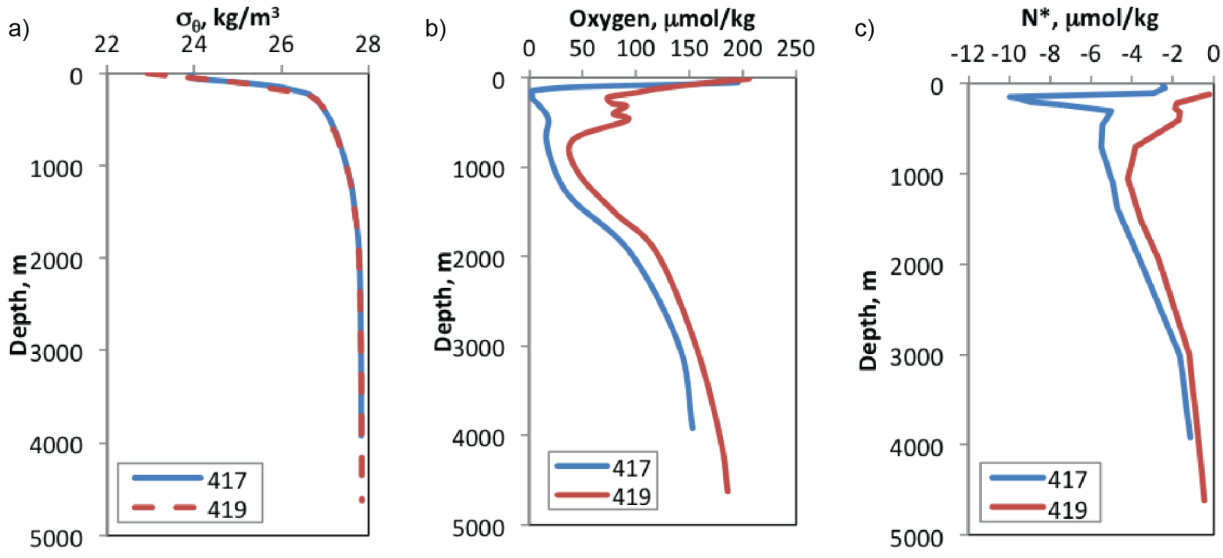

**Figure 4.12 [Cr] and $\delta^{53}Cr$ - $\sigma_\theta$ relationships with 4th-order polynomial fittings at station 419 in the Arabian Sea (100m to 1000m)**

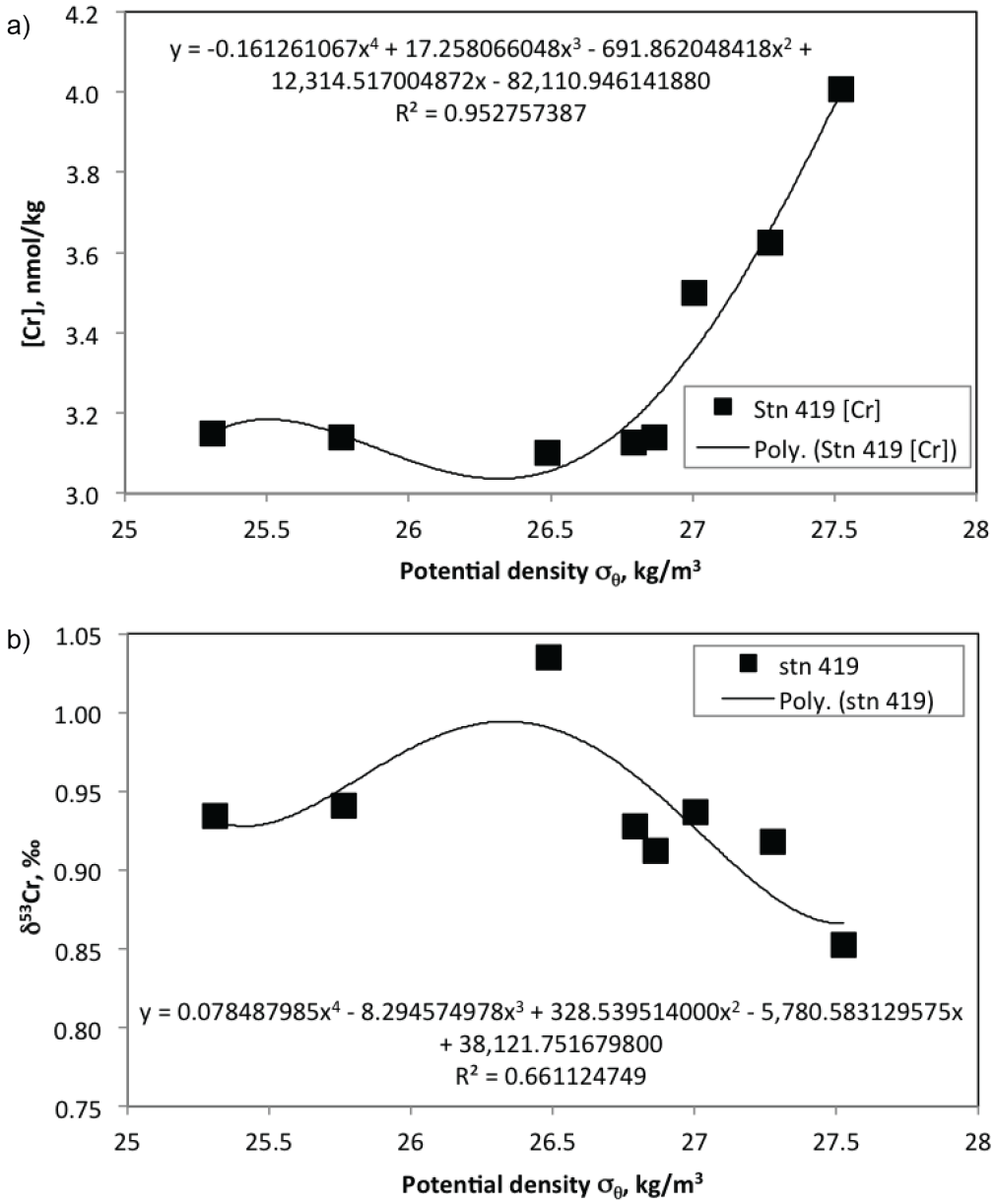

**Figure 4.13 Total dissolved Cr concentration and isotopic composition of station 417 in the Arabian Sea compared with station 419 at isopycnal surfaces**

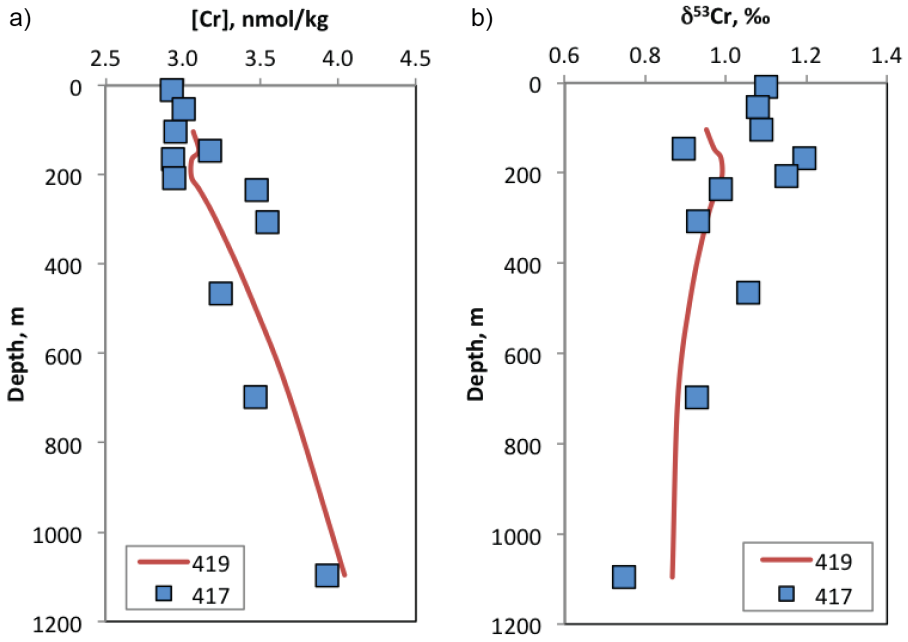

**Figure 4.14 $\delta^{53}$Cr versus ln[Cr] in nmol/kg of ETSP and Arabian Sea stations**

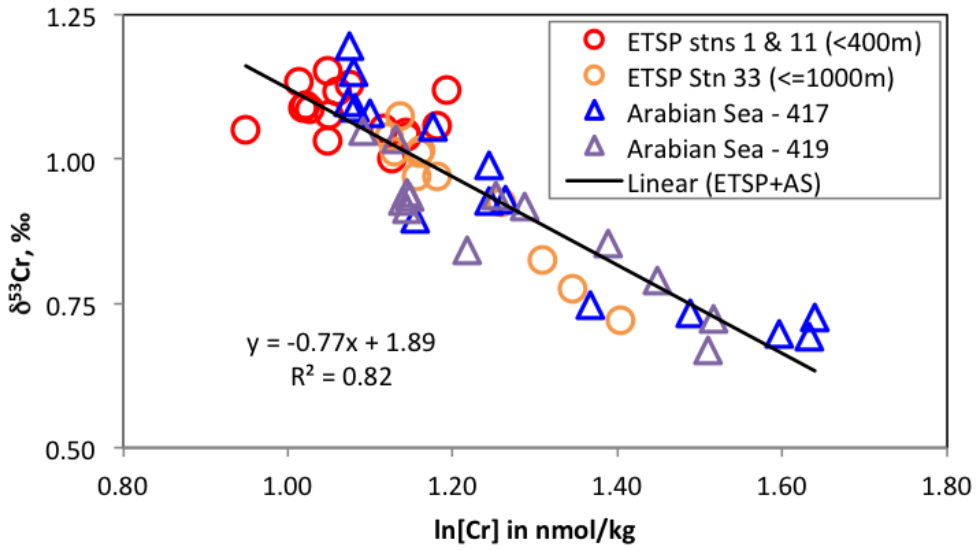


**Figure 4.15 a) Cr(III) concentration, b) [Cr(III)]/[$Cr_{tot}$] ratio and c) $\delta^{53}$Cr(III) of station P2 in ETNP ODZ and station 11 in ETSP ODZ**

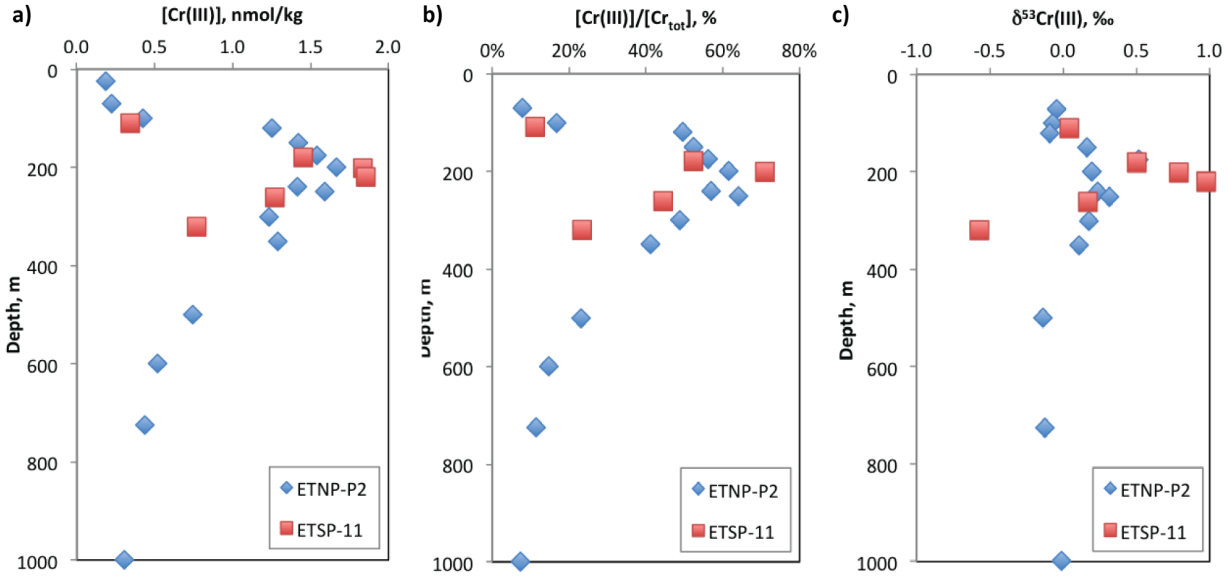

**References**


Babbin, A. R., Peters, B. D., Mordy, C. W., Widner, B., Casciotti, K. L., & Ward, B. B. (2017). Multiple metabolisms constrain the anaerobic nitrite budget in the Eastern Tropical South Pacific. *Global Biogeochemical Cycles*, *31*(2), 258-271.

Banse, K., & McClain, C. R. (1986). Winter blooms of phytoplankton in the Arabian Sea as observed by the Coastal Zone Color Scanner. *Marine Ecology Progress Series*, 201-211.

Barber, R. T., Marra, J., Bidigare, R. C., Codispoti, L. A., Halpern, D., Johnson, Z., ... & Smith, S. L. (2001). Primary productivity and its regulation in the Arabian Sea during 1995. *Deep Sea Research Part II: Topical Studies in Oceanography*, *48*(6-7), 1127-1172.

Buck, K. N., Sedwick, P. N., Sohst, B., & Carlson, C. A. (2018). Organic complexation of iron in the eastern tropical South Pacific: results from US GEOTRACES Eastern Pacific Zonal Transect (GEOTRACES cruise GP16). *Marine Chemistry*, *201*, 229-241.

Codispoti, L. A., & Christensen, J. P. (1985). Nitrification, denitrification and nitrous oxide cycling in the eastern tropical South Pacific Ocean. *Marine chemistry*, *16*(4), 277-300.

Cutter, G. A., & Bruland, K. W. (2012). Rapid and noncontaminating sampling system for trace elements in global ocean surveys. *Limnology and Oceanography: Methods*, *10*(6), 425-436.

Cutter, G. A., Moffett, J. W., Nielsdóttir, M. C., & Sanial, V. (2018). Multiple oxidation state trace elements in suboxic waters off Peru: In situ redox processes and advective/diffusive horizontal transport. *Marine Chemistry*, *201*, 77-89.

Dean, W. E., Piper, D. Z., & Peterson, L. C. (1999). Molybdenum accumulation in Cariaco basin sediment over the past 24 ky: a record of water-column anoxia and climate. *Geology*, *27*(6), 507-510.

Devol, A. H., Uhlenhopp, A. G., Naqvi, S. W. A., Brandes, J. A., Jayakumar, D. A., Naik, H., ... & Yoshinari, T. (2006). Denitrification rates and excess nitrogen gas concentrations in the Arabian Sea oxygen deficient zone. *Deep Sea Research Part I: Oceanographic Research Papers*, *53*(9), 1533-1547.

Evans, N., Boles, E., Kwiecinski, J. V., Mullen, S., Wolf, M., Devol, A. H., ... & Moffett, J. W. (2020). The role of water masses in shaping the distribution of redox active compounds in the Eastern Tropical North Pacific oxygen deficient zone and influencing low oxygen concentrations in the eastern Pacific Ocean. *Limnology and Oceanography*, *65*(8), 1688-1705.

Farrenkopf, A. M., Luther III, G. W., Truesdale, V. W., & Van der Weijden, C. H. (1997). Sub-surface iodide maxima: evidence for biologically catalyzed redox cycling in Arabian Sea OMZ during the SW intermonsoon. *Deep Sea Research Part II: Topical Studies in Oceanography*, *44*(6-7), 1391-1409.

Fiedler, P. C., & Talley, L. D. (2006). Hydrography of the eastern tropical Pacific: A review. *Progress in Oceanography*, *69*(2-4), 143-180.

Gueguen, B., Reinhard, C. T., Algeo, T. J., Peterson, L. C., Nielsen, S. G., Wang, X., ... & Planavsky, N. J. (2016). The chromium isotope composition of reducing and oxic marine sediments. *Geochimica et Cosmochimica Acta, 184*, 1-19.

Janssen, D. J., Rickli, J., Abbott, A. N., Ellwood, M. J., Twining, B. S., Ohnemus, D. C., ... & Jaccard, S. L. (2021). Release from biogenic particles, benthic fluxes, and deep water circulation control Cr and δ 53 Cr distributions in the ocean interior.

Johnson, G. C., & McTaggart, K. E. (2010). Equatorial Pacific 13 C water eddies in the eastern subtropical South Pacific Ocean. *Journal of Physical Oceanography*, *40*(1), 226-236.

Kadko, D. (2017). Upwelling and primary production during the US GEOTRACES East Pacific Zonal Transect. *Global Biogeochemical Cycles*, *31*(2), 218-232.

Karstensen, J., Stramma, L., & Visbeck, M. (2008). Oxygen minimum zones in the eastern tropical Atlantic and Pacific oceans. *Progress in Oceanography*, *77*(4), 331-350.

Kessler, W. S. (2006). The circulation of the eastern tropical Pacific: A review. *Progress in Oceanography*, *69*(2-4), 181-217.

Lewis, B. L., & Luther III, G. W. (2000). Processes controlling the distribution and cycling of manganese in the oxygen minimum zone of the Arabian Sea. *Deep Sea Research Part II: Topical Studies in Oceanography*, *47*(7-8), 1541-1561.

Lyons, T. W., Werne, J. P., Hollander, D. J., & Murray, R. W. (2003). Contrasting sulfur geochemistry and Fe/Al and Mo/Al ratios across the last oxic-to-anoxic transition in the Cariaco Basin, Venezuela. *Chemical Geology*, *195*(1-4), 131-157.

Moffett, J. W., Goepfert, T. J., & Naqvi, S. W. A. (2007). Reduced iron associated with secondary nitrite maxima in the Arabian Sea. *Deep Sea Research Part I: Oceanographic Research Papers*, *54*(8), 1341-1349.

Moffett, J. W., Vedamati, J., Goepfert, T. J., Pratihary, A., Gauns, M., & Naqvi, S. W. A. (2015). Biogeochemistry of iron in the Arabian Sea. *Limnology and Oceanography*, *60*(5), 1671-1688.

Moffett, J. W., & German, C. R. (2020). Distribution of iron in the Western Indian Ocean and the Eastern tropical South pacific: An inter-basin comparison. *Chemical Geology*, *532*, 119334.

Moriyasu, R., Evans, N., Bolster, K. M., Hardisty, D. S., & Moffett, J. W. (2020). The distribution and redox speciation of iodine in the Eastern Tropical North Pacific Ocean. *Global Biogeochemical Cycles*, *34*(2), e2019GB006302.

Morrison, J. M., Codispoti, L. A., Gaurin, S., Jones, B., Manghnani, V., & Zheng, Z. (1998). Seasonal variation of hydrographic and nutrient fields during the US JGOFS Arabian Sea Process Study. *Deep Sea Research Part II: Topical Studies in Oceanography*, *45*(10-11), 2053-2101.

Morrison, J. M., Codispoti, L. A., Smith, S. L., Wishner, K., Flagg, C., Gardner, W. D., ... & Gundersen, J. S. (1999). The oxygen minimum zone in the Arabian Sea during 1995. *Deep Sea Research Part II: Topical Studies in Oceanography*, *46*(8-9), 1903-1931.

Nasemann, P., Janssen, D. J., Rickli, J., Grasse, P., Frank, M., & Jaccard, S. L. (2020). Chromium reduction and associated stable isotope fractionation restricted to anoxic shelf waters in the Peruvian Oxygen Minimum Zone. *Geochimica et cosmochimica acta*, *285*, 207-224.

Olson, D. B., Hitchcock, G. L., Fine, R. A., & Warren, B. A. (1993). Maintenance of the low-oxygen layer in the central Arabian Sea. *Deep Sea Research Part II: Topical Studies in Oceanography*, *40*(3), 673-685.

Pennington, J. T., Mahoney, K. L., Kuwahara, V. S., Kolber, D. D., Calienes, R., & Chavez, F. P. (2006). Primary production in the eastern tropical Pacific: A review. *Progress in oceanography*, *69*(2-4), 285-317.

Peters, B. D., Jenkins, W. J., Swift, J. H., German, C. R., Moffett, J. W., Cutter, G. A., ... & Casciotti, K. L. (2018). Water mass analysis of the 2013 US GEOTRACES eastern Pacific zonal transect (GP16). *Marine Chemistry*, *201*, 6-19.

Reinhard, C. T., Planavsky, N. J., Wang, X., Fischer, W. W., Johnson, T. M., & Lyons, T. W. (2014). The isotopic composition of authigenic chromium in anoxic marine sediments: A case study from the Cariaco Basin. *Earth and Planetary Science Letters*, *407*, 9-18.

Saager, P. M., De Baar, H. J., & Burkill, P. H. (1989). Manganese and iron in Indian Ocean waters. *Geochimica et Cosmochimica Acta*, *53*(9), 2259-2267.

Stramma, L., Johnson, G. C., Firing, E., & Schmidtko, S. (2010). Eastern Pacific oxygen minimum zones: Supply paths and multidecadal changes. *Journal of Geophysical Research: Oceans*, *115*(C9).

Thunell, R. C., Sigman, D. M., Muller‐Karger, F., Astor, Y., & Varela, R. (2004). Nitrogen isotope dynamics of the Cariaco Basin, Venezuela. *Global Biogeochemical Cycles*, *18*(3).

Ward, B. B., Devol, A. H., Rich, J. J., Chang, B. X., Bulow, S. E., Naik, H., ... & Jayakumar, A. (2009). Denitrification as the dominant nitrogen loss process in the Arabian Sea. *Nature*, *461*(7260), 78-81.

# Chapter 5: Conclusions and outlook

## 5.1 Analytical method for seawater Cr(III) and Cr(VI) isotopes

In Chapter 2, I present a seawater Cr(III) and Cr(VI) isotope method modified from a total dissolved Cr isotope method. Pre-concentration with $Mg(OH)_2$ co-precipitation can quantitatively recover Cr(III) from seawater starting at near neutral pH. Double spike equilibration for ≤12 hours of addition does not cause Cr loss to container walls and yields consistent [Cr(III)] and $\delta^{53}$Cr(III) values. Both frozen samples and fresh seawater samples can produce reliable [Cr(III)] and $\delta^{53}$Cr(III) data. However, [Cr(III)] obtained from $Mg(OH)_2$ co-precipitation is two to three times larger than that by Chelex extraction. Despite the Cr(III) concentration difference between the two Cr(III) extraction methods, $\delta^{53}$Cr(III) values from the two methods are identical. I hypothesize that organically-bound Cr(III) is responsible for the difference - Cr(III) complexes that can be scavenged by $Mg(OH)_2$ may be either thermodynamically too strong to be bound by Chelex, or kinetically too slow to dissociate. If this hypothesis is true, it would suggest no isotopic partitioning between organically bound Cr(III) and inorganic Cr(III).

## 5.2 Cr cycling in global oxygen deficient zones

I analyzed seawater samples for total dissolved Cr isotopes from three major ODZs - ETNP, ETSP, and Arabian Sea ODZs. In all three cases, I compared the Cr isotope data in the ODZ with a nearby oxic station in the same ocean basin. Cr(III) isotopes were analyzed for ETNP and ETSP ODZs.

In all three ODZs, I observed [Cr] depletion and heavier $\delta^{53}$Cr in the upper core of the ODZ when comparing ODZ stations to the oxic reference station. These signals maximize at ~200m within the potential density from 26 to 26.5 kg/m$^3$. The extent of the depletion and enrichment of heavier isotopes varies from basin to basin, and appears to depend on the distance from the coast. At the same Cr depletion maximum, a Cr(III) maximum is observed in ETNP and ETSP ODZs. The Cr(III) is ~1‰ lighter than total dissolved Cr. This confirms that Cr(VI) reduction is occurring in the ODZ. Lighter Cr(VI) is preferentially reduced to Cr(III), which is subsequently scavenged onto particles and sinks to deeper oceans. Assuming a nearby oxic station as the source water of the ODZ, I determined the isotopic fractionation factor of Cr(VI)

reduction to be -1.29 ± 0.04 ‰ for ETNP and ETSP ODZs. Similar mechanisms might control Cr reduction in both ODZs. Cr(III), Fe(II), secondary nitrite and local particle maxima co-occur in the upper core of the ODZ within the potential density from 26 to 26.5 kg/m$^3$. This suggests a linkage between Cr reduction and microbial activities, especially that of denitrifiers. However, direct evidence is still lacking to confirm this hypothesis. Our shipboard incubations (Appendix 2) demonstrate neither Fe(II) nor microbes are reducing Cr directly. Other soluble reducing agents should be responsible for this process.

By comparing the Cr data in the ODZ with an oxic station in the same basin, I am able to calculate the scavenged Cr and its isotopic composition in ETNP and ETSP ODZs. The scavenged Cr concentration can be up to 0.9 nmol/kg in the open ocean and 1.15 nmol/kg in the anoxic slope bottom waters. The two ODZs have a weighted average $\delta^{53}$Cr of 0.5 ± 0.4‰ for scavenged Cr. Scavenged Cr averages +0.3 ± 0.4‰ relative to dissolved Cr(III). The Cr reduction fractionation factor (-1.29 ± 0.04 ‰) and the isotope partitioning during scavenging (+0.3 ± 0.4‰) are in agreement with the apparent fractionation factor derived from the global Cr array (-0.8‰).

### 5.3 Implications for sedimentary Cr isotopes interpretation

Two reports on the Cariaco Basin sedimentary $\delta^{53}$Cr claimed that the authigenic $\delta^{53}$Cr in anoxic marine sediments can preserve deepwater $\delta^{53}$Cr (Reinhard et al., 2014; Gueguen et al., 2016). However, their arguments were based on a problematic Cr dataset in the Argentine Basin (Bonnand et al., 2013). In Appendix 1, we report an updated $\delta^{53}$Cr dataset in the Argentine Basin, which has an average $\delta^{53}$Cr of 0.99 ± 0.22‰ (2SD, n=9) throughout the water column with no evident vertical variation. Our dataset is consistent with another new $\delta^{53}$Cr dataset in the Atlantic Ocean (Goring-Harford et al., 2018). If we compare the new $\delta^{53}$Cr dataset of the Atlantic with the authigenic $\delta^{53}$Cr from the Cariaco Basin sediments, the authigenic Cr is lighter than seawater $\delta^{53}$Cr, therefore not recording deepwater $\delta^{53}$Cr signatures. However, it is still questionable whether the euxinic Cariaco Basin should preserve Atlantic seawater $\delta^{53}$Cr. It may be more likely to record a local partial reduction and scavenging signal for Cr that has lighter $\delta^{53}$Cr as we have seen in scavenged Cr of the ETNP and ETSP ODZs. With an euxinic bottom that does not allow scavenged Cr to be oxidatively released back to the water column, the sedimentary Cr may record scavenged $\delta^{53}$Cr if diagenesis does not induce significant isotope

fractionation. A more comprehensive assessment of this hypothesis awaits measurements of seawater $\delta^{53}Cr$ in the Cariaco Basin.

The calculated scavenged $\delta^{53}Cr$ in this study agrees with authigenic $\delta^{53}Cr$ in oxic, reducing and anoxic sediments (see 4.3.4). Although the authigenic $\delta^{53}Cr$ in the Peru Margin is also comparable to Pacific deepwater $\delta^{53}Cr$ (~0.6-0.7‰), it is more of a coincidence that both the deep Pacific and scavenged Cr is lighter than that in the thermocline. Moreover, considering the fast Cr(VI) reduction seen in our incubations (see Appendix 2), Cr may also have a fast turnover rate in reducing environments. This is somewhat reflected in large authigenic Cr enrichments in reducing/anoxic sediments, which may be related to larger carbon export within reducing/anoxic waters (Devol et al., 2001). Therefore, it is more valid to consider sedimentary $\delta^{53}Cr$ as an archive for local redox conditions rather than preserving deepwater $\delta^{53}Cr$ signatures.

**5.4 Outlook**

Different Cr(III) results from $Mg(OH)_2$ co-precipitation and chelex extraction seem to indicate two Cr(III) pools that have different binding activities with organic chelators. It is possible that the two pools are complexed Cr(III) and inorganic Cr(III) (or complexed Cr(III) that is readily converted to inorganic Cr(III) as it is scavenged by the $Mg(OH)_2$). The two-fold concentration difference between the two methods indicates that organically-bound Cr(III) could be a significant pool in the ODZ. It might also play an important role in stabilizing Cr(III) and keeping it from being scavenged. These organic ligands may have a microbial origin given the co-occurrence of Cr(III) maximum with the particle maximum and secondary nitrite maximum. Therefore, it is crucial to identify this complexed Cr(III) pool. Preliminary data have demonstrated complexed Cr in the ODZ waters (personal communication from Lydia Babcock-Adams). However, the ligand chemistry of Cr is little studied. The difficulties lie in an extreme stability of Cr(III) complexes, thus the kinetic barrier of dissociating Cr(III) complexes. Therefore, any breakthrough in investigating Cr(III) complexes would highly advance our understanding of the Cr(III) cycling in anoxic environments.

So far, there have been several isotope studies and kinetics studies showing different possible Cr reduction mechanisms. However, most of these studies are conducted at high Cr levels. At the nanomolar level of Cr in seawater, it is still unclear which mechanism is responsible. Our incubation experiments rule out Fe(II) and denitrifiers as the responsible

reductants. Meta-genomics and incubations with nitrite may be helpful to investigate the microbial role in Cr reduction in the ODZ. Other incubations at seawater level Cr with different reductants will also be worth conducting.

Recently, there have been more studies investigating the Cr cycling at seawater-sediment interfaces. Relevant topics include possible diagenesis effect on Cr burial, and benthic flux as a potential sink or source to the global ocean. A study on oceanic Cr isotopes and primary productivity indicates a potential of Cr isotopes as a paleo-productivity proxy (Janssen et al., 2020). This needs to be scrutinized with the knowledge of the diagenesis effect on Cr burial. Contrasting porewater Cr data are reported indicating benthic flux as either a Cr sink or source in different ocean basins. More work on Cr isotopes in marine sediments is needed to evaluate their role in the global ocean Cr cycle.

**References**

Bonnand, P., James, R. H., Parkinson, I. J., Connelly, D. P., & Fairchild, I. J. (2013). The chromium isotopic composition of seawater and marine carbonates. *Earth and Planetary Science Letters*, *382*, 10-20.

Devol, A. H., & Hartnett, H. E. (2001). Role of the oxygen‐deficient zone in transfer of organic carbon to the deep ocean. *Limnology and Oceanography*, *46*(7), 1684-1690.

Goring-Harford, H. J., Klar, J. K., Pearce, C. R., Connelly, D. P., Achterberg, E. P., & James, R. H. (2018). Behaviour of chromium isotopes in the eastern sub-tropical Atlantic Oxygen Minimum Zone. *Geochimica et Cosmochimica Acta*, *236*, 41-59.

Gueguen, B., Reinhard, C. T., Algeo, T. J., Peterson, L. C., Nielsen, S. G., Wang, X., ... & Planavsky, N. J. (2016). The chromium isotope composition of reducing and oxic marine sediments. Geochimica et Cosmochimica Acta, 184, 1-19.

Janssen, D. J., Rickli, J., Quay, P. D., White, A. E., Nasemann, P., & Jaccard, S. L. (2020). Biological control of chromium redox and stable isotope composition in the surface ocean. *Global biogeochemical cycles*, *34*(1), e2019GB006397.

Reinhard, C. T., Planavsky, N. J., Wang, X., Fischer, W. W., Johnson, T. M., & Lyons, T. W. (2014). The isotopic composition of authigenic chromium in anoxic marine sediments: A case study from the Cariaco Basin. *Earth and Planetary Science Letters*, *407*, 9-18.

Schoenberg, R., Zink, S., Staubwasser, M., & von Blanckenburg, F. (2008). The stable Cr isotope inventory of solid Earth reservoirs determined by double spike MC-ICP-MS. *Chemical Geology*, *249*(3-4), 294-306.

# Appendix

**Appendix 1. Argentine Basin Cr profiles**

Cr concentration profiles in the North Atlantic and Pacific Oceans are somewhat nutrient-like (Jeandel and Minster, 1987; Moos and Boyle, 2019). However, one published Cr profile in the Argentine Basin shows the highest [Cr] anywhere in the open ocean, ranging from 5.80 to 6.50 nmol/L with no systematic variation with depth (Bonnand et al., 2013) despite normal nutrient concentration profiles and clearly inconsistent with a global [Cr]-nutrient correlation. In order to evaluate that report, we obtained samples from the central Argentine Basin (Figure A1.1 and Table A1.1) and measured Cr(III) and total dissolved Cr concentrations and total Cr isotopes.

250mL seawater samples were collected from the Argentine Basin from 3 casts during R/V Atlantis cruise AT39-03 in January 2018 and kept frozen before analysis. Frozen samples were filtered using 0.2μm Nuclepore filter membrane immediately after thawing. [Cr(III)] measurements were made on a seawater pH subsample by adding a $^{53}$Cr(III) isotope spike followed by double $Mg(OH)_2$ co-precipitation. The remaining subsamples were acidified to pH <2 for 10 days at 60°C, which shifts the Eh-pH stability field to convert Cr(VI) to Cr(III), followed by the procedures of total dissolved Cr isotope analysis described in chapter 2.

The average [Cr(III)] of 12 samples is 0.26 ± 0.03 nmol/L (Table A1.2), which is consistent with previous observations and the thermodynamic favorability of Cr(VI) in oxic waters. Our measurements give [Cr] ranging from 3.02 to 4.00 nmol/L, with a relatively uniform concentration from the surface to 3000m underlain by a slight increase from 3000m to 5000m (Table A1.3 and Figure A1.2). The Cr concentration is slightly larger than North Atlantic profiles varying from 2.40 to 3.34 nmol/kg (Jeandel and Minster, 1987; Goring-Harford et al., 2018). It is similar to a Cr profile in the Drake Passage increasing with depth from 3.61 to 3.87 nmol/kg in the upper 1000m (Rickli et al., 2019). The average of $\delta^{53}$Cr is 0.99 ± 0.22‰ (2SD, n=9) without obvious variation with depth. This Cr isotope profile is also similar to North Atlantic and Drake Passage $\delta^{53}$Cr profiles (Goring-Harford et al., 2018; Rickli et al., 2019). Both Cr concentrations and isotopic compositions in this study are different from those reported in Bonnand et al.'s paper (~6 nM and ~0.50 ‰). The Cr concentration and isotope profile of this study lies between North Atlantic and North Pacific Oceans (Jeandel and Minster, 1987; Goring-Harford et al.,

2018; Moos and Boyle, 2019). On the $\delta^{53}Cr$ - ln[Cr] plot, the data of this study cluster around North Atlantic surface water and tropical North Pacific waters (Figure A1.3).

Therefore, our South Atlantic Ocean Cr data fits into the current understanding about Cr being a nutrient-like element accumulating along the global thermohaline circulation. And both the Cr concentrations and its isotopic compositions in the South Atlantic Ocean fit onto the global Cr distribution.

## Appendix 2. Shipboard incubations of Cr(VI) reduction by Fe(II)

*In this part, the shipboard incubations were conducted by Kenneth Bolster (University of Southern California), and the Cr isotope analysis was done by me.*

### A2.1 Experiments

These incubations were conducted on cruise KM1920 in September 2019 at stations P2 and P3 (see Figure 3.1.1 for station locations). Four depths (150m, 180m, 225m, 300m) at P2 and one depth (300m) at P3 near the secondary nitrite maximum were selected for incubations.

Seawater samples were taken from the same trace metal clean Niskin bottles as described in Chapter 3. For each depth, seawater was $N_2$-pressurized into four 2L transparent polycarbonate bottles in a glove bag with flowing $N_2$ and lights off. Among the four bottles of seawater, two of them were unfiltered while the other two were filtered with a 0.2 μm Acropak capsule (Figure A2.1). Incubations with filtered and unfiltered seawater were designed to test whether particulate materials were involved in Cr reduction. Fe(II) spike was added to incubation bottles prior to sampling to reach an initial Fe(II) concentration of 5 nmol/kg at the beginning of each incubation. When sampling was done, one bag of $O_2$ scrubber (Thermo Scientific Anaerogen) was opened and put inside the glove bag, which was sealed with clips and put in a cold room (13°C) for 24-48 hours. The detailed incubation conditions were listed in Table A2.1. Once being taken out of the cold room in 24-48 hours, all samples were filtered through a 0.2 μm PES Supor membrane with a peristaltic pump in a glove bag with flowing $N_2$. Of the two 2L replicates of each condition (filtered and unfiltered), 1L was taken from one replicate and kept frozen for Cr(III) analysis, while another 1L was taken from the other replicate and stored at room temperature for total dissolved Cr analysis (Figure A2.1.1). Initial Cr(III) and total dissolved Cr concentration and isotopes were also measured from filtered samples at each depth prior to incubations.

### A2.2 Results

Cr(III) and total dissolved Cr data is shown in Table A2.2 and Figures A2.2 and A2.3. For both Cr(III) and total dissolved Cr, there is no difference in concentration and isotopic composition between filtered and unfiltered seawater as the incubation media. Among the four depths where the incubations were conducted, a [Cr(III)] increase by 0.3 to 0.5 nmol/kg was

observed at 150m, 180m and 225m, which is in the range of where we see Cr(III) maximum at station P2. At two depths (150m and 180m) where we measured $\delta^{53}$Cr, Cr(III) gets heavier by 0.3 to 0.4‰. However, at 300m, [Cr(III)] did not change after the incubation. As for total dissolved Cr, there is no change in concentration or isotopic composition for all of the depths.

### A2.3 Discussion

The observed proceedingly heavier Cr(III) signal after incubation is consistent with a closed-system Rayleigh fractionation model that the product (Cr(III)) gets heavier as the reduction proceeds with a negative isotope effect. The Cr isotope fractionation factor during the incubation is on the same order of magnitude as that of ODZ samples (Figure A2.4). This indicates that the Cr reduction occurring during the incubation may be what is actually happening in the ODZ.

Despite the generation of Cr(III), none of the incubations see changes in total dissolved Cr. This indicates that the generated Cr(III) is not removed by the newly-formed iron-oxyhydroxide at the timescale of hours to days. This result is also consistent with Arctic bottom water particulate Cr and Fe data (personal communication from Phoebe Lam). Based on the low particulate Cr/Fe ratio of 0.0039, Cr removal would not be observed in our incubations.

#### A2.3.1 Cr reduction by Fe(II)?

As discussed in 3.3.5, Cr(VI) reduction by Fe(II) was kinetically favorable at seawater pH and temperature, but these studies are limited at μM-levels of Cr(VI) and Fe(II) (Sedlak and Chan, 1997; Pettine et al., 1998). Our shipboard incubation using anoxic seawater with spiked Fe(II) as medium allows us to look into this mechanism in a closer-to-reality manner. Fe(II) concentration prior to incubation and the formation of iron oxyhydroxide after incubation were also measured by Kenneth Bolster (personal communication). The following calculation and discussion will be based on data from the upper three depths where we observed Cr(III) increase (Table A2.3) and a pseudo first-order kinetics assumption.

$$\frac{d[Cr]}{dt} = k \times [Cr(VI)] \times [Fe(II)]$$

$$\frac{d[Cr]}{dt} = k' \times [Cr(VI)]$$

$$k' = \frac{ln[Cr(VI]_0 - ln[Cr(VI)]_t}{t}$$

$$k = \frac{k'}{[Fe(II)]}$$

The average rate constant ($k$) of Cr(VI) reduction by Fe(II) is 0.066 ± 0.012 $(nmol/kg)^{-1} \cdot d^{-1}$ (SD, n=3). Using a rate constant formula for Cr(VI) reduction by Fe(II) (Pettine et al., 1998), we calculate a rate constant of 0.008 $nM^{-1} \cdot d^{-1}$ at incubation conditions (13°C, seawater pH and ionic strength). This experimental estimate is one order of magnitude lower than incubation numbers. Based on iron oxyhydroxide formation data (personal communication from Bolster) and the 3:1 stoichiometry of Fe(II):Cr(VI) in the reaction, Cr(III) gain would be 0.002 to 0.023 nmol/kg, which is at least one order of magnitude lower than direct Cr(III) measurements. Therefore, the Cr(VI) was not reduced by Fe(II) during the incubation. Other reducing agents should be responsible for this process.

### A2.3.2 Microbially-mediated Cr reduction?

The filtered/unfiltered incubation pairs can shed some light on the microbial mediation mechanism. No difference between filtered and unfiltered pairs in all Cr data suggests that particles larger than 0.2 μm are not involved in Cr reduction within the timescale of 1 to 2 days. However, soluble enzymes may catalyze this process. Studies of cell free extracts from Cr(VI) reducing bacteria show that the Cr(VI) reduction was associated with the soluble fraction of the cells (Thatoi et al., 2014).

## Figures and Tables

**Figure A1.1 A map of sampling sites in the Argentine Basin**

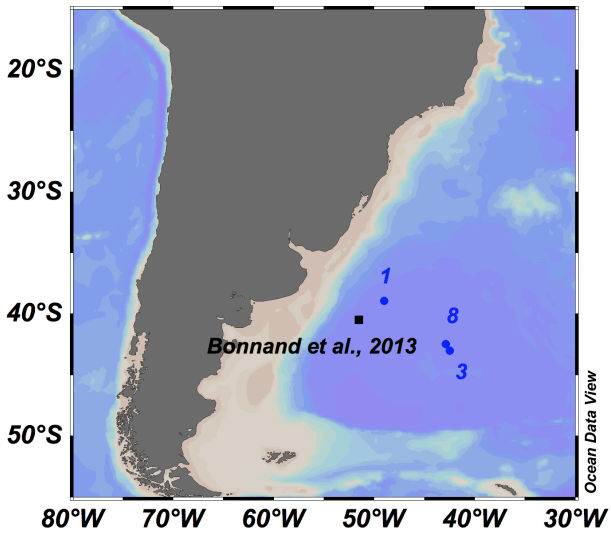


**Table A1.1 Locations of sampling sites in the Argentine Basin**

| Cast # | Latitude (°S) | Longitude(°W) |
|---|---|---|
| 1 | 38.95 | 49.01 |
| 3 | 43.01 | 42.48 |
| 8 | 42.49 | 42.86 |

**Table A1.2 [Cr(III)] data in the Argentine Basin**

| Cast # | Depth (m) | [Cr(III)] (nM) |
|---|---|---|
| 1 | 5 | 0.24 |
| 8 | 100 | 0.25 |
| 3 | 160 | 0.29 |
| 3 | 300 | 0.31 |
| 3 | 500 | 0.29 |
| 3 | 1000 | 0.27 |
| 3 | 1500 | 0.24 |
| 3 | 2000 | 0.30 |
| 3 | 2500 | 0.24 |
| 3 | 3000 | 0.14 |
| 8 | 4000 | 0.24 |
| 8 | 5000 | 0.25 |
| Average | | 0.26 |
| 2SD, n=12 | | 0.03 |

**Table A1.3 Cr concentration and isotope data in the Argentine Basin**

| Depth | $\delta^{53}$Cr (‰) | 2SD (internal) | [Cr] (nM) |
|---|---|---|---|
| 53 | 1.03 | 0.08 | 3.41 |
| 100 | 1.00 | 0.12 | 3.43 |
| 500 | 1.01 | 0.08 | 3.02 |
| 1000 | 0.96 | 0.07 | 3.80 |
| 2139 | 1.08 | 0.04 | 3.22 |
| 2741 | 0.88 | 0.03 | 3.52 |
| 3252 | 1.07 | 0.12 | 3.65 |
| 4213 | 0.77 | 0.04 | 3.71 |

**Figure A1.2 Profiles of a) $\delta^{53}Cr$ and b) Cr concentration of this study and c) silica concentration at a nearby SAVE station 293 (43.21°S, 41.21°W)**

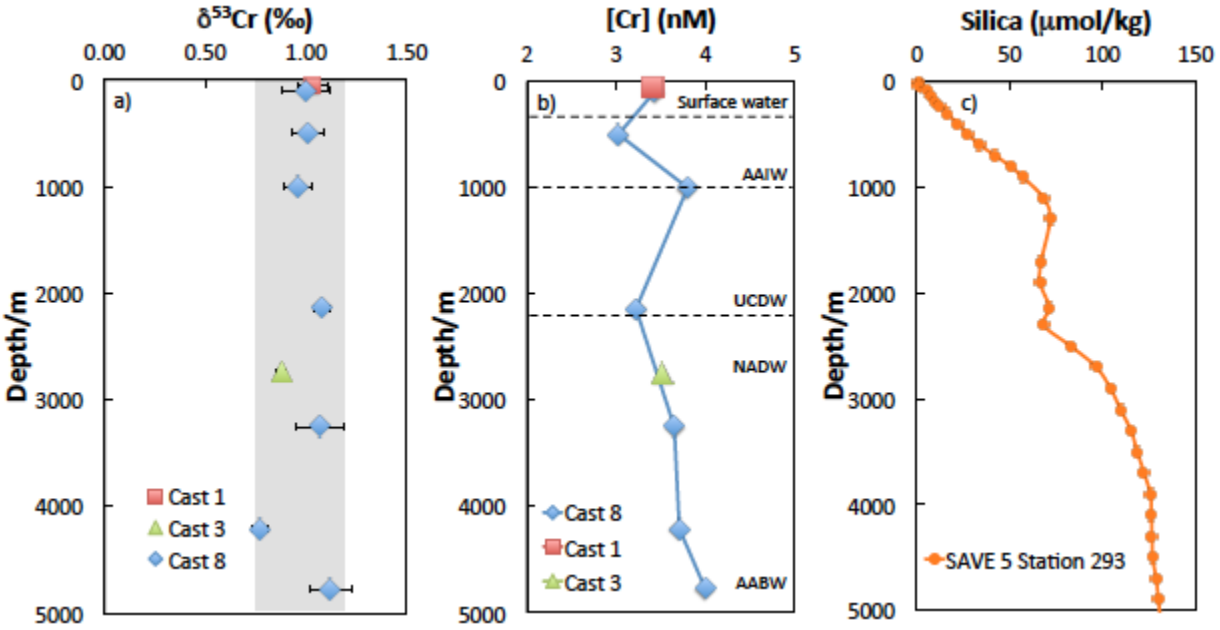

**Figure A1.3 $\delta^{53}Cr$ versus ln[Cr] (Bonnand et al., 2013, Scheiderich et al., 2015; Moos and Boyle, 2019)**

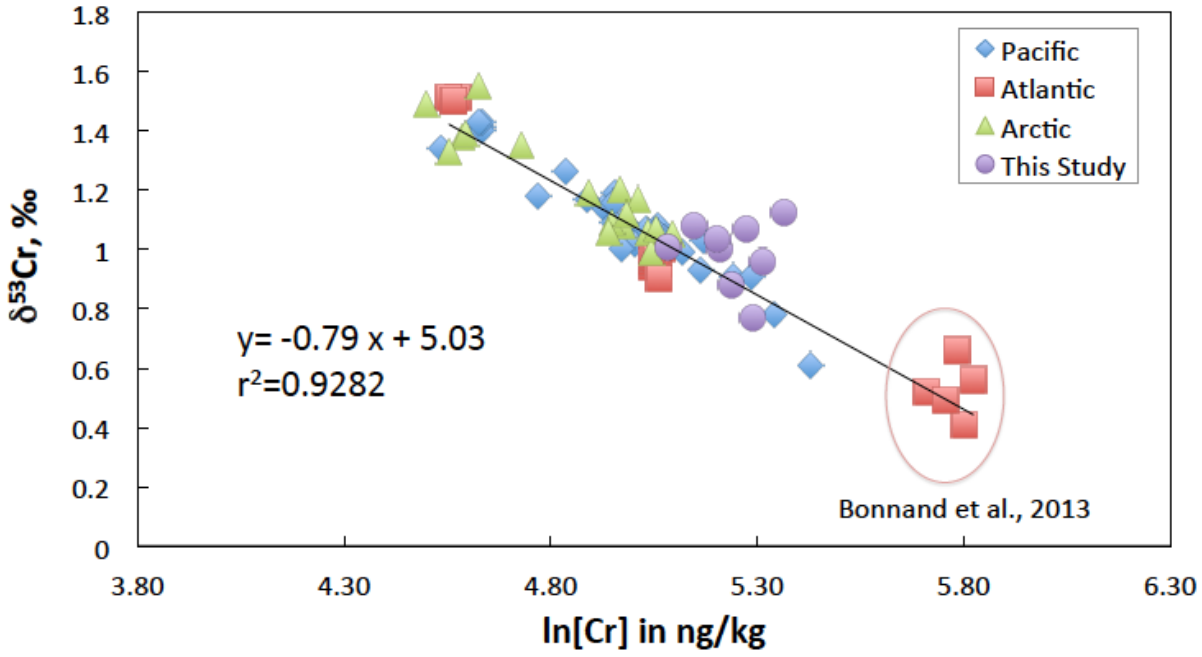

**Figure A2.1 A schematic diagram of incubation setup and Cr sampling**

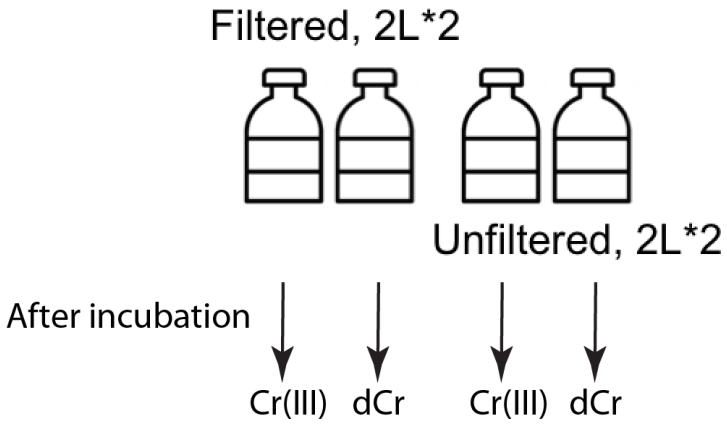


**Table A2.1 Incubation sample depths and incubation duration**

| Station | Depth (m) | Incubation duration (day) |
|---|---|---|
| P2 | 150 | 1 |
| P2 | 180 | 1 |
| P2 | 225 | 1 |
| P2 | 300 | 1 |
| P3 | 300 | 1.56 |

**Table A2.2 Cr(III) and total Cr concentration and isotope ratios prior to and after incubations**

| Inc # | Station | Depth (m) | | Cr(III) | | $Cr_{tot}$ | |
|---|---|---|---|---|---|---|---|
| | | | | [Cr(III)] (nmol/kg) | $\delta^{53}$Cr(III) (‰) | [$Cr_{tot}$] (nmol/kg) | $\delta^{53}$Cr (‰) |
| 1 | P2 | 150 | Initial | 1.23 | 0.29 | 2.32 | 1.24 |
| | | | Filtered | 1.71 | 0.64 | 2.51 | 1.25 |
| | | | Unfiltered | 1.64 | 0.58 | 2.51 | 1.31 |
| 2 | P2 | 180 | Initial | 1.35 | 0.39 | 2.49 | 1.26 |
| | | | Filtered | 1.82 | 0.64 | 2.71 | 1.14 |
| | | | Unfiltered | 1.84 | 0.72 | 2.51 | 1.35 |
| 3 | P2 | 225 | Initial | 1.30 | | 2.42 | 1.19 |
| | | | Filtered | 1.68 | | 2.43 | 1.19 |
| | | | Unfiltered | 1.56 | | 2.41 | 1.17 |
| 4 | P2 | 300 | Initial | 1.29 | | 2.52 | 1.17 |
| | | | Filtered | 1.21 | | 2.51 | 1.22 |
| | | | Unfiltered | 1.24 | | 2.50 | 1.19 |
| 5 | P3 | 300 | Initial | | | 2.57 | 1.05 |
| | | | Filtered | | | 2.56 | 1.24 |
| | | | Unfiltered | | | 2.57 | 1.26 |

**Figure A2.2 Cr(III) concentration and isotope profiles prior to and after incubations (UF denotes unfiltered samples as incubation medium; F denotes filtered samples as incubation medium)**

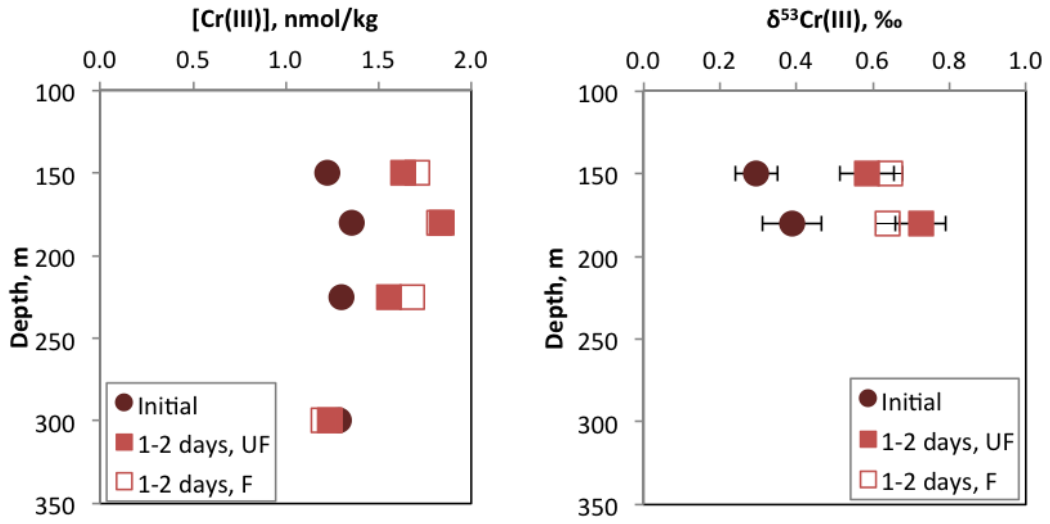


**Figure A2.3 Total dissolved Cr concentration and isotope ratio profiles prior to and after incubations**

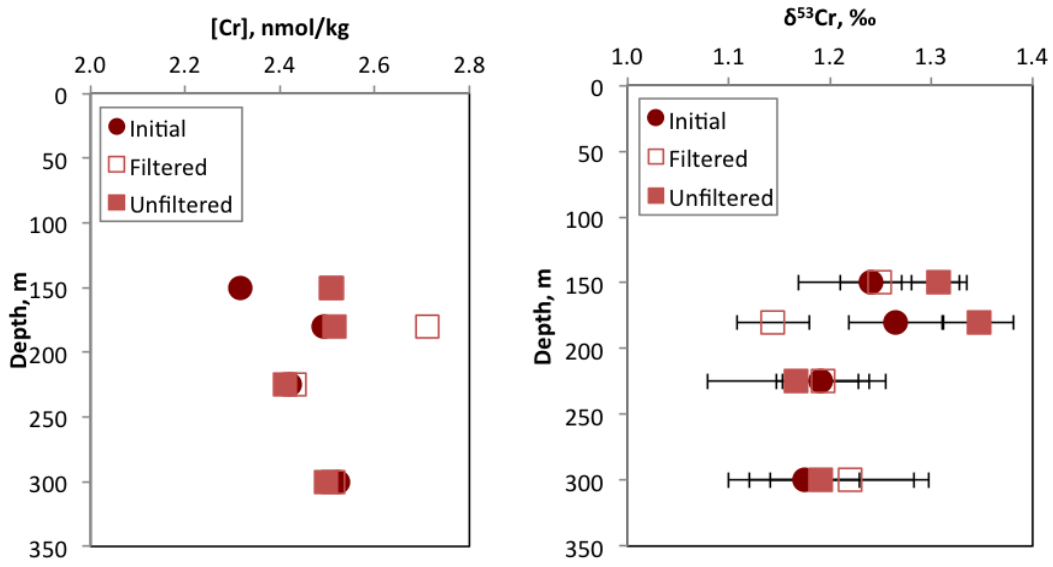

**Table A2.3 Reaction rate constants of Cr(VI) reduction assuming Fe(II) as the reductant**

| Incubation # | Depth (m) | $[Fe(II)]_{initial}$ (nM) | k' ($d^{-1}$) | k ($(nmol/kg)^{-1}$ $d^{-1}$) |
|---|---|---|---|---|
| 1 | 150 | 5 | 0.27 | 0.053 |
| 2 | 180 | 5 | 0.25 | 0.078 |
| 3 | 225 | 5 | 0.34 | 0.068 |
| Average (n=3) | | | 0.29 | 0.066 |
| SD (n=3) | | | 0.05 | 0.012 |

**Figure A2.4 Rayleigh fractionation relationship including incubation Cr data**

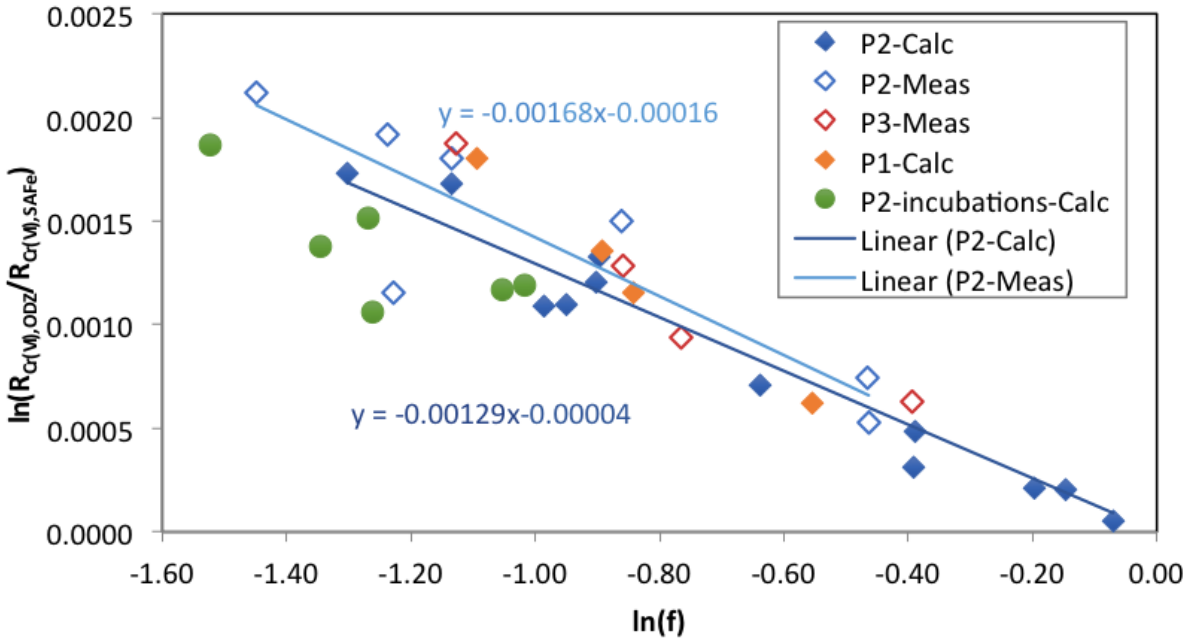

**References**


Bonnand, P., James, R. H., Parkinson, I. J., Connelly, D. P., & Fairchild, I. J. (2013). The chromium isotopic composition of seawater and marine carbonates. *Earth and Planetary Science Letters*, *382*, 10-20.

Goring-Harford, H. J., Klar, J. K., Pearce, C. R., Connelly, D. P., Achterberg, E. P., & James, R. H. (2018). Behaviour of chromium isotopes in the eastern sub-tropical Atlantic Oxygen Minimum Zone. *Geochimica et Cosmochimica Acta*, *236*, 41-59.

Gueguen, B., Reinhard, C. T., Algeo, T. J., Peterson, L. C., Nielsen, S. G., Wang, X., ... & Planavsky, N. J. (2016). The chromium isotope composition of reducing and oxic marine sediments. *Geochimica et Cosmochimica Acta, 184*, 1-19.

Jeandel, C., & Minster, J. F. (1987). Chromium behavior in the ocean: Global versus regional processes. *Global Biogeochemical Cycles, 1*(2), 131-154.

Moos, S. B., & Boyle, E. A. (2019). Determination of accurate and precise chromium isotope ratios in seawater samples by MC-ICP-MS illustrated by analysis of SAFe Station in the North Pacific Ocean. *Chemical Geology*, *511*, 481-493.

Pettine, M., D'ottone, L., Campanella, L., Millero, F. J., & Passino, R. (1998). The reduction of chromium (VI) by iron (II) in aqueous solutions. *Geochimica et cosmochimica acta*, *62*(9), 1509-1519.

Rickli, J., Janssen, D. J., Hassler, C., Ellwood, M. J., & Jaccard, S. L. (2019). Chromium biogeochemistry and stable isotope distribution in the Southern Ocean. *Geochimica et cosmochimica acta, 262*, 188-206.

Sedlak, D. L., & Chan, P. G. (1997). Reduction of hexavalent chromium by ferrous iron. *Geochimica et Cosmochimica Acta*, *61*(11), 2185-2192.

Thatoi, H., Das, S., Mishra, J., Rath, B. P., & Das, N. (2014). Bacterial chromate reductase, a potential enzyme for bioremediation of hexavalent chromium: a review. *Journal of Environmental Management, 146,* 383-399.